

LITHIUM ISOTOPIC ABUNDANCES IN METAL-POOR HALO STARS *

MARTIN ASPLUND

Research School of Astronomy and Astrophysics, Mt. Stromlo Observatory, Cotter Road, Weston, ACT 2611, Australia

DAVID L. LAMBERT

The W.J. McDonald Observatory, The University of Texas at Austin, Austin, TX 78712-1083, USA

POUL ERIK NISSEN

Department of Physics and Astronomy, Aarhus University, DK-8000, Aarhus C, Denmark

FRANCESCA PRIMAS

European Southern Observatory, Karl-Schwarzschild Str. 2, D-85748 Garching b. München, Germany

AND

VERNE V. SMITH

National Optical Astronomy Observatory, P.O. Box 26732, Tucson, AZ 85726, USA

Accepted by ApJ

ABSTRACT

Very high-quality spectra of 24 metal-poor halo dwarfs and subgiants have been acquired with ESO's VLT/UVES for the purpose of determining Li isotopic abundances. The derived 1D, non-LTE ${}^7\text{Li}$ abundances from the Li I 670.8 nm line reveal a pronounced dependence on metallicity but with negligible scatter around this trend. Very good agreement is found between the abundances from the Li I 670.8 nm line and the Li I 610.4 nm line. The estimated primordial ${}^7\text{Li}$ abundance is ${}^7\text{Li}/\text{H} = 1.1 - 1.5 \cdot 10^{-10}$, which is a factor of three to four lower than predicted from standard Big Bang nucleosynthesis with the baryon density inferred from the cosmic microwave background. Interestingly, ${}^6\text{Li}$ is detected in nine of our 24 stars at the $\geq 2\sigma$ significance level. Our observations suggest the existence of a ${}^6\text{Li}$ plateau at the level of $\log \epsilon_{{}^6\text{Li}} \approx 0.8$; however, taking into account predictions for ${}^6\text{Li}$ destruction during the pre-main sequence evolution tilts the plateau such that the ${}^6\text{Li}$ abundances apparently increase with metallicity. Our most noteworthy result is the detection of ${}^6\text{Li}$ in the very metal-poor star LP 815-43. Such a high ${}^6\text{Li}$ abundance during these early Galactic epochs is very difficult to achieve by Galactic cosmic ray spallation and α -fusion reactions. It is concluded that both Li isotopes have a pre-Galactic origin. Possible ${}^6\text{Li}$ production channels include proto-galactic shocks and late-decaying or annihilating supersymmetric particles during the era of Big Bang nucleosynthesis. The presence of ${}^6\text{Li}$ limits the possible degree of stellar ${}^7\text{Li}$ depletion and thus sharpens the discrepancy with standard Big Bang nucleosynthesis.

Subject headings: Stars: abundances – Stars: atmospheres – Stars: Population II – Galaxy: evolution – Cosmology: early Universe

1. INTRODUCTION

Lithium's two stable isotopes – ${}^6\text{Li}$ and ${}^7\text{Li}$ – continue to pose intriguing questions for astrophysicists concerned with understanding the origins of this light element. These questions concern the abundance of lithium in cool interstellar gas and every type of star in which lines of neutral lithium are either detected or are potentially detectable. In this paper, we address by new observations questions about the origin of the lithium seen in the atmospheres of metal-poor stars. In particular, we provide an adequate set of determinations of the isotopic abundance ratio ${}^6\text{Li}/{}^7\text{Li}$ with which to constrain some theoretical ideas on the origins of the rare ${}^6\text{Li}$ isotope and of the majority ${}^7\text{Li}$ isotope for which the Big Bang is widely identified as the initial and major origin.

An observational link of ${}^7\text{Li}$ with the Big Bang was

promoted first by Spite & Spite (1982) who showed that the lithium abundance in the warmest metal-poor dwarfs was independent of metallicity for $[\text{Fe}/\text{H}] < -1.5$. Their derived abundance of lithium in the dwarfs was given as $\log \epsilon_{\text{Li}} = 2.05 \pm 0.15$ on the usual scale where $\log \epsilon_{\text{H}} = 12.00$. The constant lithium abundance defining what is commonly called 'the Spite plateau' suggested that this may be the lithium abundance in pre-Galactic gas provided by the Big Bang. In the succeeding years, many observers have reinvestigated the lithium abundance of the Spite plateau but the lithium (${}^7\text{Li}$) abundance has strayed little from the Spites' original estimate. Here, we also present a new determination of the plateau's lithium abundance as extrapolated to zero metallicity that remains faithful to the 1982 estimate.

Early observations showed that the lithium on the plateau was primarily ${}^7\text{Li}$, as expected from a standard Big Bang: Maurice et al. (1984) set an upper limit ${}^6\text{Li}/{}^7\text{Li} < 0.1$ for a couple of stars. The first

*BASED ON OBSERVATIONS COLLECTED AT THE EUROPEAN SOUTHERN OBSERVATORY, PARANAL, CHILE (OBSERVING PROGRAMS 65.L-0131, 68.D-0091 AND 273.D-5043)

probable detection of ${}^6\text{Li}$ in a very metal-poor star was reported by Smith et al. (1993) for HD 84937 with ${}^6\text{Li}/{}^7\text{Li} = 0.06 \pm 0.03$. Confirmation was provided by Hobbs & Thorburn (1994, 1997), Smith et al. (1998) and subsequently by Cayrel et al. (1999) who obtained ${}^6\text{Li}/{}^7\text{Li} = 0.052 \pm 0.019$. Smith et al. (1998) observed seven single stars and reported ${}^6\text{Li}$ in one additional very metal-poor star (BD +26°3578, also known as HD 338529). Cayrel et al. provided a possible detection of ${}^6\text{Li}$ in BD +42°2667 as did Nissen et al. (2000) for G 271-162. Non-detections gave upper limits variously in the range ${}^6\text{Li}/{}^7\text{Li} < 0.03 - 0.10$.

Two questions now face students of the abundances of ${}^6\text{Li}$ and ${}^7\text{Li}$ in very metal-poor stars. First, predictions of the nucleosynthesis by the Big Bang are tightly constrained because analysis of the anisotropies of the cosmic microwave background determine the one free parameter in a standard cosmological models that sets the abundances (relative to ${}^1\text{H}$) of the products ${}^2\text{H}$, ${}^3\text{He}$, ${}^4\text{He}$, and ${}^7\text{Li}$. The free parameter is the ratio of baryons to photons $\eta = n_b/n_\gamma$ or equivalently the fraction of the critical density Ω_b provided by baryons: $\Omega_b = 3.652 \times 10^7 \eta/h^2$ where h is the Hubble constant in units of $100 \text{ km s}^{-1} \text{ Mpc}^{-1}$. The recent WMAP-based analysis of the cosmic microwave background implies $\Omega_b h^2 = 0.0224 \pm 0.0009$ (Spergel et al. 2003), which in standard Big Bang nucleosynthesis corresponds to an abundance of $\log \epsilon_{\text{Li}} = 2.65 \pm 0.10$ (Coc et al. 2004; Cuoco et al. 2004; Cyburt 2004). This predicted abundance of ${}^7\text{Li}$ is about 0.5 dex or a factor of three larger than the measured abundance of lithium on the Spite plateau. Thus, one key question has become – How does one bridge the 0.5 dex gap between observation and prediction?

The second question arises from the detections of ${}^6\text{Li}$. Our results suggest that there may be a ${}^6\text{Li}$ plateau parallel to the Spite plateau for ${}^7\text{Li}$ with the implication that the major fraction of the ${}^6\text{Li}$ (and presumably some of the ${}^7\text{Li}$) may have been synthesised prior to the onset of star formation in the Galaxy. The ${}^6\text{Li}$ abundance of the plateau exceeds by a large factor the ${}^6\text{Li}$ expected from a standard Big Bang. Thus, our second key question is – How does one account for the high abundance of ${}^6\text{Li}$ in some metal-poor stars?

Our principal concern in undertaking the observations reported here was to extend high-precision measurements of ${}^6\text{Li}$ to more metal-poor stars and to lower metallicities. The observations and the analysis techniques are described below in Sections 2 and 3, respectively. Section 4 deals with the determination of stellar parameters, abundances, and macroturbulent velocities. The derivation of the Li isotopic abundances from the observed line shapes of the Li I 670.8 nm resonance line is outlined in Section 5, while the analysis of the subordinate Li I 610.4 nm line is presented in Section 6. In Section 7, we take up the two questions just outlined: How can one reconcile the predicted ${}^7\text{Li}$ abundance using the WMAP-based $\Omega_b h^2$ with the measurement of the abundance for the Spite plateau? How does one account for those ${}^6\text{Li}$ abundances that greatly exceed the Big Bang prediction?

2. OBSERVATIONS AND DATA REDUCTION

2.1. Selection of Stars

Programme stars were selected from the *uvby- β* catalogue of Schuster & Nissen (1988) and from the Li abundance survey of very metal-poor stars by Ryan et al. (1999). In order to be able to study the possible evolution of the Li isotopes in the Galactic halo, we aimed at a group of stars covering the metallicity range $-3.0 < [\text{Fe}/\text{H}] < -1.0$ and situated in the turnoff region of the Hertzsprung-Russell-diagram, where the upper convection zone of the stars is relatively thin so that proton destruction of Li is minimal. Furthermore, the stars had to be brighter than $V \sim 11$ in order to obtain very high resolution spectra with sufficiently high S/N . Finally, known double-lined spectroscopic binaries were avoided.

2.2. Spectroscopic Observations

Spectra of 23 stars were obtained with UVES (Dekker et al. 2000) on the ESO VLT 8.2m Kueyen telescope during three observing runs: July 23-25, 2000; February 5-7, 2002, and August 28-31, 2004 (5.5 hours in service mode). About 1/3 of the time during the first two periods was lost due to high humidity. The seeing varied from about $0.5''$ most of the time in July 2000 to occasionally more than $2''$ in February 2002. One of the nights in July 2000 was interrupted by “Target of Opportunity” observations - later compensated by service observations on August 4, 2000.

In order to obtain a spectral resolution of about $R \simeq 120\,000$, we used image slicer #3, which for an entrance aperture of $1.5'' \times 2''$ produces five slices each $0.3''$ wide. Thanks to the image slicer, the efficiency of UVES was quite good even during periods with bad seeing. In average conditions a S/N of about 500 per spectral bin (0.00268 nm at the Li I 670.8 nm line) could be obtained for a $V \sim 11.0$ star in 2 hours. The total integration time was always split into at least three separate exposures so that cosmic rays hits on the CCD could be removed by comparison of the different spectra.

The July 2000 and February 2002 spectra were taken in the red arm of UVES with cross disperser #3 and a central wavelength of 705 nm. With this non-standard setting, the EEV CCD covers the spectral region 600 - 700 nm in 15 echelle orders, while the MIT CCD covers the region 710 - 820 nm in 11 orders. We note that the Li I 670.8 nm line is well centered on the EEV chip and that the orders are separated by more than 140 pixels so that despite of the large width of the orders (about 70 pixels) due to the image slicer, there is ample interorder space for measuring the CCD background including scattered light. Furthermore, the sky spectrum could be monitored through an extension of the entrance slit beyond the position of the image slicer. For further details we refer to Dekker et al. (2002).

The service observations in August 2004 were carried out with a standard UVES setting of the red arm (cross disperser #3, central wavelength 600 nm). In this setting, the EEV chip covers the 500 - 595 nm spectral region, and the MIT from 605 to 700 nm. The primary purpose with this alternative setting was to check an interesting Li isotopic abundance ratio obtained for the very metal-poor star LP 815-43 based on the July 2000 observations.

Further details about the spectroscopic observations are given in Table 1. In addition to the 23 stars listed here, G 271-162 is also included in the present paper.

Its spectrum was obtained during the commissioning of UVES in October 1999 with the same setting of UVES as in July 2000 and February 2002 but without the use of the image slicer, which was not available at the time. Instead the star was continuously moved along the slit to simulate the effect of the image slicer. This star has already been analyzed by Nissen et al. (2000) but is re-analyzed here for comparison purposes.

2.3. Data Reduction

The spectra have been reduced using standard tasks in the IRAF echelle package with the following steps included: *i*) bias subtraction, *ii*) fitting a 2-dimensional polynomial to the flux in the interorder regions and subtraction of scattered light, *iii*) pixel-by-pixel division with a normalized flat field exposed without the image slicer, *iv*) tracing and extraction of the echelle orders, *v*) corresponding extraction of a thorium calibration spectrum, *vi*) wavelength calibration, *vii*) rectification of the echelle orders by fitting cubic spline functions with a wavelength scale of about 0.5 nm to the continuum, *viii*) correction for the Doppler shift of the spectral lines.

For some stars this procedure was carried out for the individual slicer spectra, which were then combined to one spectrum by applying weights according to the exposure level of the slices. The resulting spectra were compared to spectra obtained by extraction with a long slit covering all five slices. The difference between the two sets of spectra is marginal in terms of S/N and resolution. Hence, the simpler long slit extraction was applied for all stars as our final reduction procedure. Furthermore, we note that the echelle orders are not merged, which means that lines near the edges of the orders, e.g. the oxygen triplet at 777.4 nm, can be measured in two consecutive orders.

The sky background spectrum turned out to be negligible for all stars observed on July 23-25, 2000, August 4, 2000, and February 5-6, 2002. On these dates the Moon was close to first or last quarter. The observations of LP 815-43 on August 30 - 31, 2004, however, took place during full Moon conditions, and the sky spectrum (corresponding to the extent of the five slices) turned out to be about 1% of the signal in the spectrum of LP 815-43. Hence, in this case the sky spectrum was subtracted.

The wavelength calibration is based on 20-40 thorium lines per echelle order. The rms of a third order polynomial transformation between pixel and wavelength is of the order of 0.12 pm (1.2 mÅ). In addition, the Th lines can be used to check the resolution of UVES; the intrinsic width of a typical Th line is negligible compared to the measured width (Hobbs et al. 1999). The profiles of the Th lines are well approximated by Gaussians, but the resolving power as defined from the FWHM of the Th lines ($R = \lambda/\Delta\lambda_{\text{FWHM}}$) varies along a given spectral order from about 100 000 to 130 000 on the EEV chip. As can be seen in Fig. 1, we achieved slightly higher resolving power during our first observing run in July 2000 than in February 2002. The lower resolution for the August 2004 spectra is caused by charge diffusion in the MIT chip, which, as mentioned above, was used in that period. In any case, the large number of Th lines available, enable us to map the variation of the resolving power along an echelle order. Hence, the actual instrumental broadening for a given stellar line is known and

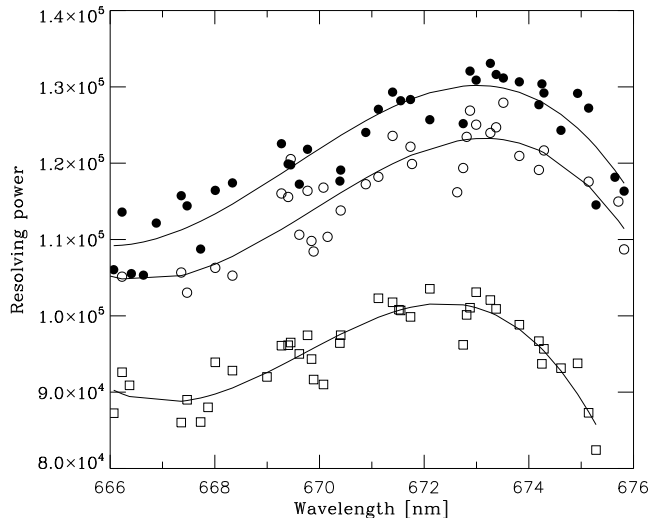


FIG. 1.— Measured resolving power of UVES based on the FWHM of thorium lines in the echelle order containing the Li I 670.8 nm line. Filled circles: July 2000 (EEV CCD); Open circles: February 2002 (EEV CCD); open squares: August 2004 (MIT CCD). The curves are 3rd order fits to each set of data.

can be applied in connection with the spectrum synthesis.

In addition to increasing the efficiency, the image slicer in UVES also serves to broaden the spectrum over a larger area of the CCD. This helps to minimize problems in the flat-fielding, i.e., to reduce the amplitude of any residual fringing existing after the flat-fielding. From exposures of bright B-type stars during the July 2000 observations we estimate that the residual fringing is less than about 0.1%. For some unknown reason, the residual fringing turned out to be larger for the February 2002 spectra, reaching an amplitude of about 0.3% on a wavelength scale that could affect the profiles of the spectral lines. Hence, we decided to determine a “residual fringe function” from the continua of several very metal-poor stars observed in February 2002 taking advantage of the fact that these stars have only a few spectral lines, which are shifted to different positions in the spectra due to large differences in radial velocities. This residual fringe function is well defined and was applied to all spectra observed in February 2002. A similar procedure was applied to the spectra of LP815-43 obtained on August 30-31, 2004; in this case the spectrum of HD 140283 from August 28, 2004 was used to define the residual fringe function.

As a test of the quality of the spectra and of possible problems with the correction for residual fringing in particular, we compare in Fig. 2 the Li I spectra of HD 140283 ($[\text{Fe}/\text{H}] = -2.4$) obtained in July 2000 and Feb. 2002. As seen, there is no significant trend in the residuals, and the rms of the difference is 0.0016 corresponding to a S/N of about 600. This is close to what one would expect for the S/N values of each spectrum given in Table 1. A similar comparison of the spectra of HD 140283 from July 2000 and August 2004 does reveal a significant trend in the residuals, but this is mainly due to the lower resolution of the August 2004 spectrum.

The S/N of the spectra in the region around the Li I

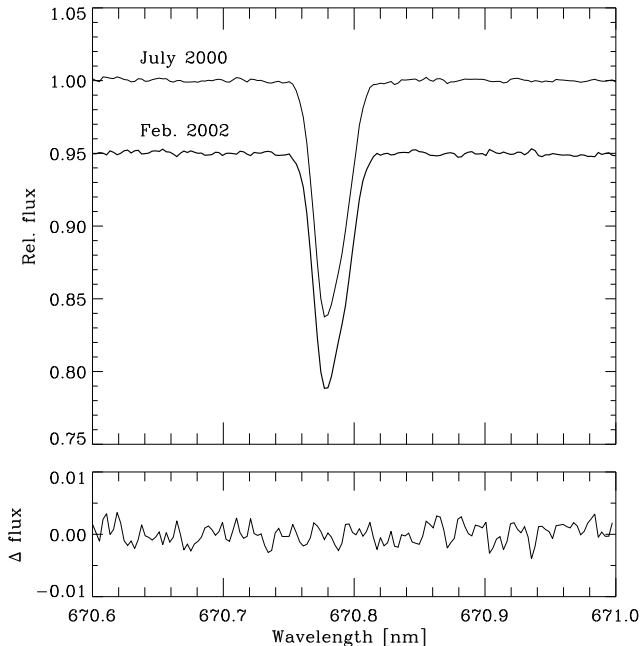


FIG. 2.— Comparison of the Li I region in the July 2000 spectrum of HD 140283 with the February 2002 spectrum (shifted by 0.05). The lower panel shows the difference between the two spectra.

670.8 nm line ranges from about 400 for some of the very metal-poor stars to more than 1000 for the relatively bright star HD 140283. All but two of the stars have $S/N > 500$. Representative spectra are shown in Fig. 3 for a range of metallicities.

2.4. Radial Velocities and Binary Stars

Our conclusions regarding the lithium isotope ratio could be compromised if our targets are binaries. We have searched available databases for evidence suggesting that our program stars are not single. The extensive radial velocity survey of Carney et al. (1994) contains 11 of our 23 stars. One of them, G 126-062, is reported as a single-lined binary; the orbital solution by Latham et al. (2002) gives a period of 219 days and a radial velocity amplitude of $K = 4.8 \text{ km s}^{-1}$. In addition, Carney et al. list BD +03°0740 as a suspected binary. Another accurate survey, that of Nordström et al. (2004) based on radial velocities measured with the Coravel spectrometer, contains eight of our stars but except for G 126-062 none of them are noted as binaries. Finally, Ryan et al. (1999) have nine of the most metal-poor stars in common with us, but again there is no evidence of radial velocity variations.

To supplement these studies we have determined radial velocities for all our stars. The values are based on the measured Doppler shifts of four of the lines that are used in Sect. 4.5 to determine the macroturbulent velocity broadening. The following laboratory wavelengths from the NIST database are adopted: Ca I 612.2217 nm, Ca I 616.2173 nm, Fe I 623.0726 nm and Ca I 643.9075 nm. In determining the radial velocity one should ideally correct for gravitational redshift and convective blueshift, but as the net effect is expected to be below 0.5 km s^{-1} we have

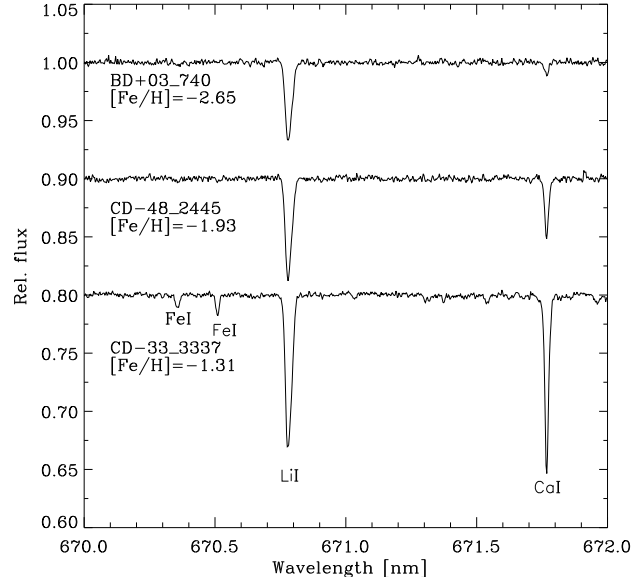


FIG. 3.— Sample spectra around the Li I 670.8 nm line with the spectra of CD -48°2445 and CD -33°3337 shifted 0.10 and 0.20, respectively. Note, that the region between the Li I and the Ca I lines in the spectrum of CD -33°3337 is affected by several faint lines, which are not identified on the figure.

not made such a correction.

The measured radial velocities (corrected to heliocentric values using the IRAF task *rvcorrect*) are given in Table 1. The accuracy of the velocities depends on the stability of UVES because the thorium comparison spectrum was obtained only a few times per night. Comparing the radial velocities for stars observed on different nights we estimate that the precision is $\pm 0.3 \text{ km s}^{-1}$, i.e. similar or slightly better than the precision obtained in the radial velocity surveys mentioned above. A comparison to the data in these three sources and those in the Li isotope study of Smith et al. (1998) gives the following mean differences (us - them) and rms dispersions of the differences (excluding G 126-062):

$$\begin{aligned} \text{Carney et al. (1994): } \Delta v_r &= +0.6 \pm 0.4 \text{ km s}^{-1} \text{ (10),} \\ \text{Nordström et al. (2004): } \Delta v_r &= -0.4 \pm 0.6 \text{ km s}^{-1} \text{ (7),} \\ \text{Ryan et al. (1999): } \Delta v_r &= +0.5 \pm 0.3 \text{ km s}^{-1} \text{ (9),} \\ \text{Smith et al. (1998): } \Delta v_r &= -0.4 \pm 0.4 \text{ km s}^{-1} \text{ (7),} \end{aligned}$$

where the number within parenthesis denotes the number of stars in each comparison. Evidently, there are small systematic differences in the zero point of the radial velocities, but the small rms dispersions are as expected; hence, no additional evidence for binarity is revealed. In particular, we note that BD +03°0740 that was suspected to be a binary by Carney et al. is included in three of the four comparisons and shows no sign of variability.

Out of the 23 stars in Table 1, there are only three (HD 213657, CD -33°3337 and CD -48°2445) for which our radial velocities could not be compared to other accurate sources. The spectra of these stars show no evidence of lines from a companion; the same is true for the other stars including G 126-062. Hence, we feel confident that all stellar spectra can be used for determining the Li isotopic ratio.

3. ANALYSIS: METHODS, MODELS AND INPUT DATA

3.1. *Stellar Model Atmospheres*

In the present study, we have made use of both 1D LTE hydrostatic and time-dependent 3D hydrodynamical stellar model atmospheres. One-dimensional model atmospheres with convection treated by the mixing length theory for the particular stellar parameters of our sample have been generated with the MARCS code (Gustafsson et al. 1975; Asplund et al. 1997), which includes realistic continuous and line opacities for a wide range of atomic and molecular species. The radiative transfer in the construction of the model atmospheres is treated by opacity sampling. As all our stars are metal-poor, the chemical composition of the models have an overabundance of the α -elements of $[\alpha/\text{Fe}] = +0.5$ and a helium abundance of $\log \epsilon_{\text{He}} = 10.93$ (Asplund et al. 2005). This He abundance corresponds to a He mass fraction of $Y = 0.253$, which is close to the expected value from standard Big Bang nucleosynthesis (e.g. Steigman 2005). For test purposes we have also employed theoretical 1D Kurucz model atmospheres without convective overshoot as computed by Castelli et al. (1997). Those models are based on very much the same approximations and assumptions as our standard MARCS models and have been interpolated to the specific stellar parameters of our sample from the available grid of models.

A novel feature of our analysis compared with the pioneering works on Li isotopic abundances in metal-poor stars of Andersen et al. (1984), Smith et al. (1993, 1998), Hobbs & Thorburn (1994, 1997), Nissen et al. (1999), Hobbs et al. (1999) and Cayrel et al. (1999)¹, is our use also of time-dependent 3D hydrodynamical stellar model atmospheres for the stars for which such 3D models with appropriate stellar parameters exist. The 3D model atmospheres of metal-poor stars are taken from Asplund et al. (1999) and Asplund & García Pérez (2001). In short, the models have been constructed by solving the standard hydrodynamical equations of conservation of mass, momentum and energy coupled with a simultaneous solution of the 3D radiative transfer in a representative volume of the stellar atmosphere and near sub-surface layers (e.g. Stein & Nordlund 1998; Asplund et al. 2000). The 3D models are based on realistic continuous and line opacities and equation-of-state computed for the appropriate $[\text{Fe}/\text{H}]$ under the assumption of LTE and opacity binning (Nordlund 1982). At any given time the simulation box is sufficiently large to cover at least ten upflowing regions (granules). The time sequence for each simulation employed is at least one convective turnover time divided into thirty or more individual snapshots to give statistically significant results for the spatially and temporally averaged line profiles. In contrast to the 1D model atmospheres, no mixing length theory enters for the calculation of the convective energy flux. Instead, the time-dependent hydrodynamical simulation automatically and self-consistently predicts the convection efficiency as a function of depth for the given stellar parameters.

¹ We recognize even earlier observational studies by, for example, Herbig (1964), Feast (1966) and Cohen (1972) who attempted to derive Li isotopic abundances using both the center-of-gravity and profile fitting methods. These works were restricted to Galactic disk stars and yielded no convincing ${}^6\text{Li}$ detections.

3.2. *Spectral Line Formation*

The spectral line formation is treated under the assumption of (strong) LTE making the source function equal to the Planck function: $S_\nu(\tau) = B_\nu[T(\tau)]$, i.e. continuum scattering is treated as an absorption. The lines used in our study are located at wavelengths at which Rayleigh and electron scattering make a negligible contribution to the source function; we have ensured that identical results are obtained with the code used herein and the code BSYN from the Uppsala spectrum synthesis package that treats continuum scattering properly within the LTE framework. The radiative transfer is solved with a Fortran implementation of the Feautrier method to which is coupled an IDL routine for the χ^2 -analysis to find the optimum solution in terms of element abundance, wavelength shift, continuum normalization and extra broadening beyond the instrumental broadening (1D: macroturbulence and rotation, 3D: rotation only). The rotational broadening is performed through a disk-integration of the angle-dependent intensity profiles. In the 1D case, microturbulence is prescribed and not part of the χ^2 -optimization while the parameter does not enter the 3D calculations. The same code is able to handle both 1D and 3D geometries with otherwise identical calculations, which is a great advantage when investigating the possible systematic errors when relying on 1D plane-parallel model atmospheres. The background continuous opacities are taken from the MARCS project (Gustafsson et al. 1975; Asplund et al. 1997; Gustafsson et al., in preparation). We have verified that identical ${}^6\text{Li}/{}^7\text{Li}$ ratios and absolute Li abundances to within 0.01 dex would result with the independent spectrum synthesis code BSYN which comes as part of the Uppsala package.

The resulting velocity field from the predicted convection and waves in the 3D models introduce Doppler shifts, which translate to shifts and asymmetries of spectral lines. These will depend on the line formation depths and the atmospheric conditions (in particular temperature, pressure and velocity) for the individual lines, making the detailed line shapes sensitive probes of the stellar atmospheres. As will become clear in Sect. 5.7, this results in a significant improvement in the ability to reproduce the detailed shapes of spectral lines (e.g. Dravins & Nordlund 1990; Asplund et al. 2000; Nissen et al. 2000; Allende Prieto et al. 2002). Since the presence of ${}^6\text{Li}$ in the stellar atmosphere manifests itself as an asymmetry in the Li I 670.8 nm line in excess of the unresolved fine structure of the ${}^7\text{Li}$ line, it is clearly important to have an understanding of other possible mechanisms which can introduce line asymmetries, such as convection. It should be emphasized that no microturbulence or macroturbulence is necessary for the calculation of the line formation in 3D.

Our final ${}^6\text{Li}/{}^7\text{Li}$ ratios will be taken from the 1D analysis rather than from the 3D calculations. Partly, this is due to the simple fact that 3D models do not yet exist for all combinations of stellar parameters of our sample. Another reason is that the very steep photospheric temperature gradients in 3D simulations of metal-poor stars are likely conducive to significant departures from LTE, at least for neutral minority species (Asplund et al. 1999). This has already been confirmed by detailed

multi-level 3D non-LTE calculations for Li (Asplund et al. 2003; Barklem et al. 2003) which showed significant over-ionization of neutral lithium but the lithium abundance from 3D non-LTE calculations was not greatly different from 1D non-LTE calculations. Likewise, one may expect similarly large 3D non-LTE effects for many of our calibration lines of for example Fe I and Ca I used to determine the intrinsic atmospheric line broadening (Asplund et al. 1999; Asplund 2005). Perhaps, more important will be the line asymmetries inherent in predictions for 3D model atmospheres and which will depend somewhat on the thermodynamic conditions (LTE or non-LTE). Under these circumstances, the derived ${}^6\text{Li}/{}^7\text{Li}$ ratios from a 3D LTE analysis may be prone to systematic errors. While the above-mentioned 3D non-LTE studies based on only a couple of snapshots from a simulation are expected to provide a good estimate of the overall Li line *strength* and thus the Li abundance, predicting the detailed line *shape* requires taking the temporal average of many more snapshots to obtain statistically significant profiles. Unfortunately, performing 3D non-LTE calculations for long time-sequences for a stellar sample our size even for a relatively simple atom like Li is beyond reach of current computers. Therefore, the here presented 3D LTE calculations will mainly serve as a test of the 1D results for the Li isotopic ratios to assess possible systematic errors.

3.3. Atomic Data

The basic data for the Li I 670.8 nm resonance line is fortunately very well-known. The wavelengths for the individual hyperfine and isotope components are taken from the highly precise frequency measurements reported by Sansonetti et al. (1995), which are accurate to within 0.01 pm (0.1 mÅ). The gf -values for the different ${}^7\text{Li}$ and ${}^6\text{Li}$ components are based on the calculations by Yan et al. (1998, see also Yan & Drake 1995) that give $f = 0.7467871 \pm 0.0000010$ and $f = 0.7467527 \pm 0.0000010$ for the ${}^7\text{Li}$ and ${}^6\text{Li}$ doublets. Recent experimental values are very similar to the theoretical calculations. For example, the radiative lifetime of the $2p$ upper level (27.11 ± 0.06 ns) measured by Volz & Schmoranzler (1996) is very similar to the prediction by Yan et al. (27.117301 ± 0.000036 ns). Our adopted wavelengths and gf -values are the same as in Hobbs et al. (1999) and Smith et al. (1998). The transition probabilities and wavelengths for the isotope and hyperfine components for the subordinate Li I 610.4 nm were also taken from Sansonetti et al. (1995) and Yan et al. (1998). While not important for the Li I lines, we note for completeness that we use the accurate pressure broadening data of Barklem et al. (2000b).

The transition probabilities for the lines of other species employed in the present study are taken from a variety of sources, all of which are expected to be accurate and thus not introduce any severe systematic errors. The $\log gf$ -values for the Fe II lines are from Biémont et al. (1994) while those of the Fe I lines are from O'Brian et al. (1991). Both of those should be accurate to within ± 0.03 dex. The corresponding data for the O I triplet at 777 nm comes from Wiese et al. (1996): $\log gf = 0.369$, 0.223 , and 0.002 . The transition probabilities for the Ca I lines are from Smith & Raggett (1981) and for the K I line ($\log gf = -0.17$) from Reader et al. (1980). Hyperfine

and isotope splitting have been taken into account for the K I line although the effects turned out to be negligible. We emphasize that the exact choice of transition probability for our calibration lines used in our determination of the Li isotopic abundances is of no consequence for the determination of the line broadening in the χ^2 -analysis. The excitation potential of the lower level for the lines is taken from the NIST database while the radiative broadening comes from the VALD database. For neutral lines we rely on the pressure broadening from Barklem et al. (2000b) while for Fe II the classical Unsöld theory with an enhancement factor of 2.0 has been adopted; the recent improvements in computing line broadening for Fe II lines by Barklem & Asplund-Johansson (2005) only became available after our analysis was completed. We emphasize that as our Fe II lines are all weak ($W_\lambda \lesssim 4$ pm), the exact treatment of the pressure broadening for these lines is of no importance for our purposes.

4. STELLAR PARAMETERS

4.1. Effective Temperature

In a previous paper by Nissen et al. (2002) on oxygen abundances derived from the [O I] line in a subset of the same UVES spectra as employed here, the effective temperature was derived from the $b - y$ and $V - K$ colour indices calibrated on the infrared flux method (Alonso et al. 1996). The 1σ relative error of T_{eff} was estimated to be about ± 70 K with the largest contribution coming from the uncertainty in the interstellar reddening $\Delta(E(b - y)) \simeq \pm 0.01$. Since it is of great importance for our discussion of the total Li abundance in the stars to obtain a higher precision of T_{eff} , we derive here the effective temperature from the profile of the H α line, which is very sensitive to temperature and practically independent of interstellar reddening.

The H α line is well centered in one of the echelle orders on the EEV CCD. The main problem in getting an accurate profile is to determine the echelle blaze function of the H α order. The method of fitting cubic spline functions to the continuum, which works well for narrow, well isolated lines like the Li I line, cannot be applied to a broad line like H α . Hence, we made a special reduction of the H α echelle order taking advantage of the fact that the blaze function varies smoothly and slowly with echelle order. This allows us to determine the blaze function of the H α order by interpolating in the blaze functions of the two adjacent orders. A similar technique has been successfully applied by Barklem et al. (2002) and Korn (2002) for various echelle spectrographs, including UVES.

The H α profile is affected by a few metallic lines and several telluric H $_2$ O lines, but due to the high resolution of the spectra these narrow absorption lines can easily be removed by interpolating the H α profile over the disturbing lines.

The observed H α profiles have been compared to theoretical profiles computed for MARCS model atmospheres using the Uppsala LTE spectrum synthesis code BSYN. Stark broadening is based on calculations of Stehlé & Hutcheon (1999) with the model microfield method, and self-broadening of hydrogen from Barklem et al. (2000a) is included. The profiles are computed for models having the same gravity and metallicity as the star but with a range of effective temperatures embracing the value es-

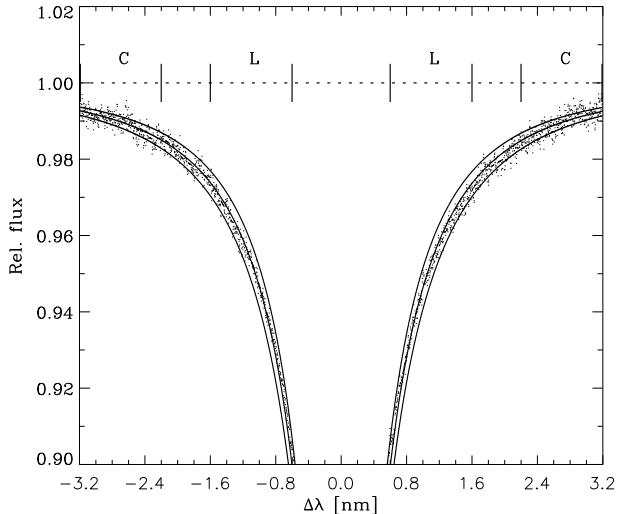


FIG. 4.— Observed $H\alpha$ profile for BD +03°0740 (dots) compared to theoretical profiles calculated for atmospheric models with the gravity and metallicity of the star ($\log g = 4.04$, $[\text{Fe}/\text{H}] = -2.65$) and three values of the effective temperature: $T_{\text{eff}} = 6170$ K, 6270 K (best fit), and 6370 K. The spectral bands used in the definition of the $H\alpha$ index is marked.

timated from the colour of the star. An improved T_{eff} is then determined from χ^2 -fitting to the observed profile (see Fig. 4). The region within ± 0.6 nm from the center is not included in the fit because the core of $H\alpha$ is affected by deviations from LTE (Przybilla & Butler 2004; Barklem, in preparation). Furthermore, we note that the continuum setting is considered as a free parameter in the fit, because the true continuum is ill-defined due to the limited width of the $H\alpha$ echelle order. As an alternative to the χ^2 -fitting we have also determined T_{eff} from an $H\alpha$ index defined as the ratio between the flux in the two regions marked by ‘C’ in Fig. 4 to the flux in the regions marked by ‘L’. Comparison with model atmosphere calculations of the index then yields T_{eff} . As with the χ^2 -fitting, the derived T_{eff} does not depend on the continuum normalization.

The two methods to determine T_{eff} give consistent results within ± 20 K. We also note that the T_{eff} derived for a given star from spectra observed on different nights is extremely stable with variations being less than ± 15 K. The calculated $H\alpha$ profile is relatively insensitive to errors in the gravity and the metallicity of the models. Altogether, we estimate that *relative* temperatures for our sample of metal-poor turnoff stars are determined with a 1σ precision of about ± 30 K. As discussed in Sect. 4.3, the good agreement between Fe abundances derived from Fe I and Fe II lines, respectively, suggests that this small error estimate is realistic.

The *absolute* temperature scale is, however, more uncertain than ± 30 K, as it depends on the theory of hydrogen line broadening among other things. Had instead the older Ali & Griem (1966) theory of resonance broadening been applied instead of the more complete self-broadening theory of Barklem et al. (2000a), the T_{eff} derived would be raised by about 100 K. In addition, there are uncertainties in the absolute T_{eff} values of at least 100 K arising from the current generation of 1D model

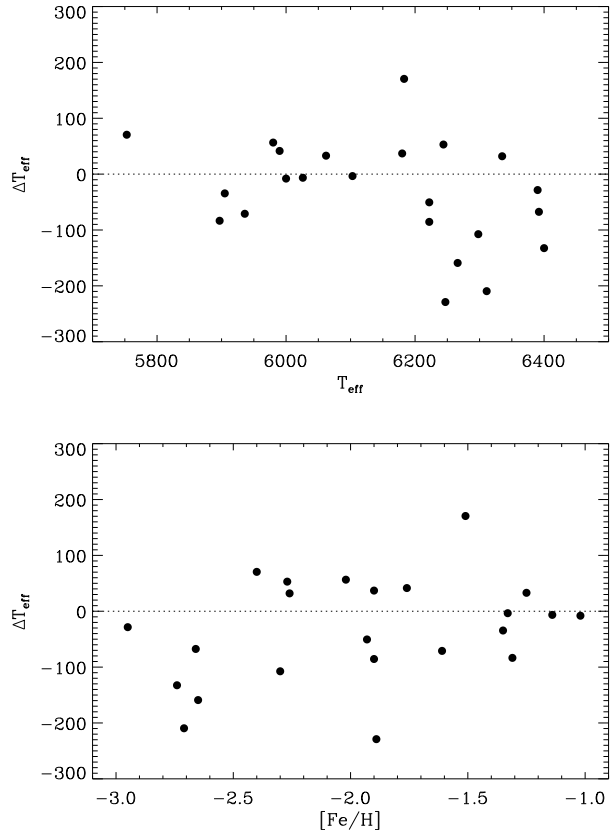


FIG. 5.— Difference in T_{eff} as estimated from $H\alpha$ and from $(b-y)$ and $(V-K)$ photometry calibrated on the infrared flux method as a function of T_{eff} (upper panel) and $[\text{Fe}/\text{H}]$ (lower panel).

atmospheres, which may not capture the effects of convection in a realistic manner. Detailed statistical equilibrium calculations for H I based on available $e^- + \text{H I}$ and $\text{H I} + \text{H I}$ collision cross-sections and 1D model atmospheres reveal no departures from LTE for the wings of $H\alpha$ while the line cores are much better described (Przybilla & Butler 2004; Barklem, in preparation). For completeness, we note that the adopted He abundance has no effect on the $H\alpha$ -based T_{eff} : a 0.2 dex lower He abundance, as perhaps induced by elemental diffusion in the star, would only increase T_{eff} by about 8 K.

The temperatures derived from $H\alpha$ are given in Table 2. When compared to the effective temperatures in Nissen et al. (2002, 2004) determined from $b-y$ and $V-K$ calibrated on the infrared flux method, good agreement for the majority of the stars is found: the mean difference is $\Delta T_{\text{eff}} = -34 \pm 95$ K. A few stars show large differences: the $H\alpha$ -based T_{eff} for G 126-062 is 170 K higher while for two stars (G 020-024 and BD -13°3442) the photometric temperatures are higher by about 200 K. The reason for the latter is probably an overestimate of the reddening for the two stars in Nissen et al. (2002, 2004). Overall the agreement is quite satisfactory, and there are no obvious trends in the temperature differences with T_{eff} or $[\text{Fe}/\text{H}]$, as seen in Fig. 5. We are thus unable to find any evidence from $H\alpha$ for the very hot T_{eff} -scale of Melendéz & Ramírez (2004) and Ramírez & Melendéz (2005a,b) based on their reapplication of the infrared flux method.

4.2. Surface Gravity and Absolute Magnitude

The surface gravity is determined from the fundamental relation

$$\log \frac{g}{g_{\odot}} = \log \frac{\mathcal{M}}{\mathcal{M}_{\odot}} + 4 \log \frac{T_{\text{eff}}}{T_{\text{eff},\odot}} + 0.4(M_{\text{bol}} - M_{\text{bol},\odot}) \quad (1)$$

where \mathcal{M} is the mass of the star and M_{bol} the absolute bolometric magnitude.

The absolute visual magnitude M_V is derived from the Hipparcos parallax (ESA 1997), if available, and also from Strömgren photometry using the method and calibrations in Nissen et al. (2002, 2004). The only exception from the procedure described by Nissen et al. is that we used the spectroscopic $H\alpha$ index (Sect. 4.1) instead of the photometric $H\beta$ index to derive the interstellar reddening excess. This provides a more precise estimate of $E(b-y)$, and consequently the limit for performing a correction of the Strömgren photometry for interstellar absorption and reddening was set at $E(b-y) > 0.010$ instead of $E(b-y) > 0.015$ in Nissen et al. (2002, 2004).

If the parallax is available with an accuracy $\Delta\pi/\pi < 0.3$, the mean value of $M_{V,\text{phot}}$ and $M_{V,\text{par}}$ is adopted for M_V , otherwise $M_{V,\text{phot}}$. The bolometric correction is taken from Alonso et al. (1995), and the mass of a star is derived by comparing its position in the $M_V - \log T_{\text{eff}}$ diagram with evolutionary tracks calculated by Vandenberg et al. (2000).

As the determination of $\log g$ depends on T_{eff} directly and $[\text{Fe}/\text{H}]$ indirectly the determination of the stellar parameters has to be iterated. The final values are given in Table 2 together with values for $[\text{Fe}/\text{H}]$ and $[\text{O}/\text{H}]$ (Sect. 4.3 and Sect. 4.4) and the microturbulence ξ_{turb} (Sect. 4.5). The internal error of the derived value of $\log g$ is dominated by the error of M_V , which we have estimated to be $\Delta M_V = \pm 0.20$. This corresponds to $\Delta \log g = \pm 0.08$ dex. While the Vandenberg et al. (2000) models do not include the effects of diffusion, this translates to the surface gravity possibly being overestimated by at most 0.04 dex (e.g. Proffitt & Michaud 1991). We note that this effect is much too small to impact any of our conclusions in what follows.

The upper panel in Fig. 6 shows the $M_V - \log T_{\text{eff}}$ diagram for stars with $[\text{Fe}/\text{H}] < -1.7$ compared to two sets of evolutionary tracks from Vandenberg et al. (2000) corresponding to $[\text{Fe}/\text{H}] = -2.31$ (the mean metallicity of the stars) and -2.01 , respectively, and an α -element enhancement of $[\alpha/\text{Fe}] = +0.3$. Except HD 19445 (a main sequence star) and HD 140283 (a subgiant), the stars are close to the turnoff. Some of the scatter in T_{eff} around the turnoff can be attributed to differences in $[\text{Fe}/\text{H}]$ with the most metal-poor stars being warmest. The lower panel of Fig. 6 shows the location of the eight stars with $[\text{Fe}/\text{H}] > -1.7$ in the HR-diagram. They have a mean metallicity of $[\text{Fe}/\text{H}] = -1.33$. Again all stars except perhaps HD 106038 are classified as turnoff stars. As discussed in Sect. 7.1, HD 106038 has a peculiar high Li abundance.

4.3. Metallicity

Iron abundances have been determined as described in detail by Nissen et al. (2002) from 13 Fe II lines, six of which are in our spectra. The remaining seven lines lie

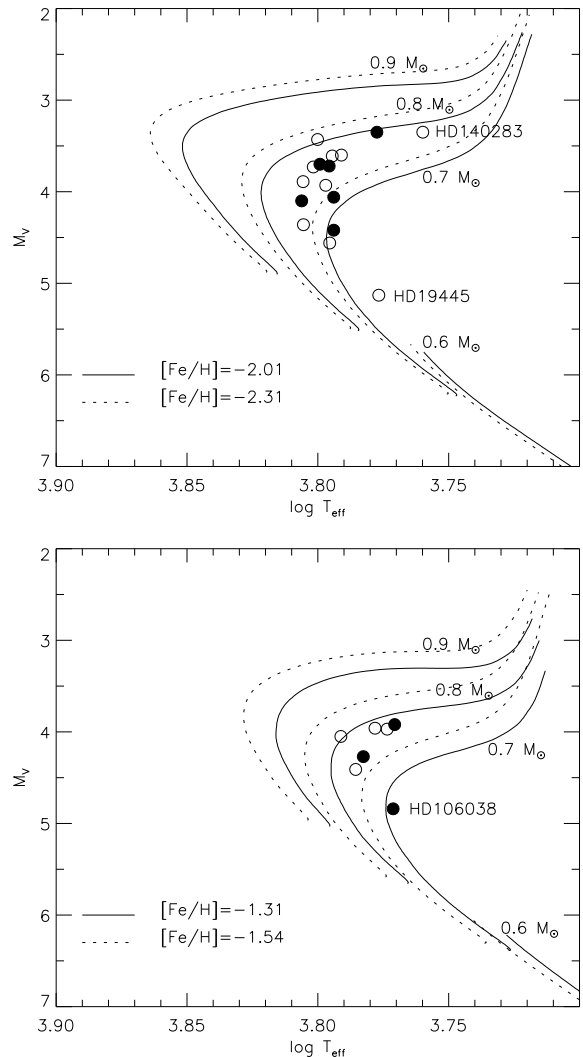


FIG. 6.— HR-diagram for stars with $[\text{Fe}/\text{H}] < -1.7$ (Upper panel) and for stars with $[\text{Fe}/\text{H}] > -1.7$ (Lower panel). Filled circles refer to stars with a $\geq 2\sigma$ detection of ${}^6\text{Li}$, and open circles to stars with no clear detection of ${}^6\text{Li}$. The displayed evolutionary tracks are from Vandenberg et al. (2000).

in the spectral region 490 - 550 nm and were measured from UVES spectra with $R \simeq 55\,000$ and $S/N \simeq 300$ obtained with the primary aim of determining beryllium abundances (Primas et al., in preparation). For the very metal-poor stars BD +09°2190, BD +03°0740 and BD -13°3442 only two of the Fe II lines (519.76 and 523.46 nm) could be measured reliably. For these stars, we added the somewhat stronger Fe II 492.32 nm line to improve the precision of $[\text{Fe}/\text{H}]$. For the most metal-poor star in our sample, CD -33°1173, we do not have a spectrum in the 490 - 550 nm region. Hence, $[\text{Fe}/\text{H}]$ could not be determined from Fe II lines, but was estimated from Fe I lines taking into account the offset of 0.08 dex between $[\text{Fe}/\text{H}]$ from Fe II and Fe I lines discussed below. The Fe II lines were also measured in the solar flux spectrum (Kurucz et al. 1984), allowing differential iron abundances $[\text{Fe}/\text{H}]$ to be determined without knowledge of the exact oscillator strengths of the lines. We note that for an adopted solar iron abundance of $\log \epsilon_{\text{Fe}} = 7.50$,

the gf -values derived from the solar spectrum agree well with those of Biémont et al. (1991) using the MARCS solar model atmosphere.

The Fe abundances for the Sun and our sample of stars were determined from the observed Fe II line strengths using the Uppsala EQWIDTH program together with 1D MARCS model atmospheres having the appropriate stellar parameters. As T_{eff} , $\log g$ and $[\text{Fe}/\text{H}]$ are interlinked, the determination of $[\text{Fe}/\text{H}]$ is an iterative procedure, with the final values listed in Table 2. The microturbulence ξ_{turb} used in these calculations was adjusted such that the derived Fe abundances show no trend with line strength. For $[\text{Fe}/\text{H}] \lesssim -2.0$, the employed Fe II lines are weak and, hence, the derived Fe abundances are practically independent of ξ_{turb} . For those stars, a microturbulence of 1.5 km s^{-1} has been adopted.

The error in $[\text{Fe}/\text{H}]$ induced by the uncertainties in T_{eff} is small: $\Delta[\text{Fe}/\text{H}] \lesssim \pm 0.02$ dex. Since Fe II is the dominant ionization stage in the line formation region of these stars, the derived Fe II based abundance is dependent on $\log g$: an error in $\log g$ of ± 0.1 translates to an error in $[\text{Fe}/\text{H}]$ of ± 0.035 . Adding in quadrature the error indicated by the line-to-line scatter with those arising from the uncertainties in T_{eff} and $\log g$ implies a statistical error of ± 0.05 dex in $[\text{Fe}/\text{H}]$. The systematic error in $[\text{Fe}/\text{H}]$ may be somewhat larger.

In addition, we have measured Fe abundances based on up to 11 weak Fe I lines using gf -values from O’Brian et al. (1991). As shown in Fig. 7, the Fe I lines systematically give $[\text{Fe}/\text{H}]$ values slightly lower than those from Fe II lines. The average difference, $[\text{Fe II}/\text{H}] - [\text{Fe I}/\text{H}]$, is 0.08 dex with an rms scatter of only 0.041 dex. The expected scatter arising from the adopted errors, $\Delta T_{\text{eff}} = \pm 30 \text{ K}$ and $\Delta \log g = \pm 0.08$ dex, is 0.046 dex, i.e., not significantly different from the observed scatter. This suggests that the estimated precision of T_{eff} and $\log g$ is realistic.

The difference in the derived Fe abundances from Fe I and Fe II lines could reflect departures from LTE, most likely for Fe I (see discussion in Asplund 2005) or erroneous stellar parameters (e.g., T_{eff} too low by about 100 K). The small abundance differences and the lack of a trend in $[\text{Fe II}/\text{H}] - [\text{Fe I}/\text{H}]$ with either T_{eff} or $[\text{Fe}/\text{H}]$ is a strong argument against pronounced departures from LTE for 1D atmospheres, as claimed for example by Thévenin & Idiart (1999).

Our $[\text{Fe}/\text{H}]$ values are systematically higher by about 0.2 dex than those of Ryan et al. (1999) for the 11 stars in common. Ryan et al. adopted literature values of $[\text{Fe}/\text{H}]$ mainly based on Fe I lines, with a supporting role played by a calibration of medium resolution spectra. It is likely that this 0.2 dex difference is largely attributable to the discrepancy between Fe I and Fe II lines mentioned above, the lower T_{eff} -scale of Ryan et al. and/or differences in the adopted gf -values. Given the remaining uncertainties surrounding Fe I lines in terms of possible departures from LTE, we believe it is wise to rely on Fe II lines for the estimate of $[\text{Fe}/\text{H}]$.

4.4. Oxygen abundance

Oxygen may be a preferred alternative to iron in tracking the evolution of the lithium isotopes in the early Galaxy. Oxygen is synthesised primarily in the most massive stars and distributed when those stars explode

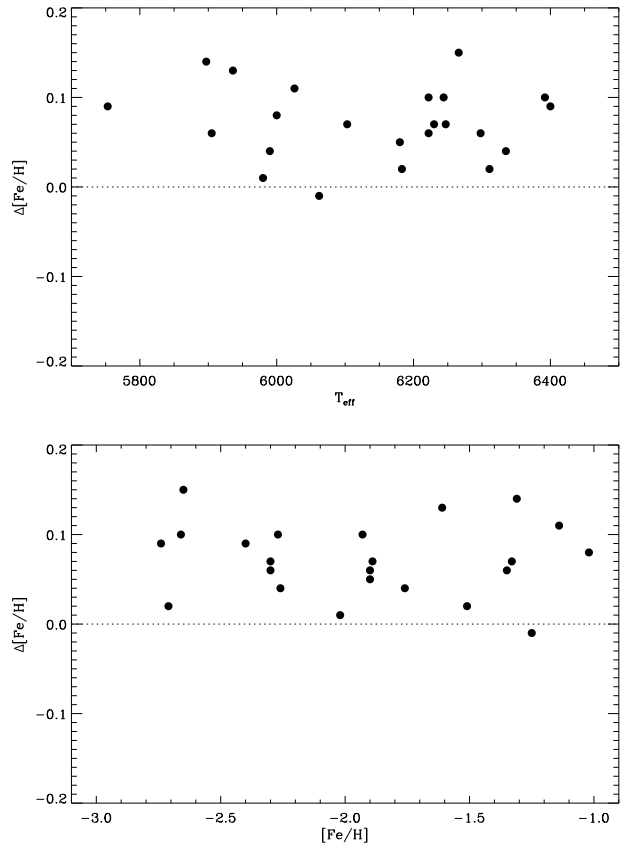


FIG. 7.— Differences in $[\text{Fe}/\text{H}]$ estimated from Fe II and Fe I lines as a function of T_{eff} (upper panel) and $[\text{Fe}/\text{H}]$ (lower panel). While there is an offset of about 0.1 dex, there are no obvious trends with stellar parameters. This difference may signal differential non-LTE effects for Fe I relative to the Sun or slightly too low adopted T_{eff} by about 100 K.

as Type II supernovae; ${}^7\text{Li}$ may also be made in these supernovae by the ν -process (Woosley et al. 1990). Also, when spallation is an effective mode of lithium synthesis, spallation of oxygen nuclei is the dominant mechanism. Iron is also a product of Type II supernovae but in contrast to oxygen its yield is dependent on the mass cut between the stellar remnant (neutron star or black hole) and the ejecta and iron is also a product of Type Ia supernovae. The latter factor is not a major concern here as our stars have a metallicity below that at which Type Ia supernovae are generally considered to begin their contributions.

The O abundances for our program stars have been derived from the O I triplet at 777 nm. Unfortunately, the alternative abundance indicator, the [O I] line at 630 nm, is undetectable for $[\text{Fe}/\text{H}] \lesssim -2.5$, even with the very high S/N of our spectra. We have, therefore, opted for using the same diagnostic for the entire sample. The O I triplet typically yields somewhat higher O abundances than the forbidden [O I] line at low metallicity (see discussion in Asplund 2005 and references therein).

The O I 777.1, 777.4 and 777.5 nm lines are located towards the edges of two consecutive echelle orders from which the equivalent widths were measured and averaged (weighted by their respective S/N). The results for the July 2000 spectra have already been presented in Nis-

sen et al. (2002) to which we now add nine stars from February 2002. From the equivalent widths the 1D LTE O abundances were derived using the stellar parameters listed in Table 2; it should be noted that the O abundances for the July 2000 targets differ slightly from those given in Nissen et al. (2002) due to our use of $H\alpha$ -based T_{eff} rather than the photometric values employed in our previous study. We have also computed 1D non-LTE abundance corrections for the O I triplet lines in an identical fashion to the calculations presented in Nissen et al. (2002). These non-LTE corrections are always negative and typically $-0.1\dots -0.2$ dex but reach -0.3 dex at the lowest $[\text{Fe}/\text{H}]$. Our final adopted O abundances given in Table 2 include these non-LTE corrections. These abundances are referenced relative to the same solar O abundance from a 1D solar model atmosphere as adopted in Nissen et al. (2002), i.e. $\log \epsilon_{\text{O}} = 8.74$, which is 0.08 dex higher than the current best estimate based on 3D hydrodynamical model atmospheres (Asplund et al. 2004, 2005).

Nissen et al. (2005a) have discussed in some detail the trend and scatter of $[\text{O}/\text{Fe}]$ as a function of $[\text{Fe}/\text{H}]$ for our sample. Here we just note that $[\text{O}/\text{Fe}]$ increases from about 0.4 dex at $[\text{Fe}/\text{H}] = -1.0$ to 0.6 dex at $[\text{Fe}/\text{H}] = -3.0$. The scatter in $[\text{O}/\text{Fe}]$ around a linear fit to the data ($[\text{O}/\text{Fe}] = -0.11 [\text{Fe}/\text{H}] + 0.31$) is 0.08 dex with a large contribution coming from a relatively low $[\text{O}/\text{Fe}]$ in HD 160617, a star that is known to belong to the rare class of nitrogen-rich subdwarfs (Bessell & Norris 1982).

4.5. Spectral Line Broadening

In order to extract the lithium isotopic ratio from the profile of Li I 670.8 nm line, it is paramount to have an accurate understanding of the intrinsic spectral line broadening. This broadening comes in various forms all of which must be taken into account: thermal, pressure, radiative, rotational and Doppler broadening. Thermal broadening can be directly computed from the known temperature structure of the stellar atmosphere while the pressure and radiative broadening are, in principle at least, known atomic properties specific for each transitions.

It is well-known that the observed spectral lines are always broader than predicted solely from the thermal and atomic broadening. All stars are expected to rotate, which broadens the line profiles but does not modify the line strength. As our observations are unable to disentangle readily rotational broadening from other atmospheric broadening agents, we adopt in all cases $v_{\text{rot}} \sin i = 0.5 \text{ km s}^{-1}$ given the great age of these metal-poor halo stars (for comparison, the Sun has $v_{\text{rot}} = 1.8 \text{ km s}^{-1}$ at the equator). We have confirmed that our derived results are immune to this particular choice of $v_{\text{rot}} \sin i$. In addition, atmospheric velocity fields from convection, wave motion, turbulence and the like introduce Doppler shifts which affect the line profiles. In analyses based on 1D hydrostatic model atmospheres, one normally introduces two free parameters: microturbulence ξ_{turb} and macroturbulence ζ_{macro} , acting on small and large spatial scales, respectively. Following standard practice we determine ξ_{turb} by ensuring that the derived abundances from Fe I and Fe II lines are independent of line strength while ζ_{macro} is estimated from the observed line shapes. The form of ζ_{macro} is assumed to be Gaus-

sian. This choice was made mainly for convenience as the effects of ζ_{macro} can then be easily combined with the line broadening due to the finite instrumental resolution which is also described by a Gaussian distribution. We have performed various tests ensuring that our results in terms of Li isotopic abundances are not affected by the use of a Gaussian ζ_{macro} instead of, for example, a radial-tangential version (e.g. Gray 1992).

The lines used for determining ζ_{macro} were K I 769.9 nm, Ca I 612.2 nm, Ca I 616.2 nm, Ca I 643.9 nm, Fe I 623.0 nm, Fe II 624.7 nm and Fe II 645.6 nm. In some cases we also added the Fe I 610.2 nm and Fe I 613.6 nm lines when there was a lack of calibration lines of suitable strength compared with the Li I line. For the August 2004 observations of LP 815-43 and HD 140283, additional lines could be used since the spectra extended further to the blue, enabling the Fe II 501.8 nm, Fe I 523.3 nm, Fe I 532.4 nm, Fe I 539.7 nm, Fe I 538.3 nm, Fe I 543.4 nm, Fe I 542.4 nm, Mg I 552.8 nm, Fe I 561.2 nm, Ca I 558.9 nm and Fe I 558.7 nm lines to be covered in exchange for the K I 769.9 nm line. The K I line was broader than other lines, such as Fe I 623.0 nm, of comparable strength in most stars. This may signal significant departures from LTE which have indeed been predicted for this resonance line for metal-poor stars (Ivanova & Shimanskii 2000; Takeda et al. 2002). Good agreement was found, however, when the K I line had an equivalent width of about 2 pm, i.e., similar to that of the Li I line itself. This is consistent with the finding of Smith et al. (2001) in the case of HD 84937. We, therefore, decided not to include this line in the final estimates of ζ_{macro} and used it only as a consistency check on the mean value and scatter implied by the other lines.

When computing the average broadening parameters from the calibration lines, we have considered only lines with strengths $0.9 \leq W_{\lambda} \leq 7.5$ pm. The calibration lines included in the computation of the mean broadening are of similar line strength to the Li I 670.8 nm line, which should minimize possible systematic differences. This point is important since we have noticed that the derived ζ_{macro} is dependent on the strength of the line, as illustrated in Fig. 8 for the case of HD 106038 (a Li-rich star with a significantly stronger Li I 670.8 nm line than in the typical star of our sample: $W_{\lambda} = 6.32$ pm rather than ≈ 2 pm). In this particular instance, ζ_{macro} was computed as a mean of the four lines with $W_{\lambda} = 6 \pm 1$ pm, which is expected to give a good estimate of the intrinsic broadening for the Li I line.

5. LI ISOTOPIC ABUNDANCES FROM THE Li I 670.8 NM RESONANCE LINE

5.1. Li Isotopic Abundances

The presence of ${}^6\text{Li}$ alongwith ${}^7\text{Li}$ in the stellar atmosphere introduces additional width and asymmetry of the line profile². As outlined in Sect. 4.5, we first determine ζ_{macro} from a number of K I, Ca I, Fe I and

² We will not consider here the center-of-gravity method which is based on the wavelength shift introduced by the addition of ${}^6\text{Li}$. The nearby Ca I 671.7 nm line has served as a reference line. As discussed by Smith et al. (1998) and Cayrel et al. (1999), the presence of differential line shifts arising from convection (see, for example, Reddy et al. 2002), and the remaining uncertainties in the laboratory wavelength of the Ca I line render this method very prone to systematic errors.

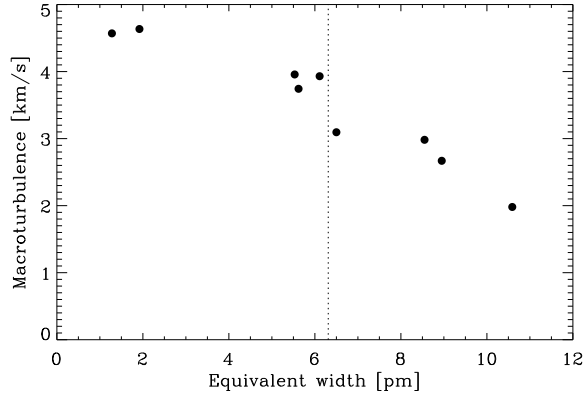


FIG. 8.— Estimated macroturbulence ζ_{macro} (assumed to be described by a Gaussian) from different lines of varying strengths in HD 106038; in addition the lines were broadened by rotation (assumed to be $v_{\text{rot}} \sin i = 0.5 \text{ km s}^{-1}$) and instrumental broadening (measured from Th lines). Note the strong correlation between ζ_{macro} and equivalent width, which emphasizes the importance of having calibration lines of similar strengths as the Li I 670.8 nm line when estimating the intrinsic line broadening. The equivalent width for the Li line in HD 106038 is denoted by the vertical dotted line.

Fe II lines. This is achieved by a χ^2 -analysis of the predicted and observed line profiles allowing the element abundance, wavelength zero-point and continuum normalization to vary besides ζ_{macro} . In most cases, ζ_{macro} could be well determined with a standard deviation of $\Delta\zeta_{\text{macro}} = \pm 0.1 - 0.2 \text{ km s}^{-1}$. Larger uncertainties of $\pm 0.3 - 0.6 \text{ km s}^{-1}$ resulted for four stars: G 126-062, CD -33°1173, HD 59392 and BD +09°2190. The estimated broadening parameters are listed in Table 3, while Figs. 9–12 show the resulting profiles for one of these calibration lines (Ca I 612.2 nm) for a few stars.

Equipped with the estimate of the macroturbulence ζ_{macro} for each star, the adopted $v_{\text{rot}} \sin i$ (0.5 km s^{-1}) and the measured instrumental broadening at 670.8 nm from Th lines, synthetic profiles of the Li I 670.8 nm line for different Li isotopic ratios were generated for the program stars using the stellar parameters listed in Table 2. Calculations were done for ${}^6\text{Li}/{}^7\text{Li}$ between -0.10 and 0.10 by step of 0.01 . Negative ${}^6\text{Li}/{}^7\text{Li}$ ratios, of course, do not exist in reality but were included in order to obtain estimates as accurate as possible for stars with very small or vanishing ${}^6\text{Li}$ content. These were produced by allowing the ${}^6\text{Li}$ components of the Li I 670.8 nm line to be in emission rather than in absorption as is the case for positive ${}^6\text{Li}/{}^7\text{Li}$ ratios. At the low metallicity of the program stars, one does not need to worry about potential blends from various atomic and molecular lines that can perturb the Li feature at solar metallicity (Nissen et al. 1999; Israelian et al. 2001, 2003; Reddy et al. 2002) and we thus computed the theoretical profile taking into account only the various components of the Li line. Test calculations revealed that this was fully justifiable for the target stars.

The comparison between the theoretical and observed profiles was quantified using a χ^2 -analysis similar to that used in most recent investigations of ${}^6\text{Li}/{}^7\text{Li}$ in late-type stars (e.g. Smith et al. 1998; Nissen et al. 1999, 2000; Israelian et al. 2001, 2003; Reddy et al. 2002;

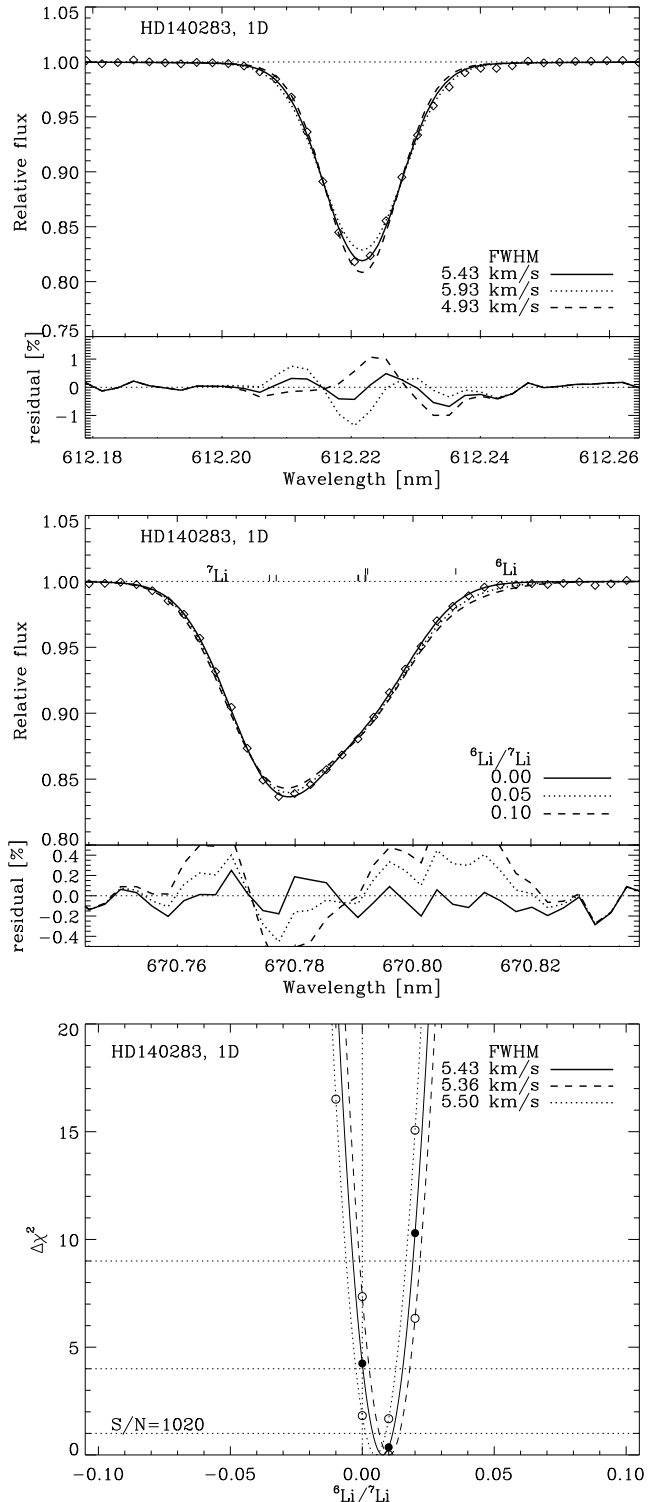


FIG. 9.— *Upper panel:* Observed Ca I 612.2 nm profile (rhombs) in HD 140283 together with the best fit theoretical 1D LTE profile (solid line). Also shown are the predictions with the macroturbulence $\zeta_{\text{macro}} \pm 0.5 \text{ km s}^{-1}$. The Gaussian FWHM is here the combination of ζ_{macro} and the instrumental broadening; the profiles have also been convolved with a stellar rotation velocity of $v_{\text{rot}} = 0.5 \text{ km s}^{-1}$. *Middle panel:* Computed Li I 670.8 nm profile for three different values for ${}^6\text{Li}/{}^7\text{Li}$ (0.00, 0.05 and 0.10) shown together with the observed line (rhombs). In each case, the Li abundance, wavelength shift and continuum level have been allowed to vary. The location of the various ${}^7\text{Li}$ and ${}^6\text{Li}$ components are indicated. *Lower panel:* Resulting $\Delta\chi^2$ for the combined Gaussian of the mean ζ_{macro} and instrumental broadening; also shown are the cases for $\zeta_{\text{macro}} \pm \Delta\zeta_{\text{macro}}$. In this star, no significant detection of ${}^6\text{Li}$ can be claimed.

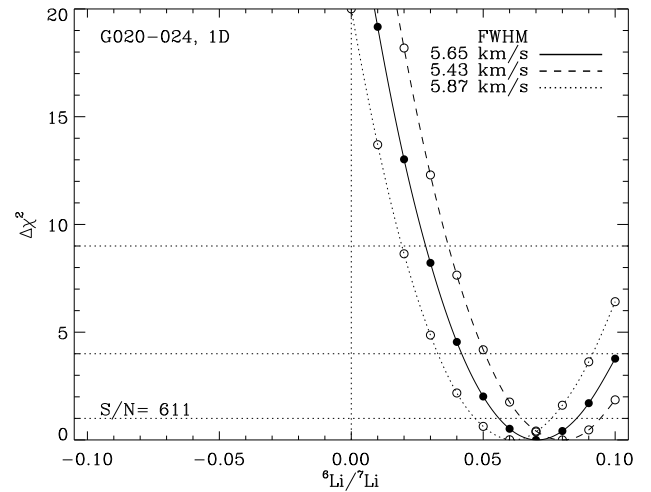
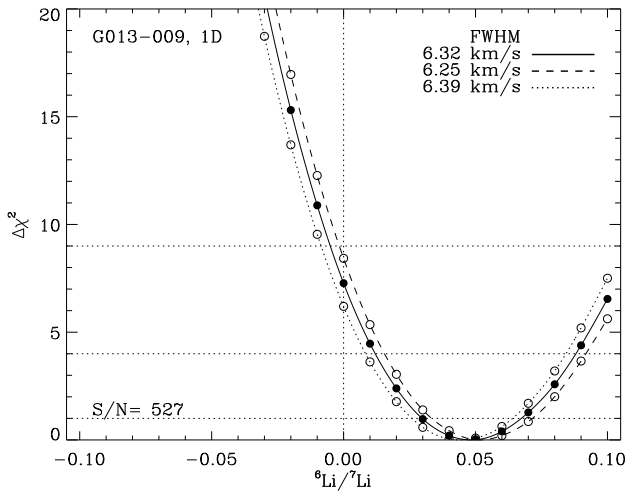
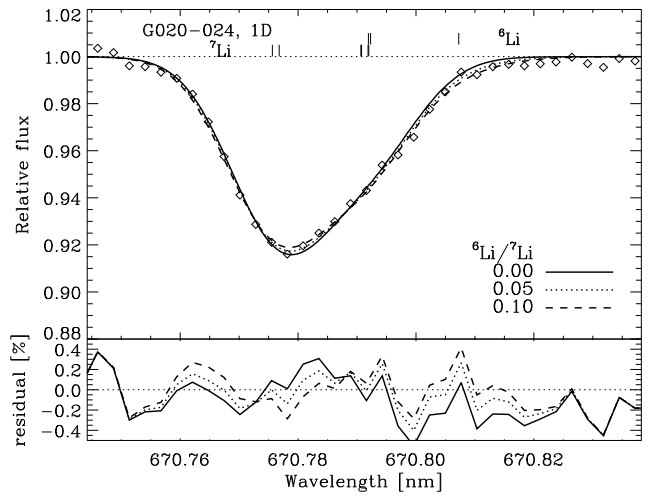
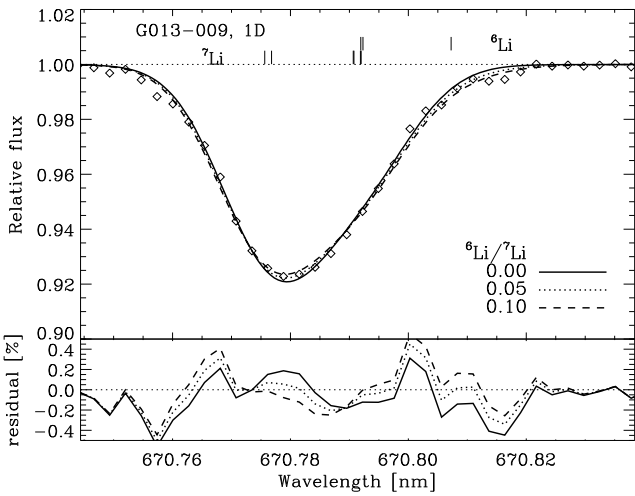
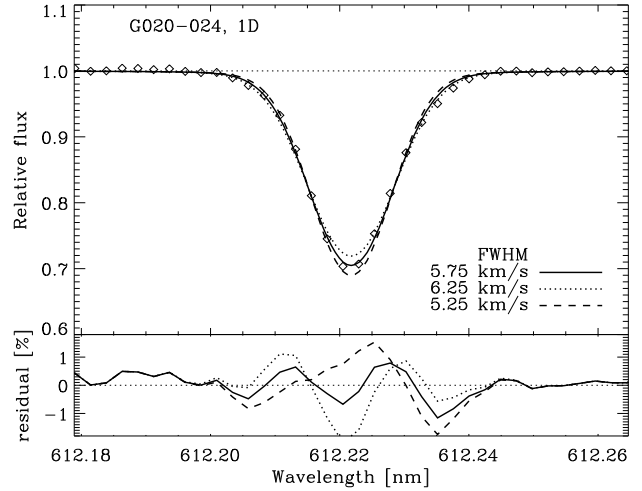
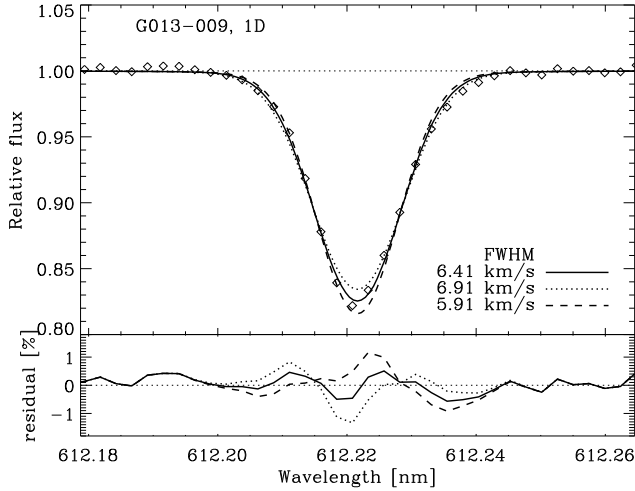


FIG. 10.— Same as Fig. 9 but for G013-009. In this star, the χ^2 -analysis indicate a $> 2\sigma$ detection of ${}^6\text{Li}$ at the level of ${}^6\text{Li}/{}^7\text{Li} = 0.05$.

FIG. 11.— Same as Fig. 9 but for G020-024. In this star, the χ^2 -analysis indicate a 4σ detection of ${}^6\text{Li}$ at the level of ${}^6\text{Li}/{}^7\text{Li} = 0.07$.

Aoki et al. 2004). The χ^2 was computed according to $\chi^2 = \sum (O_i - S_i)^2 / \sigma^2$, where O_i and S_i denote the observed and synthetic flux at wavelength point i , respectively, and $\sigma = (S/N)^{-1}$ as estimated in three nearby continuum windows. Typically 26 wavelength points

were considered across the Li line to estimate χ^2 . For each ${}^6\text{Li}/{}^7\text{Li}$, the total Li abundance, the wavelength zero-point of the observed spectrum and the continuum level were allowed to vary in order to optimize the fit and thus minimize χ^2 . The most probable value for ${}^6\text{Li}/{}^7\text{Li}$ was obtained by cubic spline interpolation of the resulting

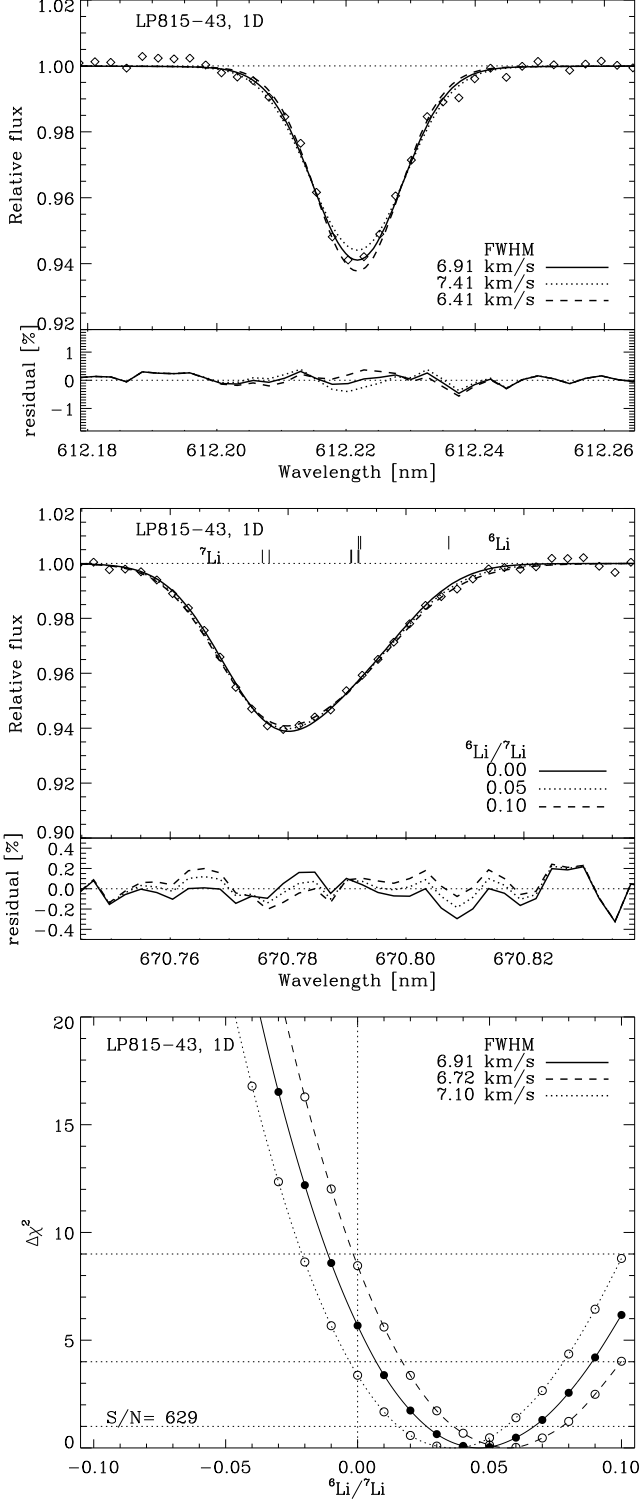


FIG. 12.— Same as Fig. 9 but for LP 815-43. In this star, the χ^2 -analysis indicate a 2σ detection of ${}^6\text{Li}$ at the level of ${}^6\text{Li}/{}^7\text{Li} = 0.05$. The observed spectrum shown here is the one from August 2004.

χ^2 values, from which the minimum χ^2_{\min} could be determined. The 1σ , 2σ and 3σ confidence limits of the determinations correspond to $\Delta\chi^2 = \chi^2 - \chi^2_{\min} = 1, 4$ and 9 , respectively. These uncertainties are determined by the noise of the spectra, which as mentioned above are

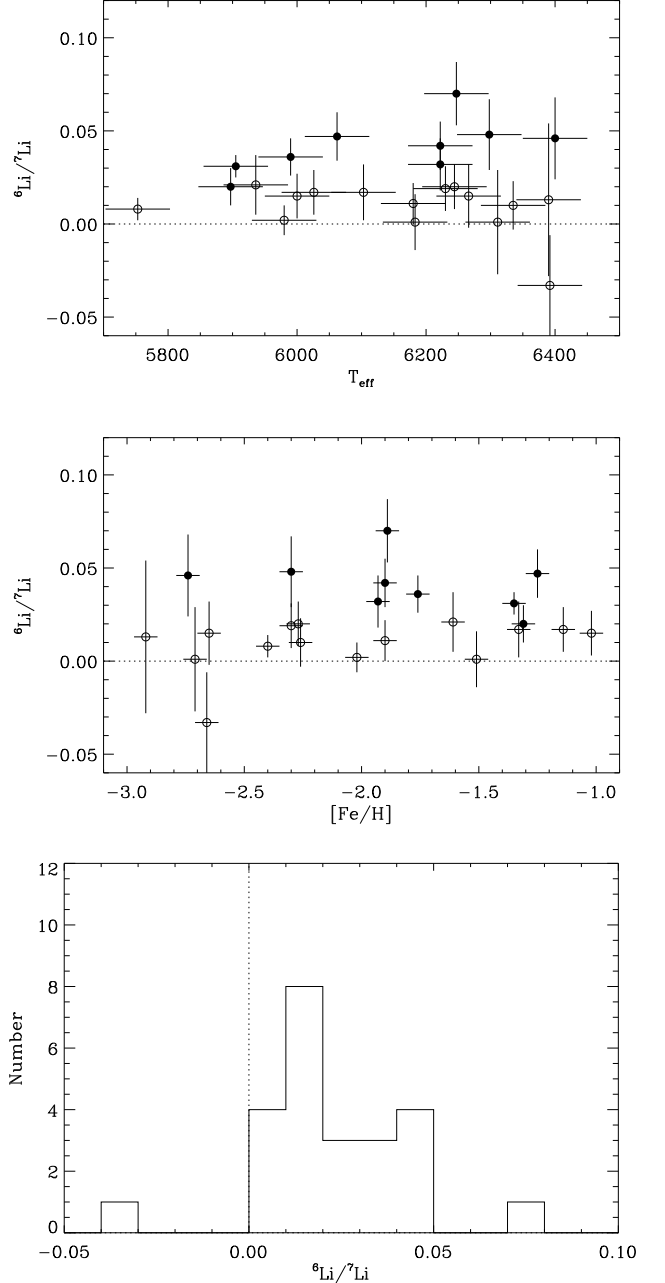


FIG. 13.— Derived ${}^6\text{Li}/{}^7\text{Li}$ as a function of T_{eff} (*Upper panel*) and $[\text{Fe}/\text{H}]$ (*Middle panel*). The stars considered to have a significant detection ($\geq 2\sigma$) of ${}^6\text{Li}$ are shown as solid circles while non-detections are plotted as open circles. Note that the non-detections do not cluster around ${}^6\text{Li}/{}^7\text{Li} = 0.00$ but rather at ≈ 0.01 . This is also illustrated as a histogram (*Lower panel*). The observed distribution is clearly not representative of a Gaussian centered at ${}^6\text{Li}/{}^7\text{Li} = 0.00$.

better than $S/N > 500$ for all but two stars that have 400 and 470, respectively. The reduced χ^2_r is in all cases close to one with the variations between stars as expected from statistical fluctuations. In addition, the χ^2 -analysis was repeated for each star with different adopted macro-turbulence parameters, $\zeta_{\text{macro}} \pm \Delta\zeta_{\text{macro}}$, where $\Delta\zeta_{\text{macro}}$ was given by the standard deviation from the various Ca and Fe lines. Examples of the observed and predicted Li I line profiles and the corresponding χ^2 values can be

found in Figs. 9–12 for a few stars. The resulting ${}^6\text{Li}/{}^7\text{Li}$ ratios and ${}^7\text{Li}$ abundances are listed in Table 3.

The errors in the derived ${}^6\text{Li}/{}^7\text{Li}$ ratios are quantified by taking the uncertainties from the finite S/N as well as the adopted ζ_{macro} and stellar parameters in quadrature. In essentially all cases, the first source dominates the error budget in spite of the extremely high S/N achieved in these observations, but for a couple of stars with poorly determined ζ_{macro} such as CD $-33^\circ 1173$ the second uncertainty drives the final error. The errors arising from the uncertainties in the stellar parameters are in all cases very minor, as discussed in detail in Sect. 5.5. We note that our error estimates are slightly more conservative than previous studies of the Li isotopic ratios in metal-poor stars, which, for example, often have relied on only one or two calibration lines to determine the line broadening.

As seen in Table 3, nine of the 24 stars fulfill our criteria of a $\geq 2\sigma$ result to be considered a significant ${}^6\text{Li}$ detection: HD 102200, HD 106038, HD 160617, G 013-009, G 020-024, CD $-30^\circ 18140$, CD $-33^\circ 3337$, CD $-48^\circ 2445$ and LP 815-43. This should be contrasted with the previous single confirmed detection of ${}^6\text{Li}$ in HD 84937 (Smith et al. 1993, 1998; Hobbs & Thorburn 1997; Cayrel et al. 1999). The stars with detected ${}^6\text{Li}$ are all very near the turn-off for their respective metallicities (Fig. 6), in accordance with the suggestion of Smith et al. (1993, 1998). In addition, we find a large number of borderline cases at the $1 - 2\sigma$ level that we do not consider significant enough to claim a positive detection. In fact, there is a tendency for the non-detections to cluster at ${}^6\text{Li}/{}^7\text{Li} \approx 0.01$, as illustrated in Fig. 13. This could be taken as a warning sign that our analysis contains an unidentified systematic error that bias the derived isotopic ratio towards too high values. We have therefore carried out tests in an attempt to identify such a problem, which are described in detail in the following subsections. In summary, no serious problem that could affect our analysis has been uncovered: no differences are found when taking into account possible ISM absorption in the Li line (Sect. 5.2), adopting an alternative χ^2 -analysis (Sect. 5.4), changing the stellar parameters within reasonable bounds (Sect. 5.5), employing a different suite of 1D model atmospheres (Sect. 5.6) or using 3D hydrodynamical model atmospheres (Sect. 5.7). Furthermore, we independently obtain the same results as some previous investigations when relying on their observations (Sect. 5.8). Finally, our confidence in the derived results is boosted by the analysis of HD 19445, which was included in our program to provide a consistency check (see, also, Smith et al. 1993). Since this star is a relatively cool ($T_{\text{eff}} = 5980$) metal-poor dwarf ($\log g = 4.42$), standard models of stellar evolution predict that ${}^6\text{Li}$ should be thoroughly destroyed on the star attaining the main sequence (see discussion in Sect. 7.3). Indeed, an analysis identical to that for all of our other stars indicate no presence of ${}^6\text{Li}$: ${}^6\text{Li}/{}^7\text{Li} = 0.002 \pm 0.008$.

We conclude that the Li isotopic ratios presented in Table 3 are reliable. We claim significant ${}^6\text{Li}$ detections only in the above-mentioned nine stars, but we can not rule out the possibility that the majority of turn-off halo stars in fact have ${}^6\text{Li}/{}^7\text{Li} \approx 0.01$ (Fig. 13). To confirm an isotopic ratio as low as 0.01 for an individual star is extremely challenging (c.f. our analysis of HD 140283 with

$S/N \approx 1000$), but confirmation should be attemptable in at least a statistical sense for a sample like ours but with even higher S/N spectra and additional calibration lines to nail down the line broadening accurately.

The Li abundances derived from the profile fitting of the Li I 670.8 nm line have been obtained under the assumption of LTE. We have applied the non-LTE abundance corrections computed by Carlsson et al. (1994) interpolated to the stellar parameters of our sample to the LTE Li abundances. These non-LTE calculations are particularly appropriate as they have been performed using similar MARCS model atmospheres as employed here. The resulting non-LTE ${}^7\text{Li}$ abundances are given in Table 3. The non-LTE abundance corrections are in all cases very small ($\Delta \log \epsilon_{\text{Li}} \lesssim 0.02$ dex) and generally negative. The scatter in Li abundances is not significantly modified by the application of these non-LTE corrections.

5.2. Is the High ${}^6\text{Li}/{}^7\text{Li}$ in LP 815-43 Real?

Due its low $[\text{Fe}/\text{H}]$, LP 815-43 will feature prominently in the discussions in Sect. 7. It is natural to inquire whether its high ${}^6\text{Li}$ abundance determined from our χ^2 -analysis is real. We note that both the spectrum of LP 815-43 obtained in July 2000 and that acquired in August 2004 imply a detection of ${}^6\text{Li}$ at the 2σ level or more. The former indicated ${}^6\text{Li}/{}^7\text{Li} = 0.078 \pm 0.033$ based on an observed spectrum with $S/N = 540$ but with only three Ca I lines to estimate the intrinsic line broadening. This result prompted us to request additional observing time for this star to improve the S/N and include more calibration lines. The combined spectrum from two nights in August 2004 has $S/N = 630$ as well as covering as many as 10 calibration lines of the right strength which importantly beat down the uncertainty in the macroturbulence to 0.19 km s^{-1} . The resulting isotopic ratio is slightly less but still implies a significant detection by our criteria: ${}^6\text{Li}/{}^7\text{Li} = 0.046 \pm 0.022$. The result from the July 2000 spectrum is fully consistent with this improved value taking the uncertainties into account. The individual spectra obtained on August 30 and 31, 2004, have $S/N = 420$ and 490, respectively. Both of these imply ${}^6\text{Li}/{}^7\text{Li} \approx 0.03 - 0.04$ but each allows only a 1σ -detection due to the reduced S/N . Finally, we note that had we adopted the better determined macroturbulence value from the August 2004 spectrum for the analysis of the July 2000 spectrum, the derived ${}^6\text{Li}/{}^7\text{Li}$ would have increased to 0.089 ± 0.027 , i.e. a 3σ -detection.

As described in Sect. 2.3, there may be residual fringing in the reduced spectrum at the level of $< 0.1\%$ of the continuum level with a typical wavelength scale of 0.1-0.2 nm. If it is as high as 0.1% and one of those depressions falls on top of the Li line, it could mean that the ${}^6\text{Li}/{}^7\text{Li}$ has been overestimated. An ad-hoc adjustment of the local continuum level by this amount would change ${}^6\text{Li}/{}^7\text{Li}$ for LP815-43 to only a 1σ detection and thus not significant by our standards (of course if instead of a depression there is a peak in the residual fringing it would increase ${}^6\text{Li}/{}^7\text{Li}$ by the corresponding amount). This illustrates clearly the challenges posed by this method to determine the Li isotopic ratio in metal-poor turn-off stars. An enlargement of the observed August 2004 spectrum is shown in Fig. 14. While there may be hints of a residual fringing at some wavelengths, there are no traces thereof in other parts of the spectrum near the Li line.

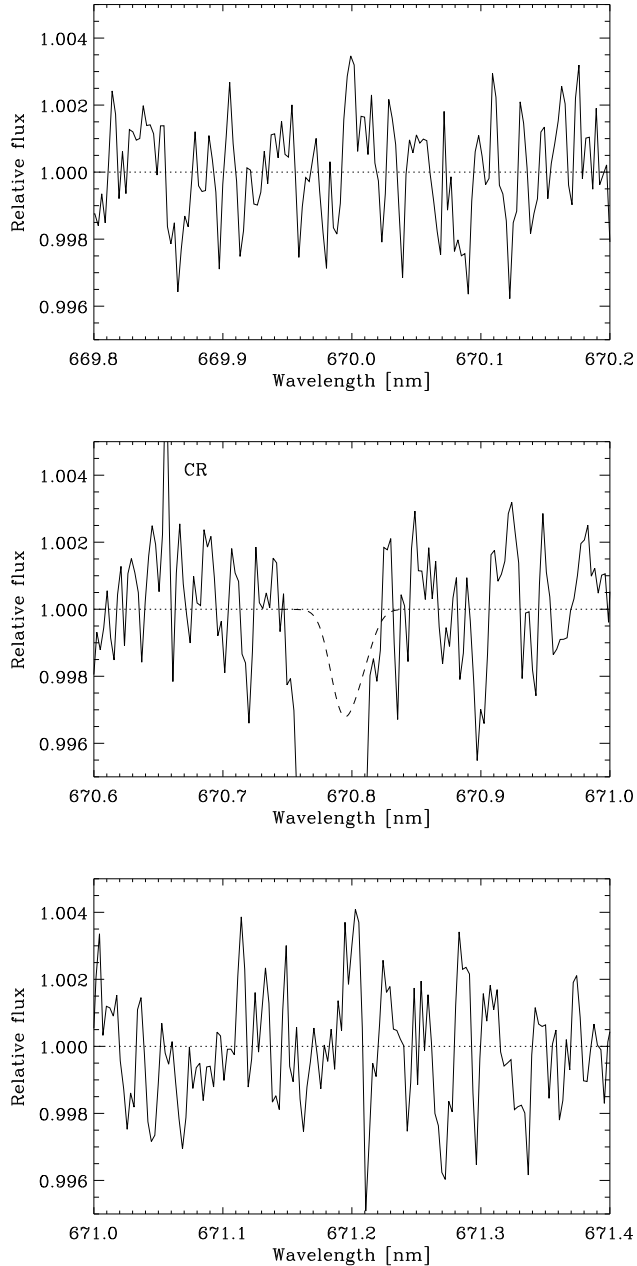


FIG. 14.— Enlargement of the August 2004 spectrum of LP 815-43 around the Li I 670.8 nm line. Note that the spike at 670.655 is a cosmic ray hit. Also shown with a dashed line is the predicted contribution of ${}^6\text{Li}$ to the Li I 670.78 nm line for ${}^6\text{Li}/{}^7\text{Li} = +0.05$.

We have tried to quantify the amount of fringing by computing the equivalent width directly integrated over a 0.08 nm window (the width of the Li line) along the echelle order with the Li line. The wavelength variation of these equivalent width measurements is slightly more pronounced than expected from pure random noise with the same S/N , suggesting the presence of fringing with a quasi-regular wavelength dependence. Adding a sinusoidal component with an amplitude of 0.05% and wavelength scale of about 0.17 nm to such pure random noise produces a similar equivalent width distribution to that observed in August 2004, as shown in Fig. 15; fringing

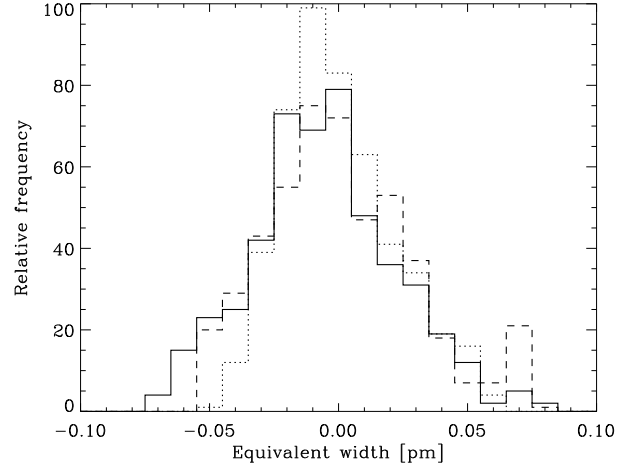


FIG. 15.— Histogram of the measured equivalent widths over a 0.08 nm window in the continuum near the Li I 670.8 nm line for the August 2004 spectrum of LP 815-43 (solid line). Also shown is the same distribution for pure random noise with the same S/N (630) as the observed spectrum (dotted line). The dashed line shows the distribution of equivalent widths for the random noise spectrum with an added sinusoidal component of amplitude 0.05% (see text for details). The similarity with the observed distribution suggests the presence of residual fringing at the 0.05% level for this star while fringing at the 0.1% level can be ruled out (not shown).

as large as 0.1% can clearly be ruled out. A similar exercise for the July 2000 spectrum suggests residual fringing with an amplitude of 0.08%. It can also be noted that the expected ${}^6\text{Li}$ contribution to the equivalent width (0.1 pm for ${}^6\text{Li}/{}^7\text{Li} = +0.046$) is very unlikely to be produced purely by chance as the observed equivalent width distribution of the nearby continuum have a typical uncertainty of 0.03 pm, consistent with our claimed 2σ detection for this star. We stress that the presence of fringing at the 0.05% level does not automatically imply that our derived ${}^6\text{Li}/{}^7\text{Li}$ for this star is overestimated as it also requires that a fringing depression rather than a peak falls on top of the Li line, something we are not able to evaluate the likelihood of. The fact that independent observations acquired in 2000 and 2004 both yield a significant presence of ${}^6\text{Li}$ in the star increases our confidence that our ${}^6\text{Li}$ detection in this star is real. We nevertheless strongly encourage further observations of this star to confirm our conclusions.

A further concern in the analysis of LP 815-43 is that lithium interstellar (ISM) absorption line may mimic the presence of ${}^6\text{Li}$ considering that the K I 769.8 nm is clearly distorted by a *blue-shifted* (-2.07 km s^{-1}) ISM line. Welty & Hobbs (2001) found in their survey of ISM absorption that $N(\text{Li I})/N(\text{K I}) = 0.0054$. Together with the difference in gf -values of the two resonance lines, the ISM Li I profile should be about 100 times weaker than the corresponding ISM K I line. The ISM K I line has a line depth of about 8% and an equivalent width of 0.97 pm. The ISM Li I line should, therefore, have an equivalent width of less than 0.01 pm (0.1 mÅ). It is, therefore, unlikely that an ISM lithium line will have a significant influence on the derived ${}^6\text{Li}/{}^7\text{Li}$.

To quantify the above estimates, we first subtracted from the K I 769.8 nm profile the expected stellar K I line

as predicted using an K abundance similar to the other four stars with similar $[\text{Fe}/\text{H}]$ and ζ_{macro} and v_{rad} from the Ca I and Fe I lines. We then fitted a Gaussian to this ISM K I profile, which was subsequently converted to a corresponding ISM Li I profile while taking into account the hyperfine structure of the Li line and the difference in overall line strength. The difference in line width of the Gaussians due to different thermal broadening of Li and K was also included. After subtraction of this blue-shifted ISM profile, we again performed a χ^2 -analysis of the remaining stellar Li I line. As expected from the above estimates, the resulting ${}^6\text{Li}/{}^7\text{Li}$ was indistinguishable from the previous value. We conclude that our derived high ${}^6\text{Li}/{}^7\text{Li}$ is not an artifact of ISM Li absorption.

5.3. Estimating Uncertainties Using Monte Carlo Calculations

As an independent means of estimating the uncertainties attached to our Li isotopic abundance analysis, we have carried out extensive Monte Carlo simulations for HD 140283. A theoretical profile of the Li I 670.8 nm line with an adopted ${}^6\text{Li}/{}^7\text{Li} = 0.02$ was treated as an observed line, to which noise corresponding to various S/N values (400, 500, 600, 700, 800, 900 and 1000) were added. All line profiles were convolved with a Gaussian of width 5 km s^{-1} and projected stellar rotational velocity of 0.5 km s^{-1} prior to introducing the effects of finite S/N . These artificial observed lines had the same wavelength sampling as our UVES spectra. We then performed a χ^2 -analysis of these profiles in an identical fashion as for our real observations with the exception that the line broadening parameters were assumed to be known beforehand. For each S/N , 100 realisations of the noisy synthetic profile were generated and exposed to the χ^2 -analysis. The scatter in the estimated ${}^6\text{Li}/{}^7\text{Li}$ gives an estimate of the accuracy with which the isotopic ratio can be determined for a given S/N . To these uncertainties should still be added the possible errors arising from uncertainties in the line broadening, continuum placement and stellar parameters.

The estimated ${}^6\text{Li}/{}^7\text{Li}$ deviated from the input value with a standard deviation of 0.010, 0.007, 0.005 and 0.004 for $S/N = 400, 600, 800$ and 1000, respectively. These estimates are consistent with the χ^2 results using the true observed profile for this star when ignoring the uncertainty stemming from the estimated errors in the adopted macroturbulence and stellar parameters. We conclude that the error estimates in Sect. 5.1 are indeed realistic.

5.4. Effects of Choice of a χ^2 Analysis

In their analysis of the Li isotopic ratio in HD 84937, Cayrel et al. (1999) adopted a slightly different technique than the one employed by us. Rather than determining the intrinsic line broadening due to macroturbulence and rotation from lines of other species, they introduced this as an additional free parameter in the χ^2 -analysis of the Li I 670.8 nm line. Only after the analysis did they confirm that the derived broadening parameter was consistent with values estimated from the Ca I 616.2 and 671.7 nm lines. The ${}^6\text{Li}/{}^7\text{Li}$ ratio Cayrel et al. obtained for this star (0.052 ± 0.019 at 1σ) is in agreement with the value (0.06 ± 0.03 at 1σ) of Smith et al. (1998) from an independent observational data set. Smith et al. used the same approach as us but with fewer calibration lines.

We have investigated how our conclusions would be modified by employing Cayrel et al.'s approach for our full sample. Our results are reasonably unchanged by adopting this alternative approach. Only in six of our 24 stars is the derived ${}^6\text{Li}/{}^7\text{Li}$ ratio changed by more than ± 0.02 . Of our nine detections at the $\gtrsim 2\sigma$ level, seven (HD 102200, HD 106038, HD 160617, G 020-024, CD $-30^\circ 18140$, CD $-33^\circ 3373$, LP 815-43) are still detections under the same criterion. While G 013-009 and CD $-48^\circ 2445$ would no longer be significant detections, three other stars would in this framework be classified as $\gtrsim 2\sigma$ detections: HD 213657, HD 298986 and BD $+03^\circ 0740$, which otherwise were only 1σ results. BD $+03^\circ 0740$ ($[\text{Fe}/\text{H}] = -2.65$) is noteworthy given its low $[\text{Fe}/\text{H}]$.

We believe that Cayrel et al.'s method is inferior to ours as it does not make full use of the information content in the observed spectra. Due to the limited wavelength coverage of their spectra, Cayrel et al. had access to only two calibration lines (Ca I 616.2 and 671.7 nm) which in HD 84937 are of quite different strength compared with the Li line. Under those circumstances it may be justified to allow also the broadening parameters to vary in the χ^2 -analysis of the Li I 670.8 nm profile when the S/N is very high as in their spectrum. One of the great advantages of the VLT/UVES is the wide wavelength coverage that provides several lines for estimating the intrinsic line broadening. We also note that the uncertainties in the estimated ${}^6\text{Li}/{}^7\text{Li}$ ratios are in general larger when Cayrel et al.'s method is used in place of our standard analysis presented in Sect. 5.1, in some cases significantly so (e.g. BD $-13^\circ 3442$: ${}^6\text{Li}/{}^7\text{Li} = 0.001 \pm 0.028$ and 0.042 ± 0.050 , respectively), while in no case was the uncertainty reduced. We conclude that the method of Cayrel et al. is less appropriate than the one employed in the present study. Nevertheless, our results would have been quite similar had we adopted this approach.

5.5. Effects of Choice of Stellar Parameters

As described in Sect. 4, the estimated uncertainties in the adopted stellar parameters in absolute terms are $\Delta T_{\text{eff}} = \pm 100 \text{ K}$, $\Delta \log g = \pm 0.2$, $\Delta [\text{Fe}/\text{H}] = \pm 0.2$ and $\Delta \xi_{\text{turb}} = \pm 0.2 \text{ km s}^{-1}$. We have repeated our Li isotopic abundance determinations for all stars using MARCS model atmospheres with modified stellar parameters by deriving new line broadening parameters and then repeating the χ^2 -analysis of the Li I 670.8 nm profile. The resulting ${}^6\text{Li}/{}^7\text{Li}$ ratios when changing the stellar parameters by $+100 \text{ K}$, $+0.2 \text{ dex}$ and $+0.5 \text{ km s}^{-1}$, respectively, are given in Table 4. Clearly, the ${}^6\text{Li}/{}^7\text{Li}$ ratios are basically immune to the uncertainties at this level in the stellar parameters: the slightly different line broadening parameters derived from the calibration lines also apply to the Li I line, leaving ${}^6\text{Li}/{}^7\text{Li}$ essentially intact. Very rarely is $\Delta {}^6\text{Li}/{}^7\text{Li}$ as large as 0.003 with the difference being ≤ 0.001 in the majority of cases. This finding is in line with those reported previously by Smith et al. (1993, 1998).

While the effects of the uncertainties in $\log g$, $[\text{Fe}/\text{H}]$ and ξ_{turb} are negligible for the derived ${}^7\text{Li}$ and ${}^6\text{Li}$ absolute abundances ($\Delta \log \epsilon_{\text{Li}} < \pm 0.01 \text{ dex}$ for our estimated stellar parameter uncertainties), this is not true when changing T_{eff} . Our calculations reveal that $\log \epsilon_{\text{Li}}$ increases with about 0.073 dex for $\Delta T_{\text{eff}} = +100 \text{ K}$, neces-

sarily quite similar to the estimate by Ryan et al. (1999).

5.6. Effects of Choice of Suite of 1D Model Atmospheres

The tendency for our derived ${}^6\text{Li}/{}^7\text{Li}$ ratios to be slightly but positively offset from zero, may raise concern that our analysis suffer from an unidentified systematic error. One possibility could be our use of MARCS model atmospheres, since Nissen et al. (1999) found a *smaller* isotopic ratio (0.033 instead of 0.041) for the disk star HD 68284 when switching from a MARCS to a Kurucz model atmosphere with identical stellar parameters. To investigate whether the choice of suite of 1D model atmospheres has any effect on the derived Li isotopic abundances, we have repeated the analysis for all stars using Kurucz model atmospheres without convective overshoot and for the same stellar parameters, as computed by Castelli et al. (1997). The resulting ${}^6\text{Li}/{}^7\text{Li}$ ratios are presented in Table 4 together with the corresponding values with MARCS model atmospheres. The changes to the isotopic ratios resulting from substitution of the Kurucz for the MARCS models are, as anticipated, negligible: $\Delta{}^6\text{Li}/{}^7\text{Li} \leq \pm 0.001$ and in no case larger than 0.003. Furthermore, the small differences can be both positive and negative.

Similarly, the effect of the Kurucz models on the absolute Li abundances is marginal³. The average difference compared with the MARCS based results is $\Delta\log \epsilon_{\text{Li}} = 0.015 \pm 0.018$ dex with the maximum difference being 0.048 for HD 102200.

For completeness, we note that the above test is based on the assumption that the stellar parameters of the model atmospheres need no adjustments when switching to a different suite of model atmospheres. Given the almost identical behaviour of our Li I, K I, Ca I, Fe I and Fe II lines in the two cases, we expect insignificant differences for both the photometric calibrations or the H α line profile fitting. In summary, our conclusions about the lithium isotopic ratio are immune and the lithium abundance insensitive to the particular brand of theoretical 1D, hydrostatic, LTE model atmospheres employed in the analysis.

5.7. Effects of 3D Hydrodynamical Model Atmospheres

In addition to the tests described above, we have also performed a similar χ^2 -analysis using the time-dependent 3D hydrodynamical model atmospheres described in Sect. 3.1 under the assumption of LTE. Since such 3D models still only exist for relatively few stellar parameter combinations, only some of our target stars could be exposed to a 3D analysis. The 3D models assigned to the various stars were based on similarity in stellar parameters; we note therefore that the here presented 3D results are obtained with somewhat different stellar parameters than adopted for the 1D calculations

³ Differences in absolute Li abundances approaching 0.1 dex would have been found had we resorted to the convective overshoot models of Kurucz (1993) instead of using the models with this option switched off (Ryan et al. 1996). These overshoot models are, however, significantly less successful in reproducing observed stellar flux distributions and their shallower temperature gradients find no support in our detailed 3D hydrodynamical simulations of stellar atmospheres with surface convection. We conclude that the overshoot models are less appropriate for abundance analyses of halo stars.

described in Sect. 5.1. As explained in Sect. 3.2, the main advantages with a 3D approach is that neither micro- nor macroturbulence enter the analysis and that the intrinsic line asymmetries arising from convective motions follow directly from the 3D line formation calculations. The projected stellar rotation velocity $v_{\text{rot}} \sin i$ must however be determined from other lines. Thus, in the χ^2 -analysis, $v_{\text{rot}} \sin i$ replaces ζ_{macro} as a free variable; the Gaussian instrumental broadening measured for each line is known from Th lines.

The results for the stars for which a 3D analysis has been carried out are given in Table 5, while Fig. 16 and Fig. 17 show examples of the achieved profile fits for the Ca I 616.21 lines for a few of the stars. It is noteworthy that the 3D analysis yields a substantial improvement in the agreement with the observed profiles of Ca and Fe lines, as also previously reported by Nissen et al. (2000). In almost all cases, the resulting χ^2 for the calibration lines are smaller than for the corresponding 1D cases; the only exceptions are for the K I 769.89, Fe II 624.76 and/or Fe II 645.64 nm lines for a few of the stars. The derived $v_{\text{rot}} \sin i$ values are between 0.1 and 3.8 km s^{-1} . The typical uncertainties in $v_{\text{rot}} \sin i$ are 0.3 km s^{-1} but in some cases can be as large as $\approx 1 \text{ km s}^{-1}$. Very little is known about the observed rotation properties of metal-poor halo stars but due to their high age one would expect them to rotate slowly (the Sun has $v_{\text{rot}} = 1.8 \text{ km s}^{-1}$). It is therefore quite possible that the estimated rotational velocities towards the higher end are overestimated. For example, Smith et al. (1998) suggest $v_{\text{rot}} \sin i < 2 - 3 \text{ km s}^{-1}$ for a typical metal-poor turn-off star. It can, however, not be ruled out at present that some of these stars actually have $v_{\text{rot}} \sin i \approx 3 \text{ km s}^{-1}$. Part of the explanation for some of the high estimated $v_{\text{rot}} \sin i$ values is that the adopted stellar parameters for the 3D models are inappropriate for some of the stars: if a too low T_{eff} or too high $\log g$ are used then the convective motions and thus the Doppler line broadening will be too small, requiring large $v_{\text{rot}} \sin i$ to compensate when fitting the observed spectral lines. Furthermore, we remind the reader that LTE has been assumed for these 3D line formation calculations while the steep temperature gradients in low metallicity 3D models can be expected to result in significant non-LTE effects (Asplund et al. 1999; Asplund 2005). We suspect that this may be the explanation for the slight correlation between $v_{\text{rot}} \sin i$ and $[\text{Fe}/\text{H}]$ in our sample, although we note that $v_{\text{rot}} \sin i$ is particularly uncertain for the two stars with $[\text{Fe}/\text{H}] \approx -1$ (HD 3567 and G 075-031) because of the quite strong calibration lines employed. We therefore urge these $v_{\text{rot}} \sin i$ values not to be taken too literally at this stage. In fact, it is encouraging that the resulting rotational velocities are at least reasonable given that there are no broadening mechanisms like micro- and macroturbulence as in 1D that can be tuned.

Interestingly, in general the 3D LTE calculations do not improve the agreement with the Li I 670.78 nm line as judged by the χ^2 -statistics. For more than half of the stars, the 3D analysis yield slightly higher minimum χ^2 -values than in 1D. The most likely explanation in our opinion for this contrasting behaviour compared with the Ca and Fe lines is that LTE is a particularly poor assumption for the Li I line in metal-poor stars; pronounced

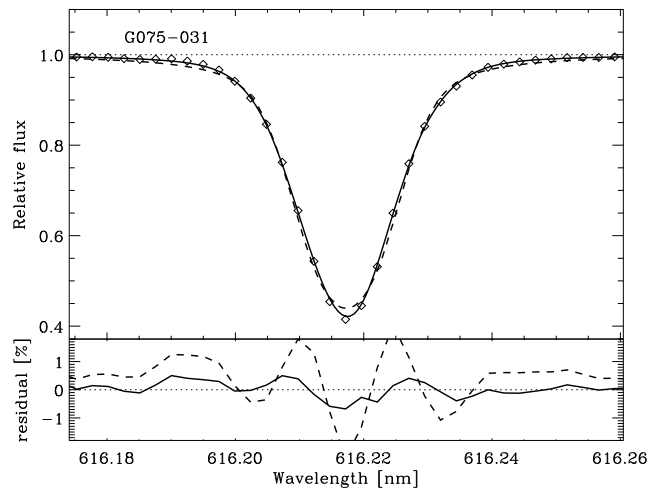
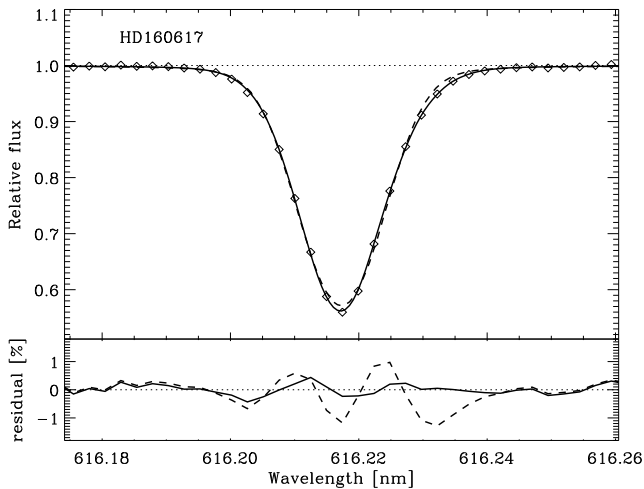
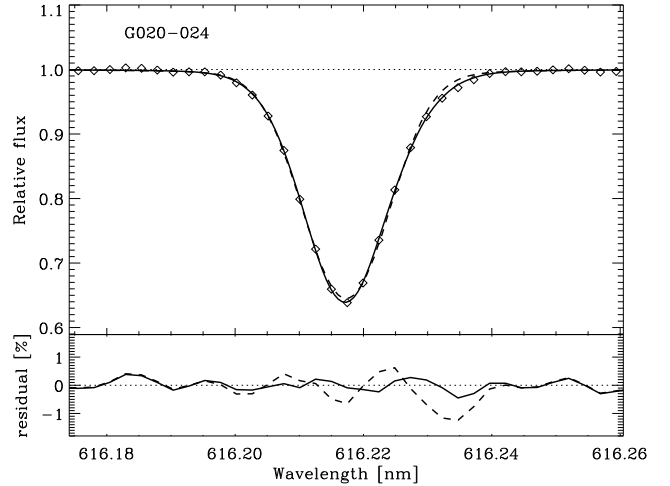
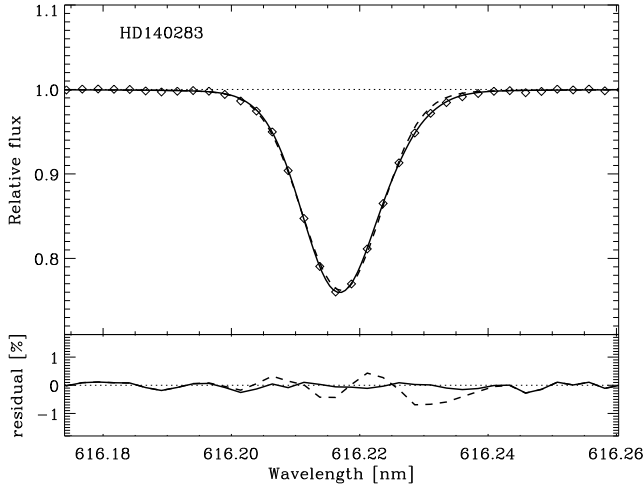


FIG. 16.— Ca I 616.21 nm line in HD 140283 (*upper panel*) and HD 160617 (*lower panel*). The solid lines correspond to the best fitting 3D profiles from a χ^2 analysis while the dashed lines are for the 1D profiles; the rhombs are the observed profiles. Also shown are the residuals between observed and predicted line profiles.

FIG. 17.— Same as Fig. 16 but for G020-024 (*upper panel*) and G075-031 (*lower panel*).

over-ionization of Li I is predicted from 3D non-LTE calculations due to the steep temperature gradients of the 3D model atmospheres (Asplund et al. 2003; Barklem et al. 2003).

An inspection of Table 5 reveals that the 1D ${}^6\text{Li}/{}^7\text{Li}$ ratios appear to be similar or lower than the ratios derived from 3D LTE calculations. Only in three stars are the 3D results noticeably smaller than for the corresponding 1D case. The smaller ${}^6\text{Li}/{}^7\text{Li}$ ratios in HD 3567 and G 075-031 are likely a reflection of the relatively high $[\text{Fe}/\text{H}]$ of these two stars, which renders the calibration lines used to determine $v_{\text{rot}} \sin i$ quite strong (equivalent widths up to 12 pm); in the case of the Sun, the impressive agreement between predicted and observed line profiles found for weak lines breaks down for such strong lines (Asplund et al. 2000). The difference between 3D and 1D for LP 815-43 is of particular interest given the prominent status this star will have when later discussing the implications of our ${}^6\text{Li}$ survey. In 3D, the derived isotopic ratio is ${}^6\text{Li}/{}^7\text{Li} = 0.036 \pm 0.021$ to be compared with the 1D value of ${}^6\text{Li}/{}^7\text{Li} = 0.046 \pm 0.022$ (both results are for

the August 2004 observations). Taking these 3D LTE calculations at face value, LP 815-43 would no longer be considered a significant ${}^6\text{Li}$ detection, although it would not be far from making the 2σ criteria.

Considering the expected severe 3D non-LTE effects on the Li I line in metal-poor stars that are not accounted for here, the 1D results are to be preferred. Indeed, one would expect also the calibration lines used to estimate $v_{\text{rot}} \sin i$ to be vulnerable to departures from LTE, in particular minority species like Ca I and Fe I (Asplund 2005). Carrying out detailed 3D non-LTE calculations for both the calibration lines and the Li I line for the necessary many simulation snapshots is unfortunately extremely computationally demanding. We will therefore have to postpone investigating this remaining issue to a future date. The preliminary 3D LTE analysis carried out here, however, has not uncovered any significant systematic errors that would suggest that our 1D-based Li isotopic ratios are overestimated in general.

5.8. Comparison with Previous Studies

A number of our targets have been investigated for their Li isotopic abundances in previous studies. Our non-detection of ${}^6\text{Li}$ is consistent with the upper lim-

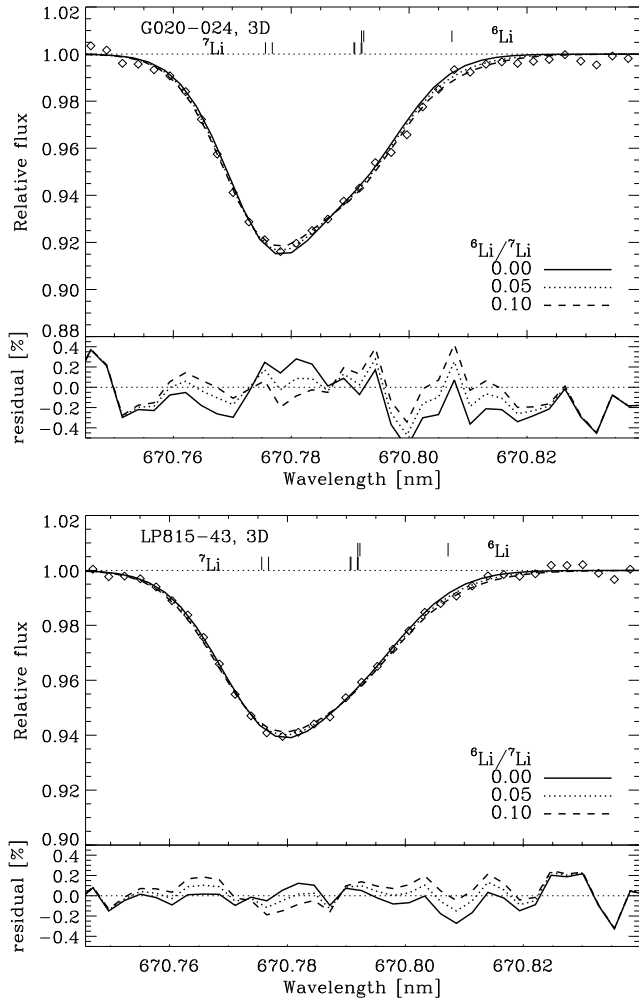


FIG. 18.— Li I 670.78 nm line in G020-024 (*upper panel*) and LP815-43 (*lower panel*) based on a 3D LTE analysis. The best fitting line profiles as judged by a χ^2 analysis for ${}^6\text{Li}/{}^7\text{Li}$ = +0.00, +0.05 and +0.10 are shown.

its reported for HD 19445, HD 140283 and BD +03°0740 by Smith et al. (1993, 1998) and Hobbs & Thorburn (1994, 1997). Our derived value for G 271-162 (${}^6\text{Li}/{}^7\text{Li} = 0.019 \pm 0.012$) does not constitute a detection of ${}^6\text{Li}$ but is very close to Nissen et al.’s (2000) result of ${}^6\text{Li}/{}^7\text{Li} = 0.02 \pm 0.01$ based on the same VLT/UVES commissioning spectra, in particular as we have here adopted a slightly more conservative estimate of the uncertainties.

More noteworthy is the result that we do not confirm the ${}^6\text{Li}$ detection for HD 338529 (also known as BD +26°3578) by Smith et al. (1998) who found ${}^6\text{Li}/{}^7\text{Li} = 0.05 \pm 0.03$. Our value of 0.010 ± 0.013 is based on a higher quality spectrum ($S/N \simeq 520$ vs 420) but the main difference can be traced to the adopted line broadening parameters. Smith et al. combined the effects of instrumental broadening and macroturbulence by convolving the synthetic spectra with a Gaussian profile, but used only the Ca I 671.78 nm line to determine the width of this Gaussian; however, this line is quite weak in HD 338529 having a line depth of only 3% at $R = 110,000$. As a result, Smith et al. could not constrain the macroturbulent velocity parameter for this star very

well (this can be seen in their Figure 6 for HD 338529, where the χ^2 as a function of macroturbulent velocity is very shallow). Our higher broadening parameter is significantly better determined as it is based on four Ca I and Fe I lines, all in very good agreement. We would also have found a significant ${}^6\text{Li}/{}^7\text{Li}$ ratio had we adopted the same macroturbulence as Smith et al. (1998). In addition, Smith et al. could only obtain upper limits: ≤ 0.06 and ≤ 0.05 (2σ) for HD 102200 and HD 160617, respectively. Again, the main difference appears to be the adopted macroturbulence parameter, which in our case is smaller than their value. Also, our spectra for these stars have significantly higher S/N . The differences in ${}^6\text{Li}/{}^7\text{Li}$ between us and Smith et al. for HD 338529 certainly serve as a warning when trying to interpret the results in terms of Li isotopic abundances for this extremely challenging method. It is clearly paramount to have exceptionally high S/N as well as well-determined intrinsic broadening parameters based on a multitude of spectral lines with similar strength as the Li I 670.8 nm line. While we have tried to accomplish both of these factors and believe that we have set a new standard in this respect, we urge the reader to exercise some caution when using our quoted Li isotopic abundances.

Deliyannis & Ryan (2000) reported a firm detection of ${}^6\text{Li}$ in the subgiant HD 140283: ${}^6\text{Li}/{}^7\text{Li} = 0.040 \pm 0.015$. No details of this analysis have as yet appeared in the literature. We are, therefore, not able to identify reasons for the discrepancy with our non-detection of ${}^6\text{Li}/{}^7\text{Li} = 0.008 \pm 0.006$. Our result for HD 140283 is, however, consistent with the upper limit of ${}^6\text{Li}/{}^7\text{Li} < 0.018$ estimated recently by Aoki et al. (2004) based on a Subaru/HDS spectrum of the quality of our VLT/UVES spectrum. Wako Aoki has kindly made available their Subaru spectrum of HD 140283 for an independent analysis by us. As we did not have access to their measured instrumental profile, we performed the analysis adopting a combined Gaussian for the instrumental and macroturbulence broadening, a case also considered by Aoki et al. Our result of ${}^6\text{Li}/{}^7\text{Li} = 0.003$ is in perfect agreement with their corresponding result of 0.002 when using their choice of calibration lines. We note that when we perform an analysis in the same way as for our own sample (i.e. using the same calibration lines and taking into account uncertainties in line broadening, S/N and stellar parameters), we find ${}^6\text{Li}/{}^7\text{Li} = 0.006 \pm 0.004$, which is in excellent agreement with the UVES result. When expanding the set of calibration lines to include in total 14 lines between 500 and 650 nm from the Subaru spectrum, the 1σ error doubles: ${}^6\text{Li}/{}^7\text{Li} = 0.007 \pm 0.009$. The exact results and uncertainties thus depend (slightly) on the particular choice of lines to estimate the line broadening, which must be borne in mind when comparing different ${}^6\text{Li}/{}^7\text{Li}$ -analyses.

6. LI ABUNDANCES FROM THE Li I 610.4 NM SUBORDINATE LINE

6.1. Analysis

The exceptionally high quality of our UVES spectra allows Li abundances to be derived from the subordinate Li I 610.36 nm line, which in these halo stars has an equivalent width of just 0.1 – 0.2 pm (1 – 2 mÅ). We have performed a similar χ^2 -analysis of a wavelength re-

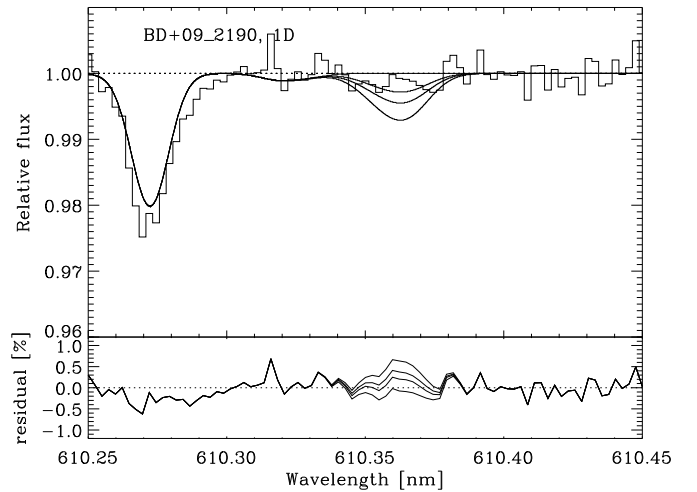
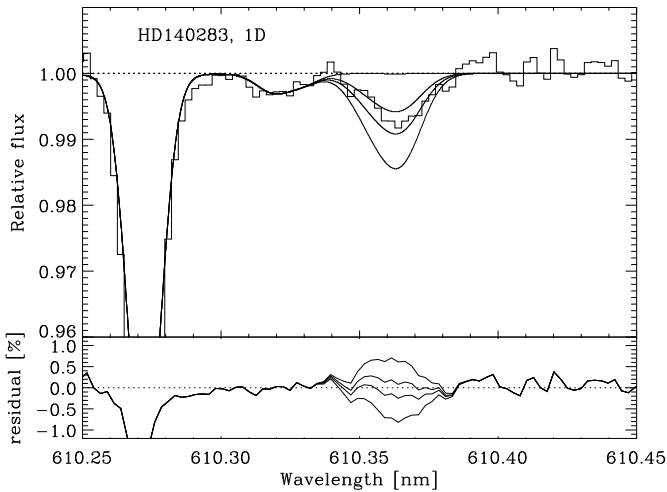
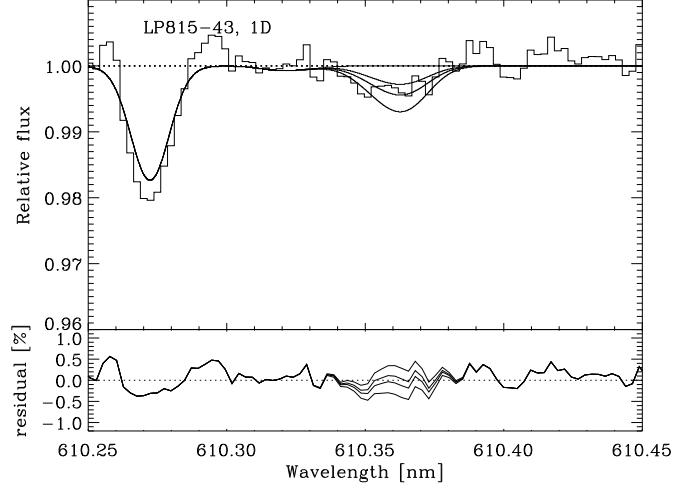
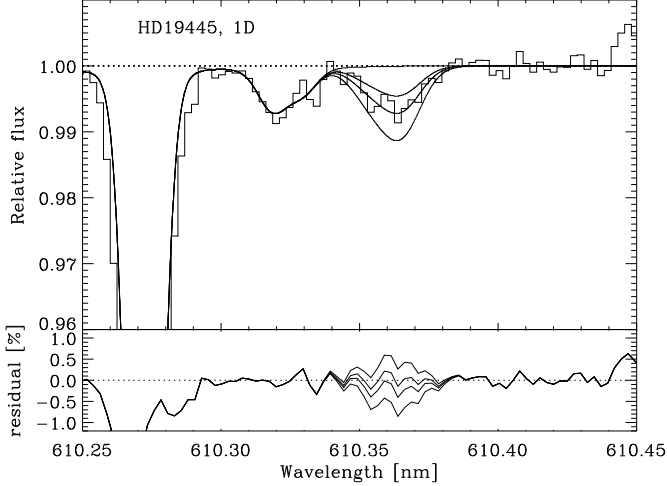


FIG. 19.— Observed and theoretical Li I 610.4 nm profiles for HD 19445 (upper panel) and HD 140283 (lower panel). The four theoretical 1D LTE profiles are computed with no Li, $\log \epsilon_{\text{Li}} = 2.0, 2.2$ and 2.4 , respectively, with the stellar parameters listed in Table 2. For each star, the residuals between the synthesis and observations are also shown.

FIG. 20.— Same as for Fig. 19 but for LP 815-43 (upper panel) and BD+09°2190 (lower panel). No significant detection of the Li I 610.4 nm line is made in the latter star according to a χ^2 -test, although there is a possible feature at the correct wavelength that would correspond to $\log \epsilon_{\text{Li}} \approx 2.0$.

gion around 610.4 nm, taking into account the hyperfine and isotope splitting for the Li line and neighboring lines of Fe I, Fe II and Ca I. The adopted Fe and Ca abundances were those implied by the other considered Fe and Ca lines. While no attempt was undertaken to optimize the agreement between observations and predictions for these Fe and Ca lines by adjusting the gf -values or elemental abundances, we emphasize that this had no impact on the derived Li abundances as the neighboring lines are quite well described and sufficiently far away from the Li feature not to cause any problems. Fig. 19 and Fig. 20 compare the synthesized profiles for different Li abundances with the observed spectra for a few stars.

The derived Li abundances from the subordinate Li I 610.4 nm line are listed in Table 3. The line is unambiguously detected in 22 of the 24 program stars with the two exceptions being the very metal-poor stars BD+03°0740 and BD+09°2190. Also for those two stars there is a tantalizing suggestion of a feature at the correct wavelength, although the χ^2 -analysis does not indicate a significant detection. As a consequence, we only give 3σ upper lim-

its to the Li abundance in these two stars.

The derived 1D LTE Li abundances from the Li I 610.4 nm line have been corrected for departures from LTE using the detailed 1D statistical equilibrium calculations of Carlsson et al. (1994). The non-LTE abundance corrections for the subordinate line are positive and slightly larger than for the resonance lines: typically $\Delta \log \epsilon_{\text{Li}} \approx +0.05$ dex. The maximum non-LTE effect occurs for the metal-poor subgiant HD 140283 (+0.09 dex).

6.2. Comparison with Results from the Li Resonance Line

Figure 21 compares the derived Li abundances from the weak subordinate Li I 610.4 nm line with those from the stronger Li I 670.8 nm resonance line. The agreement is very encouraging with a mean difference of only 0.05 ± 0.05 dex for the 22 stars with measured Li abundances. For all practical purposes, the two lines return the same lithium abundance for a given star. The differences show no obvious trends with metallicity or effective temperature. The upper limits for the Li abun-

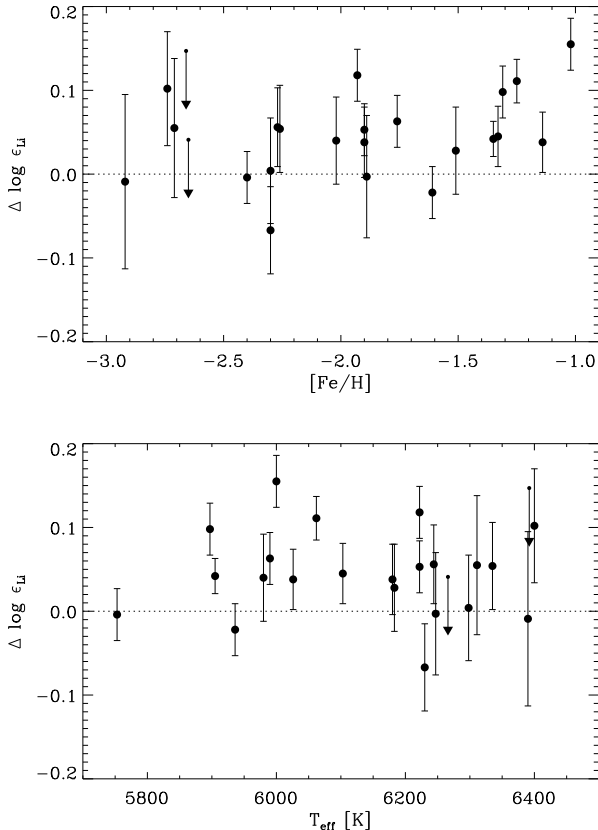


FIG. 21.— Differences in the 1D non-LTE abundances from the Li I 610.4 nm and 670.8 nm lines as a function of T_{eff} (upper panel) and $[\text{Fe}/\text{H}]$ (lower panel).

dances from the subordinate line in BD +03°0740 and BD +09°2190 are very close to the abundances from the resonance line. It is unlikely that the explanation for this minor abundance difference can be found in erroneous gf -values for either of the two lines. One (remote) possibility is that the adopted T_{eff} values are underestimated; a ≈ 150 K higher T_{eff} -scale would erase the mean difference. Another explanation could be inappropriate non-LTE abundance corrections for the 1D models. Use of 3D models with non-LTE line formation might erase the differences (Asplund et al. 2003). A study aimed at investigating the 3D non-LTE line formation for a wider range of stellar parameters as well as revisiting the 1D non-LTE abundance corrections in light of recent improvements in collisional data (Belyaev & Barklem 2003; Barklem et al. 2003) would be worthwhile.

The Li I 610.4 nm line was first detected in the halo star HD 140283 by Bonifacio & Molaro (1998). They also found very good agreement in the abundances inferred from the two Li lines. Likewise, Ford et al. (2002) derived the same abundances from the 610.4 and 670.8 nm lines for this star using a very high quality spectrum obtained with Subaru/HDS (the same spectrum as used by Aoki et al. (2004) to derive an upper limit to ${}^6\text{Li}/{}^7\text{Li}$ in this star as discussed above). However, for the other seven stars for which Ford et al. (2002) claimed a detection of the subordinate line, the derived Li abundances are 0.2 – 0.5 dex higher than suggested by the resonance

line. This is in sharp contrast with our findings. While we are not in a position to unequivocally identify the reasons for the very different conclusions of Ford et al., we suspect that the key is the quality of the observations. The S/N ratios of the spectra of Ford et al. are between 200 and 300 around the 610.4 nm line, which may still not be sufficient to detect this very weak line in metal-poor turn-off stars (note that this line is about 50% stronger in a subgiant like HD 140283 with $T_{\text{eff}} \approx 5700$ K than in a turn-off star with $T_{\text{eff}} \approx 6200$ K for the same Li abundance). Under these circumstances it is easy to overestimate the line strength due to noise and thus derive too high abundances. In comparison, our spectra have $S/N \approx 500$ or better in the relevant wavelength region. Finally, we note that our resolving power is about twice as large as obtained by Ford et al. (110 000 vs 50 000).

7. ORIGIN AND EVOLUTION OF LITHIUM

7.1. Lithium Abundance Trends and Scatter

Since our sample is relatively small and does not extend to extremely low metallicities, our discussion of the lithium abundances will be relatively brief. Furthermore, our results for the total lithium abundance are in broad agreement with many published analyses. The principal novelty from our study is an estimate of the isotopic ratio for stars on the Spite plateau.

Our data may be used to quantify the trend of the lithium abundance with metallicity (here, Fe/H or O/H), to extrapolate the trend to zero metallicity, and to determine the scatter in lithium abundance about the mean trend. In applying our data, we have excluded G 271-162 since no accurate $\text{H}\alpha$ -based T_{eff} could be derived from this star (see Sec. 4.1). In addition, the Li-rich star HD 106038 has been excluded because it has strong overabundances in Si, Ni, Y and Ba (Nissen & Schuster 1997), and a very high Be abundance relative to other halo stars of similar $[\text{Fe}/\text{H}]$ (Primas et al., in preparation). This peculiar abundance pattern suggests that the star has undergone a highly unusual nucleosynthesis enrichment, possibly due to mass transfer, which justifies its exclusion here. Such Li-rich stars as HD 106038 appear to be extremely rare. Perhaps the only known other example is the subgiant BD +23°3912 with $[\text{Fe}/\text{H}] = -1.5$ and $\log \epsilon_{\text{Li}} = 2.6$ (King et al. 1996). In addition, our sample deliberately excluded any of the rare Li-deficient halo dwarfs. The nature of these stars is currently under debate (cf. Ryan et al. 2002; Frebel et al. 2005; Aoki et al. 2006; Charbonnel & Primas 2005). Our assumption is that these stars have also undergone a very special event, a binary merger perhaps (Ryan & Elliott 2005).

From the abundances listed in Table 3, the mean ${}^7\text{Li}$ abundance of the remaining 22 stars is $\log \epsilon_{7\text{Li}} = 2.21 \pm 0.07$. As shown in Fig. 22, there is, however, a pronounced trend with metallicity, which resembles the correlation with $[\text{Fe}/\text{H}]$ found in some previous Li studies (e.g. Thorburn 1994; Norris et al. 1994; Ryan et al. 1996, 1999; Bonifacio et al. 2003, 2006). A univariate linear least-square-fit taking into account the estimated uncertainties in $[\text{Fe}/\text{H}]$ and the Li abundances (excluding HD 106038 and G 271-162 for the above reasons) implies

$$\log \epsilon_{7\text{Li}} = (2.409 \pm 0.020) + (0.103 \pm 0.010) \cdot [\text{Fe}/\text{H}]. \quad (2)$$

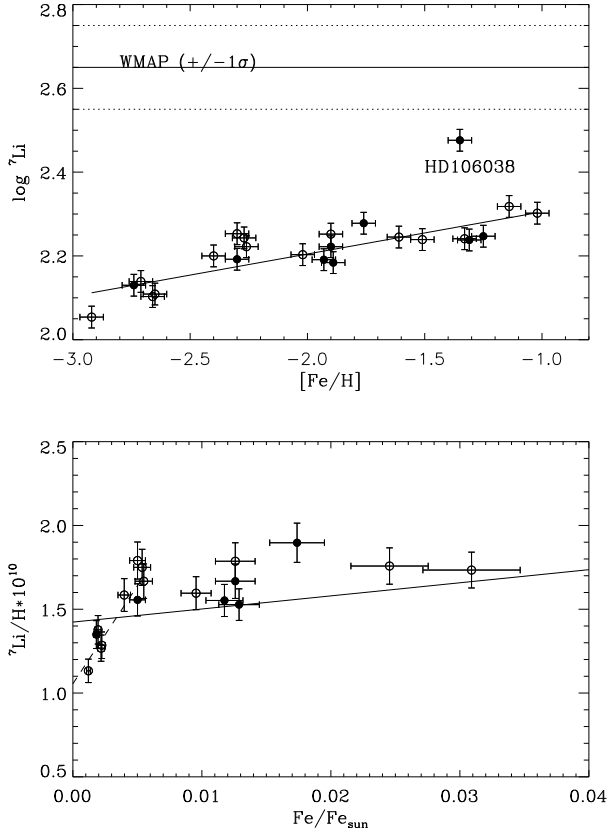


FIG. 22.— Non-LTE ${}^7\text{Li}$ abundances (1D) from the Li I 670.8 nm line as a function of metallicity; as for Fig. 13 solid circles here denote stars for which ${}^6\text{Li}$ appears to have been detected while open circles are non-detections. In the upper panel logarithmic abundances are shown ($\log \epsilon_{\text{Li}}$ vs $[\text{Fe}/\text{H}]$) while in the lower panel linear abundances (${}^7\text{Li}/\text{H}$ vs $\text{Fe}/\text{Fe}_{\odot}$) are used, which are more appropriate when extrapolating to the primordial composition. The solid lines denote the best linear fits to the data when excluding G 271-162 (no H α -based T_{eff}) and HD 106038 (abnormally high Li abundance and other peculiar abundances, see text). In the lower panel, the dashed line corresponds to the linear fit when only including the stars with $[\text{Fe}/\text{H}] < -2.2$ (G 271-162 again excluded). The horizontal solid line in the upper panel shows the predicted primordial Li abundance from Big Bang nucleosynthesis and the baryon density inferred from WMAP (Spergel et al. 2003) together with the corresponding $\pm 1\sigma$ uncertainties as dotted lines.

The observed slope is very similar in value to that presented by Ryan et al. (1999): 0.103 ± 0.010 vs 0.118 ± 0.023 for Ryan et al. The scatter around our fit is only $\sigma_{\text{obs}} = 0.033$ dex. None of the remaining 22 stars is identified as an outlier by statistical tests. Repeating the exercise using $[\text{O}/\text{H}]$ instead of $[\text{Fe}/\text{H}]$ as the independent variable yields

$$\log \epsilon_{7\text{Li}} = (2.372 \pm 0.017) + (0.115 \pm 0.011) \cdot [\text{O}/\text{H}]. \quad (3)$$

Here the non-LTE abundances from the O I 777 nm triplet have been used to estimate $[\text{O}/\text{H}]$. Again, the scatter is very small: $\sigma_{\text{obs}} = 0.034$ dex.

In Sect. 4.1 we estimated the relative precision in our adopted T_{eff} -values to be about 30 K, which would introduce an uncertainty in Li abundance of 0.022 dex. Adding also the minor uncertainties from the S/N and the other stellar parameters gives a total expected ran-

dom error of 0.026 dex. This expectation is only slightly less than the observed scatter of $\sigma_{\text{obs}} = 0.033$ dex around the linear fit. The indication is that the star-to-star scatter in lithium abundances at a given $[\text{Fe}/\text{H}]$ is very small, say 0.02 dex or less. (If the temperature error were increased to 40 K, the expected scatter in the abundances would match the observed scatter.) The observed scatter around the linear fit to our data is very similar to that found by Ryan et al., who achieved similarly high precision in T_{eff} ($\sigma_T \approx 30$ K) but utilised lower quality spectra ($S/N \approx 100 - 150$ and $R \approx 50000$). They found $\sigma_{\text{obs}} = 0.031$ dex after rejecting one star, BD +09°2190, as an outlier; we note that with the equivalent width measured from our $S/N \approx 650$ spectrum, it would no longer be considered an outlier. A different and especially a larger sample of stars may shed new light on the intrinsic scatter in the lithium abundances. For example, Nissen et al. (2005b) find that the otherwise almost identical stars G 64-12 and G 64-37 differ in their Li abundances by about 0.16 dex. Their reported observed scatter is 0.041 dex when including G 64-12 but 0.035 dex when excluding it. No doubt, any intrinsic scatter must be very small: $\lesssim 0.04$ dex.

The near-common belief has been that the primordial lithium abundance is obtainable by extrapolation of the observed abundances to zero metallicity. One supposes that extrapolation should be performed using Fe/H (or an alternative such as O/H) and not the logarithmic $[\text{Fe}/\text{H}]$ (or $[\text{O}/\text{H}]$). As seen in Fig. 22, on such a linear scale the most metal-poor stars seem to indicate a steeper slope than the less metal-poor stars, but there is no known explanation for the apparent change of slope close to the origin $\text{Fe}/\text{Fe}_{\text{sun}} = 0$. Somewhat different results are, therefore, obtained depending on which stars are included. When including only the nine stars with $[\text{Fe}/\text{H}] < -2.2$ (as usual, excluding G 271-162), the estimated primordial ${}^7\text{Li}$ abundance is ${}^7\text{Li}/\text{H} \approx 1.1 \cdot 10^{-10}$ or $\log \epsilon_{\text{Li}} \approx 2.04$. Taking all 22 stars into account results in an increase to ${}^7\text{Li}/\text{H} \approx 1.4 \cdot 10^{-10}$ or $\log \epsilon_{\text{Li}} \approx 2.15$. Very similar results are obtained using extrapolation to $\text{O}/\text{O}_{\odot} = 0$. If the presence of ${}^6\text{Li}$ at the level of that now observed for LP 815-43 is a general feature among the most metal-poor stars and it is produced in spallation or α -fusion reactions, the ${}^7\text{Li}$ abundances would have a minor non-Big Bang contribution which would reduce the estimated primordial ${}^7\text{Li}$ abundance further by about 0.05 dex (Smith et al. 1998; Ryan et al. 1999; 2000).

Our estimates of the primordial abundance do not differ significantly from the majority of published determinations, although they may be somewhat on the low side of previous estimates (e.g., Spite & Spite 1982; Thorburn 1994; Ryan et al. 1996, 1999; Bonifacio & Molaro 1997; Bonifacio et al. 2003, 2006). Our estimate of the primordial abundance is based on 1D model atmospheres and includes a correction for non-LTE effects. Presently available calculations (Asplund et al. 2003; Barklem et al. 2003; also Sec. 5.7) suggest that only a minor revision will be needed when the abundance analyses are redone using 3D models with inclusion of non-LTE effects.

It has been claimed by Melendéz & Ramírez (2004) that their new calibration of the infrared flux method (IRFM) of effective temperature determinations

(Ramírez & Melendéz 2005a,b) raises substantially the lithium abundances derived from metal-poor dwarf stars. This new T_{eff} -scale is significantly hotter at low metallicity than our $\text{H}\alpha$ -based T_{eff} -scale. It is also hotter than the IRFM calibration of Alonso et al. (1996), even though the photometric measurements required by the IRFM of the two studies agree well for the stars in common. For stars with $[\text{Fe}/\text{H}] < -3$, such as G 64-12, G 64-37 and LP 831-70, the new temperatures are 240, 460 and 320 K, respectively, higher than those estimated using the Alonso et al. ($V - K$) calibration. Ramírez & Melendéz argue that the strikingly different behaviour for the colour calibrations at low $[\text{Fe}/\text{H}]$ is due to the shortage of low metallicity stars in Alonso et al.'s sample.

A detailed scrutiny of Ramírez & Melendéz' T_{eff} -scale is beyond the scope of the present investigation. Nevertheless, it is pertinent to estimate the impact of the scale on our results. For the most metal-poor stars in our sample ($[\text{Fe}/\text{H}] < -2.6$), the T_{eff} -values of Melendéz & Ramírez (2004) are on average 182 ± 72 K higher than ours based on $\text{H}\alpha$, which increases the mean 1D non-LTE ${}^7\text{Li}$ abundance for those particular stars from $\log \epsilon_{7\text{Li}} = 2.10$ to 2.23. Independently of the new T_{eff} scale, there are reasons why Melendéz & Ramírez (2004) arrive at the significantly higher mean ${}^7\text{Li}$ abundance of $\log \epsilon_{7\text{Li}} = 2.37 \pm 0.06$ compared with our estimate: their use of convective overshoot model atmospheres ($\approx +0.1$ dex), their neglect of non-LTE corrections ($\approx +0.02$ dex) and their use of Kurucz models rather than MARCS model atmospheres ($\approx +0.02$ dex). The remaining difference with our primordial ${}^7\text{Li}$ abundance estimate stems from the extrapolation to $\text{Fe}/\text{Fe}_{\text{sun}} = 0$ in the presence of our derived slope with metallicity. Observational evidence does not favor the convective overshoot option as introduced in the Kurucz (1993) model atmospheres (e.g. Castelli et al. 1997) nor does this approach find any support in 3D hydrodynamical simulation of surface convection in metal-poor stars (Asplund et al. 1999). Non-LTE abundance corrections, while small, should be taken into account. We suggest therefore that Melendéz & Ramírez' estimate of the primordial ${}^7\text{Li}$ abundance should be revised downward by at least 0.12 dex regardless of whether or not their T_{eff} -scale is preferable to the one employed here. We note that our $\text{H}\alpha$ -based temperatures are in excellent agreement on average with the well-established IRFM ($V - K$) and ($b - y$) calibrations of Alonso et al. (1996), which seems to give little room for such large increases in T_{eff} as advocated by Melendéz & Ramírez (2004). In addition, accounting for 3D effects should push the $\text{H}\alpha$ -based T_{eff} -values downwards. More work is needed to settle the T_{eff} -scale of metal-poor stars,

Recently Bonifacio et al. (2006) have attempted to push the abundance determinations to yet lower $[\text{Fe}/\text{H}]$. In general their results agree well with ours. Their mean 1D non-LTE Li abundance for 17 stars (excluding a subgiant and a spectroscopic binary) is $\log \epsilon_{\text{Li}} = 2.17 \pm 0.09$; they argue that the expected uncertainty is about 0.08 dex from the T_{eff} -errors and quality of the spectra (median $S/N = 180$), leaving little or no room for intrinsic scatter, in particular when considering the possibility of a trend in their Li abundances with metal-

licity. Due to the small range in $[\text{Fe}/\text{H}]$ of their sample, this correlation may or may not be statistically significant by itself but when including also our results a consistent picture emerges. We note that their $\text{H}\alpha$ -based T_{eff} -scale should be very similar to ours but that their $[\text{Fe}/\text{H}]$ are likely underestimated by 0.1 – 0.2 dex due to their use of Fe I lines (Sect. 4.3); unfortunately the two samples have no stars in common, which prevents a direct comparison of the parameters and Li abundances. Interestingly, the combination of the two samples suggest a steeper slope for $[\text{Fe}/\text{H}] \lesssim -2.3$ than for higher metallicity. Whether this effect is real or spurious due to the analysis methods (1D model atmospheres, T_{eff} -scale etc) is an open question for the future. An alternative interpretation is that the intrinsic scatter increases significantly for $[\text{Fe}/\text{H}] \lesssim -2.3$.

Our major new result concerns the measurements of the lithium isotopic ratio and the apparent appearance of the analogue for ${}^6\text{Li}$ of the Spite plateau (Fig. 13). It is impossible to determine if the observed plateau is tilted, as the Spite plateau is; as shown in Sect. 7.3, when accounting for ${}^6\text{Li}$ depletion during the pre-main sequence evolution the observed ${}^6\text{Li}$ abundances apparently increase towards higher metallicity. There may be a real scatter associated with this ${}^6\text{Li}$ plateau. The average observed abundance from eight stars with a positive ${}^6\text{Li}$ detection (HD 106038 is not included) is $\log \epsilon_{6\text{Li}} = 0.82$, i.e. without accounting for any ${}^6\text{Li}$ depletion. Taking the mean ${}^6\text{Li}/{}^7\text{Li}$ of all stars but HD 106038 (unusually high Li abundance) and HD 19445 (expected to have no ${}^6\text{Li}$) together with the mean ${}^7\text{Li}$ abundance of the same stars would instead imply $\log \epsilon_{6\text{Li}} = 0.54$. To both of these estimates should be added the expected ${}^6\text{Li}$ depletion which is ≥ 0.3 dex during the pre-main sequence during which ${}^7\text{Li}$ remains largely intact, as discussed in Sect. 7.3. If, in addition, some ${}^7\text{Li}$ has been destroyed as well this would increase the ${}^6\text{Li}$ depletion further.

7.2. The Lithium Problems

Since Spite & Spite's (1982) seminal paper, the lithium abundance of metal-poor warm dwarfs has been widely equated with the abundance provided by the Big Bang. The predicted abundance from a standard Big Bang is dependent on one free parameter, namely, the baryon density. Now, the free parameter is determined independently of any inferred primordial abundances from the WMAP-observations of the anisotropies of the cosmic microwave background: ${}^7\text{Li}/\text{H} = 4.4 \pm 1.0 \cdot 10^{-10}$ or $\log \epsilon_{7\text{Li}} = 2.65 \pm 0.1$ (Coc et al. 2004; Cuoco et al. 2004; Cyburt 2004). As different calculations yield slightly different results even when adopting exactly the same baryon density, we have taken an average of the cited results. These same calculations show that very little ${}^6\text{Li}$ is synthesised, say ${}^6\text{Li}/{}^7\text{Li} \sim 10^{-5}$.

While the predictions from standard Big Bang nucleosynthesis are in good agreement with the mean deuterium abundance from the six available damped Ly- α systems (e.g. Steigman 2005 and references therein), they are in substantial conflict with the observations for Li. The ${}^7\text{Li}$ problem is now well established: the inferred primordial ${}^7\text{Li}$ abundance is about 0.5 dex less than the prediction. As will become clear from the discussion in Sect. 7.4, our survey has in addition identified a ${}^6\text{Li}$ problem: the observed high ${}^6\text{Li}$ abundance at very

low $[\text{Fe}/\text{H}]$ can not be explained by neither standard Big Bang nucleosynthesis nor apparently by Galactic cosmic ray spallation and α -fusion reactions. Possible resolutions of these problems were reviewed by Lambert (2004). It should also be noted that the problem of reconciling the inferred and predicted ${}^7\text{Li}$ abundance is not entirely decoupled from the goal of achieving an understanding of the synthesis of ${}^6\text{Li}$. Possible modes of ${}^6\text{Li}$ synthesis imply simultaneous synthesis of ${}^7\text{Li}$ but this aggravates the severity of the ${}^7\text{Li}$ problem. In turn, the presence of ${}^6\text{Li}$ constrains the possible explanations invoked for the ${}^7\text{Li}$ problem.

The solution to the ${}^7\text{Li}$ problem may lie in one or more of the following areas:

Systematic errors in the abundance analysis: The introduction of an abundance analysis based on 3D model atmospheres and non-LTE line formation for the lithium resonance and subordinate lines has not resulted in a significant upward revision of the lithium abundance obtained from 1D atmospheres and LTE or non-LTE line formation. The derived lithium abundance is dependent on the adopted T_{eff} -scale but this cannot accommodate the higher temperatures necessary to bring inferred and predicted abundance into agreement (see Sec. 4.1 and 7.1). Although the last word has not been said on the representation of the physics of the stellar atmospheres and the formation of the lithium lines, it would be extremely surprising were systematic errors in these areas be shown to resolve the lithium problem.

Present-day abundances do not reflect the primordial Li abundance: Dilution and destruction of lithium in metal-poor stars are discussed in the following section (Sec. 7.3).

Erroneous nuclear reaction rates: Nuclear reactions included in the customary networks have been well studied and uncertainties in the reaction rates at the relevant temperatures for Big Bang nucleosynthesis cannot be held responsible for the lithium problem. Coc et al.'s (2004) suggestion that addition to the network of a previously neglected reaction – ${}^7\text{Be}({}^2\text{D}, p)2\ {}^4\text{He}$ – might possibly reduce the predicted ${}^7\text{Li}$ abundance is not substantiated by a cross-section measurement (Angulo et al. 2005). (${}^7\text{Be}$ decays to ${}^7\text{Li}$ following Big Bang nucleosynthesis.) Based on the measured solar neutrino flux, Cyburt et al. (2004) have been able to show that employed nuclear data for the ${}^3\text{He}(\alpha, \gamma){}^7\text{Be}$ reaction can not be in error by a large factor as to modify the predicted ${}^7\text{Li}$ abundances significantly.

Non-standard Big Bang nucleosynthesis: Comments on the synthesis of the lithium isotopes by non-standard Big Bang models are included in our discussion of the synthesis of ${}^6\text{Li}$ in Sec. 7.4.

7.3. Lithium Destruction and Dilution in Halo Stars

Identification of the primordial lithium abundance from the Spite plateau with the abundance provided by the Big Bang rests on the assumption that the lithium abundance of the atmosphere of a star on the plateau has been unchanged since the star was formed from gas having the lithium abundance provided by the Big Bang. Perhaps, the most promising solution to the lithium problem represents a failure of this assumption. Solutions have consequences for the correction of observed

${}^6\text{Li}$ abundances to the ${}^6\text{Li}$ abundance of the gas from which a star formed.

In standard stellar models, the expected depletion of ${}^7\text{Li}$ for metal-poor turn-off stars is negligible, i.e., less than 0.02 dex (Deliyannis et al. 1990; Pinsonneault et al. 1992). A larger depletion, ≥ 0.3 dex, is predicted for ${}^6\text{Li}$ with most of this occurring during the pre-main sequence phase when ${}^6\text{Li}$ is destroyed by protons at the base of the star's deep convective envelope (e.g. Richard et al. 2005). The cross-section for destruction of ${}^6\text{Li}$ is about 60 times greater than for ${}^7\text{Li}$. Destruction of ${}^6\text{Li}$ is predicted to increase sharply with decreasing stellar mass for main sequence stars below the turn-off. Evidently, depletion (destruction) of ${}^7\text{Li}$ is according to standard models not the answer to the lithium problem but is a factor to be considered when we turn to examine synthesis of ${}^6\text{Li}$.

The search for a solution to the lithium problem then turns to investigation of non-standard models of stellar evolution (Lambert 2004). Physical processes neglected by standard models but incorporated into non-standard models in connection with halo stars in recent years include rotationally-induced mixing (e.g. Vauclair 1988; Chaboyer & Demarque 1994; Pinsonneault et al. 1999, 2002; Piau 2005), diffusion⁴ (e.g. Michaud et al. 1984; Salaris & Weiss 2001; Richard et al. 2002; 2005) and internal gravity waves (e.g. Talon & Charbonnel 2004; Charbonnel & Talon 2005), sometimes working in tandem with other mechanisms such as mass loss (e.g. Vauclair & Charbonnel 1995) and turbulent mixing. In most cases, the predictive power of these processes is restricted by their need to introduce one or more free parameters.

We comment briefly on two non-standard models drawn from the suite of proposals: rotationally-induced mixing and diffusive separation. An obvious requirement of successful non-standard models is that they provide a depletion of surface lithium by about 0.5 dex over the 10-13 Gyr life of the observed stars (we take it as given that the stars began life with the WMAP-inferred predicted lithium abundance.) Surely, a more demanding requirement (and a certain clue to the dominant process) is that this depletion be achieved uniformly over the observed sample of stars spanning a range in mass, metallicity, age, and rotational angular momentum: the depletion sought is about 0.5 dex with a star-to-star scatter of not more than about 0.03 dex. Our present interest is in identifying non-standard models that may solve the lithium problem and in obtaining an estimate of the correction to be applied to a ${}^6\text{Li}$ abundance to obtain the star's original ${}^6\text{Li}$ abundance.

A description of lithium destruction from rotationally-induced mixing depends on processes and initial conditions that are as yet poorly known, including the initial distribution of angular momentum in the star, the transport of angular momentum through the star and its loss from the surface, and attendant mixing of the interior material. To make progress requires calibrations using observations of rotational velocities and lithium abundances for stars, e.g., the Sun and stars belonging to open clusters. Calibrations have not involved metal-poor dwarfs. A probable result of rotational effects on lithium depletion is a spread in the final lithium abundance for

⁴ The term diffusion normally includes the effects of gravitational settling, thermal diffusion and radiative acceleration.

a sample of stars differing only in their rotational characteristics. One expects lithium depletion to be most severe for the stars initially rotating rapidly and least severe to vanishingly small for the slowest rotators. Then, the observed (small) spread in lithium abundances on the Spite plateau is, in principle, an indicator of rotationally-induced depletion of lithium. Conversion of the observed spread to an indicator of depletion depends on the description of rotational-induced mixing and the attendant calibrations.

The recipe and calibrations (Sun, open clusters) invoked by Pinsonneault et al. (1999) show that the depletion of ${}^7\text{Li}$ (D_7 in dex) was related to the dispersion (σ in dex) where $\sigma/D_7 \simeq 0.4$ and, hence, the required depletion by 0.5 implies $\sigma = 0.2$, a value far in excess of the observed upper limit. The depletions of ${}^7\text{Li}$ and ${}^6\text{Li}$ were predicted to be correlated: $D_7/D_6 \simeq 0.4$ yielding $D_6 \approx 1.2$ dex. Given that the observed $\log \epsilon_{6\text{Li}} \simeq 0.8$ for the stars with detected ${}^6\text{Li}$, the initial abundance would have been $\log \epsilon_{6\text{Li}} \simeq 2.0$, the value that has historically been identified with the Spite plateau for ${}^7\text{Li}$ and, more importantly, a value that implies most or all of the ${}^7\text{Li}$ came from synthesis by cosmic rays and not from the Big Bang! Pinsonneault et al. (2002) argue that the Li data of Ryan et al. (1999), who like us measured $\sigma_{\text{obs}} = 0.03$ dex, imply a most-likely ${}^7\text{Li}$ depletion of 0.13 dex although destruction factors as high as 0.3 dex were not ruled out. The corresponding ${}^6\text{Li}$ destruction is then ≥ 0.3 dex, and $\log \epsilon_{6\text{Li}} \geq 1.1$ for our stars with ${}^6\text{Li}$ detections. In summary, rotationally-induced mixing as presented in the models of Pinsonneault et al. appears not to be the solution to the ${}^7\text{Li}$ problem.

Stars on the Spite plateau have a thin convective envelope of uniform composition. Atomic diffusion occurs in the radiative zone below the convective envelope. The base of the latter mixes with and attains the composition of the top of the radiative zone. Diffusion is a slow process but is predicted to be effective in the halo dwarfs because of their great age and their thin convective envelopes. The diffusive velocity decreases with increasing density. Since the stars at the turn-off have the thinnest envelopes, the effects of diffusion on surface composition are likely to be more severe for these stars than for stars further down the main sequence. Lithium is predicted to diffuse inwards in the radiative zone and the surface abundance to decrease. Inward diffusion of lithium can result in its destruction by protons.

Model calculations including diffusion suggest that the lithium abundance for stars on the Spite plateau can be reduced to the observed level from a starting value corresponding to the WMAP-based prediction (Salaris & Weiss 2001; Richard et al. 2002; Richard et al. 2005). The earliest calculations (Michaud et al. 1984), as well as recent ones (Salaris & Weiss 2001), predicted lower lithium abundances for stars at the hot end of the plateau, in contradiction to the observations. Richard and colleagues invoke ‘turbulent diffusion’ with a recipe that restores uniform lithium abundance to the plateau; this extra turbulence could for example be induced by stellar rotation, which would limit the diffusion but not necessarily mix Li to sufficiently high temperatures where it is burnt by nuclear reactions as in the models by Pinsonneault et al. (1999, 2002) and others described above. Richard et al. (2002, 2005 and private communication)

have presented detailed calculations of the combined effects of diffusion and a parameterized recipe for turbulent diffusion. The predicted ${}^7\text{Li}$ and ${}^6\text{Li}$ depletion factors for our program stars based on their calculations are given in Table 6. We note that the pre-main sequence depletion factors are likely more uncertain than the main sequence and post-main sequence counterparts (Proffitt & Michaud 1989). Furthermore, we note that the predictions are presently available only for a very limited number of metallicities, and thus many depletion estimates in Table 6 are based on extrapolations, which likely introduce further uncertainties, in particular towards higher $[\text{Fe}/\text{H}]$. For the disk stars HD 68284 and HD 130551, in which ${}^6\text{Li}$ has been detected (Nissen et al. 1999), we estimate the pre-main sequence ${}^6\text{Li}$ depletion to be about 1 dex; these two stars have nearly identical mass and $[\text{Fe}/\text{H}]$, which explains their similarity in depletion in spite of their T_{eff} differences.

The following results are pertinent to our discussion. One, there is a recipe for the turbulent diffusion (the so-called T6.25 model) that reduces the Big Bang lithium abundance by 0.4 – 0.5 dex for turn-off stars to the observed value and preserves a largely flat plateau (Richard et al. 2005). Two, simulations suggest that stars of different ages and metallicities may have lithium quite uniformly depleted, but a quantitative comparison with the small scatter reported by us and others was not made. Third, ${}^6\text{Li}$ is partly destroyed during the pre-main sequence evolution even without any accompanying ${}^7\text{Li}$ destruction; due to the lower T_{eff} in general for our higher $[\text{Fe}/\text{H}]$ stars, the observed ${}^6\text{Li}$ plateau becomes tilted when accounting for this depletion (Fig. 23). Fourth, any substantial ${}^7\text{Li}$ destruction is accompanied by an even larger ${}^6\text{Li}$ depletion; for example, the T6.25 model which provides a 0.4 dex depletion of ${}^7\text{Li}$ predicts 1.6 dex depletion for ${}^6\text{Li}$ in LP 815-43, in addition to about 0.3 dex ${}^6\text{Li}$ destruction during the pre-main sequence phase. It then follows that the stars with ${}^6\text{Li}$ detections began with $\log \epsilon_{7\text{Li}} = 2.6$ and $\log \epsilon_{6\text{Li}} \approx 2.6$ too – not a combination that can be said to reconcile observations with the Big Bang predictions. The choice of a model that provides a smaller ${}^7\text{Li}$ depletion also gives a smaller ${}^6\text{Li}$ depletion; for example, the T6.09 model reduces ${}^7\text{Li}$ by about 0.25 dex (lithium problem is lessened but not eliminated) and ${}^6\text{Li}$ by about 0.6 dex including the pre-main sequence destruction (the initial abundance was $\log \epsilon_{6\text{Li}} \approx 1.4$). The question is whether alternative recipes for turbulent diffusion can resolve the ${}^7\text{Li}$ problem without requiring very high initial ${}^6\text{Li}$ abundances.

Although no quantitative predictions yet exist for Population II stars, a further promising candidate for Li depletion is internal gravity waves, which lead to angular momentum transport and thus mixing (e.g. García López & Spruit 1991; Talon & Charbonnel 2004; Charbonnel & Talon 2005). Recent calculations including these effects successfully reproduce both the quasi-flat solar rotation profile and the degree of Li depletion in disk open clusters as a function of age (Charbonnel & Talon 2005). We are eagerly awaiting similar modelling for metal-poor stars with predictions for the ${}^7\text{Li}$ and ${}^6\text{Li}$ depletions, in particular whether large Li depletions can be achieved while still retaining the small observed abundance scatter.

Our commentary on rotationally-induced mixing and

diffusion shows that plausible (rotationally-induced mixing) and seemingly inevitable (diffusion) processes may solve the ${}^7\text{Li}$ problem, but the observers' challenge to fit the Spite plateau's shallow slope with respect to T_{eff} and $[\text{Fe}/\text{H}]$ and its smoothness are as yet unmet. These potential solutions to the ${}^7\text{Li}$ problem indicate that the observed ${}^6\text{Li}$ abundance is almost certainly a lower bound to the initial ${}^6\text{Li}$ abundance. Some solutions lead to very high initial ${}^6\text{Li}$ abundances that, if correct, imply that our understanding of the pre-galactic and Big Bang nucleosynthesis is poor indeed.

7.4. Lithium Production in the Early Universe

The observed ${}^6\text{Li}$ abundance is several orders of magnitude larger than that predicted from the standard Big Bang. On the assumption that the standard Big Bang sequence is the correct representation of the primordial fireball, synthesis of ${}^6\text{Li}$ is attributed to collisions in the intergalactic or interstellar medium between high-energy particles (cosmic rays) and ambient nuclei. The two leading processes are the $\alpha + \alpha$ fusion reactions and spallation reactions involving protons (also, α s) and ${}^{16}\text{O}$ (also ${}^{12}\text{C}$ and ${}^{14}\text{N}$) nuclei. Both processes also produce ${}^7\text{Li}$ with ${}^7\text{Li}/{}^6\text{Li} \sim 1$ to 2 (Mercer et al. 2001). Only the spallation reactions produce ${}^9\text{Be}$, ${}^{10}\text{B}$, and ${}^{11}\text{B}$. In the classical, or direct, Galactic cosmic ray spallation scenario as formulated by Reeves et al. (1970) and Meneguzzi et al. (1971), the accelerated particles are the protons etc hitting ambient interstellar CNO nuclei. As a consequence, this reaction is secondary in nature: $[\text{Be}/\text{H}] \propto [\text{O}/\text{H}]^2$. In inverse spallation the collisions instead occur through fast CNO nuclei and interstellar protons and α -particles. Since the CNO nuclei are both produced and accelerated by supernovae, the resulting spallation yields will be essentially independent of the metallicity, a primary process: $[\text{Be}/\text{H}] \propto [\text{O}/\text{H}]$. One possible way of achieving this is through superbubbles (Higdon et al. 1998; Parizot & Drury 1999 but see Prantzos 2005, 2006 for a critique of this scenario): a sequence of supernovae in rapid succession in a cluster or OB association accelerates nuclear-process enriched material. Establishing the behaviour of $[\text{O}/\text{Fe}]$ with metallicity is clearly important for estimating the spallation production rate but unfortunately no unanimous verdict have appeared to date in this regard (e.g. Israelian et al. 1998, 2001; Boesgaard et al. 1999; Asplund & García Pérez 2001; Nissen et al. 2002; Fulbright & Johnson 2003; García Pérez et al. 2006).

Since spallation reactions are thought to be the sole process by which Be is synthesised and the Be abundance is obtainable for stars on the Spite plateau (Boesgaard et al. 1999; Primas et al., in preparation), the efficiency of a proposed scenario invoking spallation may be rather well calibrated using observed Be abundances. The simultaneous production from the $\alpha + \alpha$ fusion reactions is not simply calibratable. The observed ${}^6\text{Li}/\text{Be}$ ratio shows that the ${}^6\text{Li}$ must be produced primarily from the fusion reactions at low metallicities with Be necessarily from spallation; the meteoritic ${}^6\text{Li}/\text{Be}$ ratio (≈ 6) is a representative measure of the production ratios for spallation but the ratio is ≈ 40 for HD 84937 (Smith et al. 1998) and may reach ≈ 150 for LP 815-43 (Primas et al., in preparation). The initial ${}^6\text{Li}/\text{Be}$ ratios were likely even greater due to ${}^6\text{Li}$ depletion, underscoring the need for $\alpha + \alpha$ fusion reactions.

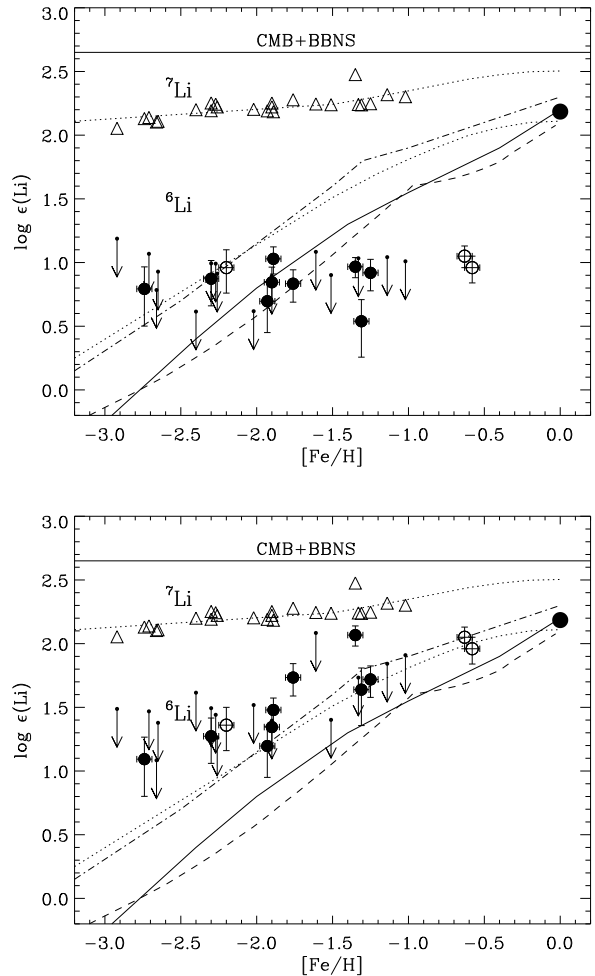


FIG. 23.— *Upper panel:* Observed logarithmic abundances of ${}^7\text{Li}$ (open triangles) and ${}^6\text{Li}$ (solid circles) as a function of $[\text{Fe}/\text{H}]$ for our program stars; 3σ upper limits to the ${}^6\text{Li}$ abundances are denoted with arrows. Also shown as open circles are the ${}^6\text{Li}$ detections in the halo turn-off star HD 84937 (Smith et al. 1993, 1998; Cayrel et al. 1999) and in the two Galactic disk stars HD 68284 and HD 130551 (Nissen et al. 1999). The large circle correspond to the solar system meteoritic ${}^6\text{Li}$ abundance (Asplund et al. 2005), while the horizontal solid line is the predicted ${}^7\text{Li}$ abundance from Big Bang nucleosynthesis and the baryon density as determined by WMAP (Spergel et al. 2003; Coc et al. 2004; Cuoco et al. 2004; Cyburt 2004). The (lower) solid, dashed, (lower) dotted and dash-dotted lines correspond to the models for cosmic ray ${}^6\text{Li}$ production by Prantzos (2006), Ramaty et al. (2000), Fields & Olive (1999) and Vangioni-Flam et al. (2000), respectively; see text for details. The higher dotted line shows the ${}^7\text{Li}$ abundance assuming the Fields & Olive model with a ${}^7\text{Li}/{}^6\text{Li}$ production ratio of 1:1.5 and a primordial abundance of $\log \epsilon_{7\text{Li}} = 2.1$. *Lower panel:* Same as in the upper panel but taking into account the predicted pre-main sequence ${}^6\text{Li}$ depletion from Richard et al. (2002, 2005; and 2005, private communication) to the observed ${}^6\text{Li}$ abundances; these are the minimum values corresponding to negligible ${}^7\text{Li}$ depletion (see Sect. 7.3 for details).

A large number of Galactic chemical evolution models including spallation and α -fusion reactions have been presented in recent years and compared with observed Li, Be and B isotopic abundances (e.g. Yoshii et al. 1997; Fields & Olive 1999; Parizot 2000; Vangioni-Flam et al. 2000; Ramaty et al. 2000; Suzuki & Yoshii 2001; Al-

ibes et al. 2002; Prantzos 2005, 2006). Four representative predictions are presented in Fig. 23: the model by Fields & Olive (1999) is based on direct cosmic ray spallation but with a very steep [O/Fe] trend (Israeli et al. 1998; Boesgaard et al. 1999); the model by Ramaty et al. (2000) is for inverse spallation with special consideration of the energetics of the light element production; the Vangioni-Flam et al. (2000) model is for inverse spallation in superbubbles with an assumed low energy ($\lesssim 30$ MeV/nucleon) cosmic ray component (Meneguzzi & Reeves 1975); and the calculations by Prantzos (2006) assume that the cosmic ray composition does not vary with time and that the light isotopes are produced as primaries, i.e. like in the inverse spallation models. These calculations fit about equally well the observed run of the Be abundance with the Fe abundance, although Ramaty et al. (2000) argue that the Fields & Olive Be production is significantly overestimated through the adoption of unrealistic Fe yields. A fair fit to the observed ${}^6\text{Li}$ abundance in HD 84937 (previously the sole data point for this isotope) when ignoring the inevitable pre-main sequence destruction is achieved for the Fields & Olive and Vangioni-Flam et al. models but it requires some assumptions to maximise ${}^6\text{Li}$ production. There are other problems and difficulties with the calculations: for example, the efficiency assumed for cosmic ray acceleration may be unrealistic given the available kinetic energy from supernovae, which may rule out the low energy cosmic ray scenario (Ramaty et al. 2000; Suzuki & Yoshii 2001; Prantzos 2005, 2006). Furthermore, several of the spallation models presented here invoke a [O/Fe] trend that is significantly higher than observed by Nissen et al. (2002) and us (Sect. 4.4); note that in addition our adopted solar O abundance is 0.1 – 0.2 dex lower than assumed by Fields & Olive and Ramaty et al. As a consequence, their predicted ${}^6\text{Li}$ abundances should be shifted downwards by ≈ 0.3 dex for $[\text{Fe}/\text{H}] \leq -2$. Finally, the subsequent downward revision by a factor of two of the measured cross-section for ${}^6\text{Li}$ production by α -fusion (Mercer et al. 2001) will further push the predictions to lower yields for all but the Prantzos model.

Now that additional ${}^6\text{Li}$ detections are available with the high ${}^6\text{Li}$ abundance in LP 815-43 in particular, it is clear that the model calculations do not reproduce the ${}^6\text{Li}$ measurements and the apparent observed ${}^6\text{Li}$ plateau. Of the here presented models, the one by Prantzos (2006, shown as a solid line in Fig. 23) is likely the most realistic as it requires the least number of assumptions in terms of maximising the production efficiency and is based on the most recent reaction cross-sections. Still we note that it makes the as yet unproven assumption that the cosmic ray composition stays constant with time and thus may well overestimate the ${}^6\text{Li}$ production. The discrepancy between models and observations at low $[\text{Fe}/\text{H}]$ is further aggravated when accounting for the pre-main sequence ${}^6\text{Li}$ depletion of ≥ 0.3 dex (Table 6), as seen in Fig. 23; invoking any significant amount of ${}^7\text{Li}$ depletion would make the situation worse still (Sect. 7.3). The inclusion of ${}^6\text{Li}$ pre-main sequence depletion tilts the ${}^6\text{Li}$ observations to follow roughly the metallicity-dependence of the models, albeit at a higher ${}^6\text{Li}$ abundance; we recall here that the pre-main sequence depletion calculations are rather uncertain and that most of the ${}^6\text{Li}$ depletion may in fact take place during the

main sequence. At face value, it seems like a remarkable coincidence that the ${}^6\text{Li}$ production from cosmic ray spallation and Li-depletion can result in a nearly flat ${}^6\text{Li}$ abundance plateau as observed. However, we do note that we are only able to detect ${}^6\text{Li}/{}^7\text{Li}$ ratios of $\gtrsim 0.02$ for observational reasons and thus would not be able to identify the stars in which the depletion is much larger than the corresponding production.

A means to boost the light element production over direct and indirect cosmic ray spallation in the interstellar medium has recently been put forward by Nakamura et al. (2006, see also Fields et al. 1996 and Nakamura & Shigeyama 2004). They speculate that the fast CNO-rich ejecta of very energetic ($\approx 10^{52}$ erg = 10^{45} J) supernovae having lost all but a small fraction of their H- and He-rich envelopes can interact directly with the circumstellar material without shock acceleration of cosmic rays. Such SNe Ic events may produce significant amounts of primary ${}^6\text{Li}$ and ${}^9\text{Be}$ under suitable conditions. Nakamura et al. (2006) have identified a parameter space that seem to explain the high ${}^6\text{Li}/\text{O}$ ratio we observe in LP 815-43 but it requires some fine-tuning in regards the explosion energy and the amount of available He in the ejecta. It remains to be seen whether real supernovae fulfill these requirements.

An additional and alternative scenario places lithium synthesis by $\alpha + \alpha$ fusion reactions during the formation of the Galaxy within the framework of hierarchical structure formation (Suzuki & Inoue 2002, 2004). Infalling and merging subgalactic clumps would have produced shocks that could have accelerated the α -particles at early epochs. Due to our incomplete understanding of the details of galaxy formation, models for the accompanying ${}^6\text{Li}$ production by necessity include several free parameters. To achieve the observed high ${}^6\text{Li}$ abundances at $[\text{Fe}/\text{H}] \leq -2.3$ requires strong structure formation shocks to have been in place very early on (≈ 0.1 Gyr after Big Bang) but vanished relatively shortly thereafter (≈ 0.1 Gyr). An argument against this scenario is that mergers in ΛCDM continue to the present day with only a relatively small dark matter halo present at early times, which would appear to make it difficult for the necessary strong shocks to have formed during the required time interval (Prantzos 2006). Rollinde et al. (2005, see also Montmerle 1977) have presented a similar scenario of pre-Galactic production of ${}^6\text{Li}$ (and ${}^7\text{Li}$) due to an ad-hoc early burst of cosmological cosmic rays, possibly due to Population III stars. The energetics of such a production were not investigated. Prantzos (2006) also speculate that accretion to a supermassive black hole such as the one believed to exist currently in the Galactic center could generate sufficient energy to accelerate the necessary cosmic rays. This scenario requires some extreme assumptions about the time of its formation and its efficiency in converting accretion energy to particle acceleration to produce sufficient ${}^6\text{Li}$ at $[\text{Fe}/\text{H}] \approx -2.7$.

The final potential site for ${}^6\text{Li}$ synthesis is the Big Bang. In a standard Big Bang much too little ${}^6\text{Li}$ is produced to explain our observations. An extension of the standard model for particle physics such as supersymmetry predicts the existence of various exotic particles, including the gravitino, axion and the neutralino; the first two of these particles are predicted to be unstable but the neutralino is likely stable. The decay and

the annihilation during or shortly after the era of Big Bang nucleosynthesis can alter the resulting light element abundances, provided the masses and life-times of these putative particles are right (e.g. Dimopoulos et al. 1988; Jedamzik 2000, 2004a,b, 2005; Kawasaki et al. 2004; Ichikawa et al. 2004). The annihilation of the neutralino can release sufficient energy to produce ${}^6\text{Li}$ by non-thermal reactions like ${}^3\text{H}(\alpha, n){}^6\text{Li}$ and ${}^3\text{He}(\alpha, p){}^6\text{Li}$ (Jedamzik 2004a). The amount of ${}^6\text{Li}$ produced depends on the mass of the neutralino and the exact annihilation channels but can reach the levels observed in some of our very metal-poor stars; this scenario does not, however, resolve the ${}^7\text{Li}$ dilemma described above. Another option to produce ${}^6\text{Li}$ is through the decay of particles like the gravitino and axion. While the electromagnetic decay routes of such particles result in ${}^3\text{He}/\text{D}$ ratios inconsistent with observations (Ellis et al. 2005), the injection of energetic nucleons through the hadronic decay about 10^3 s after Big Bang can lead to substantial ${}^6\text{Li}$ production without spoiling the agreement with D and the He isotopes. Indeed, for the right combination of particle properties, a simultaneous production of ${}^6\text{Li}$ and destruction of ${}^7\text{Li}$ appears achievable and may explain both the observed ${}^6\text{Li}$ plateau and the low ${}^7\text{Li}$ abundances in comparison with standard Big Bang nucleosynthesis (Jedamzik 2004b, 2005). Thus, both of the Li problems can conceivably be solved at the same time. While these ideas are very attractive, they rest on as yet unproven and speculative physics.

8. CONCLUDING REMARKS

Remarkable as it may have seemed in 1982 following the discovery of the Spite plateau and the near-universal association of the plateau’s lithium abundance with primordial nucleosynthesis, the debate over that association has not been stilled. Two key recent factors heating the debate have been the measurement of the Big Bang’s photon-to-baryon ratio (η) using the WMAP measurements of the anisotropies in the cosmic microwave background and the detections, here and previously, of the lighter isotope ${}^6\text{Li}$. A standard model of the Big Bang with the WMAP estimate of η predicts a lithium (${}^7\text{Li}$) abundance greater by about 0.5 dex than the value generally attributed to the Spite plateau, and a ${}^6\text{Li}$ abundance several orders of magnitude below the value reported here.

These two discrepancies resist simple resolution, as should be clear from the discussion in Section 7. One supposes that resolution of the discrepancies may be found in one or more of the following three areas:

1. *Composition of the gas from which stars on the Spite plateau formed*

Ignoring the possibility that the ${}^6\text{Li}$ was synthesised after the formation of the star, a conjecture is that ${}^6\text{Li}$ was synthesised either in a non-standard Big Bang (e.g., hadronic decays of exotic particles resulting in post-processing the ${}^7\text{Li}$ from a standard Big Bang) or through $\alpha - \alpha$ fusion reactions in the proto-Galaxy (e.g. hierarchical structure formation shocks and/or supermassive black holes). Introduction of a non-standard Big Bang may lower the predicted ${}^7\text{Li}$ abundance and increase the predicted ${}^6\text{Li}$ abundance. Qualitatively, these changes resolve both discrepancies provided that points 2 and 3 below do not come into play. Addition of lithium synthe-

sis from fusion reactions in pre-Galactic gas, as the sole additional site over a standard Big Bang, may remove the ${}^6\text{Li}$ discrepancy but may aggravate the discrepancy between the predicted ${}^7\text{Li}$ abundance and the observed abundance, unless one adopts the heresy that the WMAP estimate of η should be replaced by the lower value that results in the minimum synthesis of ${}^7\text{Li}$. (The nuclear reaction network appears to be free of significant uncertainties.)

2. *Relationship between the stars’ initial composition set 10 – 13 Gyr ago and the present composition of their stellar atmospheres*

There is tension on this point between those who stress the significance of the observed very small scatter of the lithium abundances along the Spite plateau and those who identify physical processes that ought to change the atmospheric compositions of plateau residents (Section 7.4). The very small scatter would seem to imply that the change in surface lithium abundance has been itself slight. Yet, some argue that reduction of the lithium abundance through diffusion, perhaps supplemented by rotationally-induced mixing and other processes, must occur but can result in a small star-to-star scatter of lithium abundances. The presence of ${}^6\text{Li}$, as we noted, complicates interpretations that rely on depletion/destruction of ${}^7\text{Li}$ to reduce the WMAP-based Big Bang ${}^7\text{Li}$ abundance to the observed value for the Spite plateau; very high to extraordinarily high initial ${}^6\text{Li}$ abundances may be implied. There are clearly open questions for pursuit by observers.

Diffusion does not exclusively act on lithium. Relative abundances of abundant elements are changed but these elements are not subject to destruction as lithium is. Alterations of the abundances are lessened and then removed as stars evolve from the main sequence to subgiants and then to giants. Careful comparisons of stars along this sequence might confirm that diffusion was operable in their main sequence progenitors. At present, abundance data from dwarfs and giants have given seemingly consistent results for composition as a function of metallicity, i.e., the same run of $[\text{X}/\text{Fe}]$ versus $[\text{Fe}/\text{H}]$ (e.g. Gratton et al. 2001).

3. *Measurement of the present ${}^6\text{Li}$ and ${}^7\text{Li}$ abundances*

Systematic errors are now unlikely to be uncovered that will lift the Spite plateau’s lithium abundance by the 0.5 dex to match the Big Bang WMAP-based abundance (Section 7.1). The adjustments (e.g. the necessary increase of effective temperatures by about 700 K) unless specific to lithium would result in large changes to abundances of other elements. Presently, there is generally good agreement between the compositions of metal-poor dwarfs and giants of the same metallicity and this agreement would be compromised unless adjustments were also made to the abundance analyses of giants with their very different atmospheric structures. The simplest conceivable adjustment – raising the effective temperatures by 700 K – introduces more problems than the one it solves.

Absence of systematic errors affecting the determination of the ${}^6\text{Li}/{}^7\text{Li}$ ratio cannot be so strongly dismissed: the presence of ${}^6\text{Li}$ is deduced from a slight additional asymmetry to the intrinsically asymmetric ${}^7\text{Li}$ line. The various tests outlined in Sect. 5 give confidence that

${}^6\text{Li}$ has indeed been detected. This confidence should be tested by observations of additional stars like HD 19445 for which pre-main sequence destruction of ${}^6\text{Li}$ is so great that this isotope should be undetectable. Obviously, additional ${}^6\text{Li}$ observations at very low $[\text{Fe}/\text{H}]$ would be extremely valuable, including a confirmation of our detection in LP 815-43.

The confidence commonly and frequently expressed after 1982 that primordial lithium had been discovered and measured and could be matched with a prediction from a standard Big Bang is today weakened. There remains a belief that much of the lithium is traceable to primordial nucleosynthesis but quantitative agreement between prediction and observation of the ${}^6\text{Li}$ and ${}^7\text{Li}$ abundances in stars on the Spite plateau is proving elusive. Observers will suppose that well designed additional spectroscopic analyses of metal-poor stars will provide some of the clues necessary to determining the primordial abundance of the two lithium isotopes. Theoreticians may combine these clues with other evidence and probe deeper into primordial nucleosynthesis. Interest in the lithium of the

Spite plateau is greater than in 1982, even as the lack of concordance between predictions of the standard Big Bang and measured lithium abundances has been demonstrated.

This paper has benefitted from helpful assistance, illuminating discussions and penetrating questions from numerous colleagues, including Paul Barklem, Lars Bergström, Corinne Charbonnel, Bengt Gustafsson, Susume Inoue, Karsten Jedamzik, Georges Michaud, John Norris, Keith Olive, Olivier Richard, Gary Steigman, Elisabeth Vangioni and Achim Weiss. We thank Wako Aoki for kindly providing the Subaru spectrum of HD 140283 for an independent analysis and Piercarlo Bonifacio for sharing the results of the First Stars program prior to publication. This work has been supported by the Australian Research Council through the grants DP0342613 and DP0558836. DLL acknowledges the support of the Robert A. Welch Foundation of Houston, Texas.

REFERENCES

- Ali, A.W., & Griem, H.R. 1966, *Phys. Rev.*, 144, 366
 Alibes, A., Labay, J., & Canal, R. 2002, *ApJ*, 571, 326
 Allende Prieto, C., Asplund, M., López, R.J.G., & Lambert, D.L. 2002, *ApJ*, 567, 544
 Alonso, A., Arribas, S., & Martínez-Roger, C. 1995, *A&A*, 297, 197
 Alonso, A., Arribas, S., & Martínez-Roger, C. 1996, *A&A*, 313, 873
 Andersen, J., Gustafsson, B., & Lambert, D.L. 1984, *A&A*, 136, 65
 Angulo, C., et al. 2005, *ApJ*, 630, L105
 Aoki, W., et al. 2006, *ApJ*, in press [astro-ph/0509206]
 Aoki, W., Inoue, S., Kawanomoto, S., Ryan, S.G., Smith, I.M., Suzuki, T.K., & Takada-Hidai, M. 2004, *A&A*, 428, 579
 Asplund, M. 2005, *ARA&A*, 43, 481
 Asplund, M., Carlsson, M., & Botnen, A.V. 2003, *A&A*, 399, L31
 Asplund, M., & García Pérez, A.E. 2001, *A&A*, 372, 601
 Asplund, M., Grevesse, N., Sauval, A.J. 2005, in: *Cosmic abundances as records of stellar evolution and nucleosynthesis*, Bash FN, Barnes TG (eds.), ASP Conf. series vol. 336, p. 25 [astro-ph/0410214]
 Asplund, M., Grevesse, N., Sauval, A.J., Allende Prieto, C., & Kiselman, D. 2004, *A&A*, 417, 751
 Asplund, M., Gustafsson, B., Kiselman, D., & Eriksson, K. 1997, *A&A*, 318, 521
 Asplund, M., Nordlund, Å., Trampedach, R., Allende Prieto, C., & Stein, R.F. 2000, *A&A*, 359, 729
 Asplund, M., Nordlund, Å., Trampedach, R., & Stein, R.F. 1999, *A&A*, 346, L17
 Barklem, P.S., & Asplund-Johansson, J. 2005, *A&A*, 435, 373
 Barklem, P.S., Belyaev, A.K., & Asplund, M. 2003, *A&A*, 409, L1
 Barklem, P.S., Piskunov, N., & O'Mara, B.J. 2000a, *A&A* 363, 1091
 Barklem, P.S., Piskunov, N., & O'Mara, B.J. 2000b, *A&AS*, 142, 467
 Barklem, P.S., Stempels, H.C., Allende Prieto, C., Kochukhov, O.P., Piskunov, N., & O'Mara, B.J. 2002, *A&A* 385, 951
 Belyaev, A.K., & Barklem, P.S. 2003, *Phys. Rev. A*, 68, 2703
 Bessell, M.S., & Norris, J. 1982, *ApJ*, 263, L29
 Biémont, E., Baudoux, M., Kurucz, R.L., Ansbacher, W., & Pinnington, E.H. 1991, *A&A*, 249, 539
 Boesgaard, A.M., Deliyannis, C.P., King, J.R., Ryan, S.G., Vogt, S.S., & Beers, T.C. 1999, *AJ*, 117, 1549
 Boesgaard, A.M., King, J.R., Deliyannis, C.P., & Vogt, S.S. 1999, *AJ*, 117, 492
 Bonifacio, P., & Molaro, P. 1997, *MNRAS*, 285, 847
 Bonifacio, P., & Molaro, P. 1998, *ApJ*, 500, 175
 Bonifacio, P., Molaro, P., Sivarani, T. et al. 2006, *A&A*, submitted
 Bonifacio, P., et al. 2003, *IAU Joint Discussion*, 15, 39
 Carlsson, M., Rutten, R.J., Bruls, J.H.M.J., & Shchukina, N.G. 1994, *A&A*, 288, 860
 Carney, B.W., Latham, D.W., Laird, J.B., & Aguilar, L.A. 1994, *AJ*, 107, 2240
 Castelli, F., Gratton, R.G., & Kurucz, R.L. 1997, *A&A*, 318, 841
 Cayrel, R., Spite, M., Spite, F., Vangioni-Flam, E., Cassé, M., & Audouze, J. 1999, *A&A*, 343, 923
 Chaboyer, B., & Demarque, P. 1994, *ApJ*, 433, 510
 Charbonnel, C., & Primas, F. 2005, *A&A*, 442, 961
 Charbonnel, C., & Talon, S. 2005, *Science*, 309, 2189
 Coc, A., Vangioni-Flam, E., Descouvemont, P., Adahchour, A., & Angulo, C. 2004, *ApJ*, 600, 544
 Cohen, J.G. 1972, *ApJ*, 171, 71
 Cuoco, A., Iocco, I., Mangano, G., Pisanti, O., & Serpico, P.D. 2004, *Int. J. Mod. Phys. A*, 19, 4431
 Cyburt, R.H. 2004, *Phys. Rev. D*, 70, 023505
 Cyburt, R.H., Fields, B.D., & Olive, K.A. 2004, *Phys. Rev. D*, 69, 123519
 Dekker, H., D'Odorico, S., Kaufer, A., Delabre, B., & Kotzlowski, H. 2000, *SPIE*, 4008, 534
 Dekker, H., Nissen, P.E., Kaufer, A., Primas F., D'Odorico, S., & Hanuschik, R.W. 2002, *SPIE*, 4828, 139
 Deliyannis, C.P., Demarque, P., & Kawaler, S. D. 1990, *ApJS*, 73, 21
 Deliyannis, C.P., & Ryan, S.G. 2000, *BAAS*, 32, 684
 Dimopoulos, S., Esmailzadeh, R., Starkman, G.D., & Hall, L.J. 1988, *ApJ*, 330, 545
 Dravins, D., & Nordlund, Å 1990, *A&A*, 228, 203
 Ellis, J., Olive, K.A., & Vangioni, E. 2005, *Phys. Lett. B*, 619, 30
 ESA 1997, *The Hipparcos and Tycho Catalogues*, ESA SP-1200, (Noordwijk: ESA)
 Feast, M.W. 1966, *MNRAS*, 134, 321
 Fields, B.D., Casse, M., Vangioni-Flam, E., & Nomoto, K. 1996, *ApJ*, 462, 276
 Fields, B.D., & Olive, K.A. 1999, *NewA*, 4, 255
 Fields, B.D., & Prodanović, T. 2005, *ApJ*, 623, 877
 Ford, A., Jeffries, R.D., Smalley, B., Ryan, S.G., Aoki, W., Kawanomoto, S., James, D.J. & Barnes, J.R. 2002, *A&A*, 393, 617
 Frebel, A. et al. 2005, *Nature*, 434, 871
 Fulbright, J.P., & Johnson, J.A. 2003, *ApJ*, 595, 1154
 García López, R.J., & Spruit, H.C. 1991, *A&A*, 377, 268
 García Pérez, A.E., Asplund, M., Primas, F., Nissen, P.E., & Gustafsson, B. 2006, *A&A*, in press [astro-ph/0512290]
 Gray, D.F. 1992, *The Observation and Analysis of Stellar Photospheres*, (Cambridge: CUP)
 Gratton, R. et al. 2001, *A&A*, 369, 87
 Gustafsson, B., Bell, R.A., Eriksson, K., & Nordlund, Å, 1975, *A&A* 42, 407
 Herbig, G.H. 1964, *ApJ*, 140, 702
 Higdón, J.C., Lingenfelter, R.E., & Ramaty, R. 1998, *ApJ*, 509, L33
 Hobbs, L.M., & Thorburn, J.A. 1994, *ApJ*, 428, L25
 Hobbs, L.M., & Thorburn, J.A. 1997, *ApJ*, 491, 772

- Hobbs, L.M., Thorburn, J.A., & Rebull, L.M. 1999, *ApJ*, 523, 797
- Ichikawa, K., Kawasaki, M., & Takahashi, F. 2004, *Phys. Lett. B*, 597, 1
- Israelian, G., García Lopez, R., & Rebolo, R. 1998, *ApJ*, 507, 805
- Israelian, G., Rebolo, R., García Lopez, R., Ramón, J., Bonifacio, P., Molaro, P., Basri, G., & Shchukina, N. 2001, *ApJ*, 551, 833
- Israelian, G., Santos, N.C., Mayor, M., & Rebolo, R. 2001, *Nature*, 411, 163
- Israelian, G., Santos, N.C., Mayor, M., & Rebolo, R. 2003, *A&A*, 405, 753
- Ivanova, D.V., & Shimanskii, V.V. 2000, *Astron. Rep.*, 44, 376
- Jedamzik, K. 2004, *Phys. Rev. Lett.*, 84, 3248
- Jedamzik, K. 2004a, *Phys. Rev. D*, 70, 083510
- Jedamzik, K. 2004b, *Phys. Rev. D*, 70, 063524
- Jedamzik, K., Choi, K.-Y., Roszkowski, L., & Ruiz de Austri, R. 2005, preprint [astro-ph/0512044]
- Kawasaki, M., Kohri, K., & Moroi, T. 2005, *Phys. Rev. D*, 71, 083502
- King, J.R., Deliyannis, C.P., & Boesgaard, A.M. 1996, *AJ*, 112, 2839
- Korn, A.J. 2002, in *ESO Astrophysics Symposia Ser., Scientific Drivers for ESO Future VLT/VLTI Instrumentation*, ed. J. Bergeron & G. Monnet (Heidelberg: Springer), 199
- Kurucz, R.L. 1993, *CD-ROMS # 1*, 13, 18 (Washington, DC: US Government Printing Office)
- Kurucz, R.L., Furenlid, I., Brault, J., & Testerman, L. 1984, *Solar Flux Atlas from 296 to 1300 nm* (New Mexico: National Solar Observatory)
- Lambert, D.L. 2004, in *American Institute of Physics CP743, The New Cosmology*, ed. R.E. Allen, D.V. Nanopoulos, & C.N. Pope, (New York: AIP), 206
- Latham, D.W., Stefanik, R.P., Torres, G., Davis, R.J., Mazeh, T., Carney, B.W., Laird, J.B., & Morse, J.A. 2002, *AJ*, 124, 1144
- Maurice, E., Spite, F., & Spite, M. 1984, *A&A*, 132, 278
- Melendéz, J., & Ramírez, I. 2004, *ApJ*, 615, L33
- Meneguzzi, A., Audouze, J., & Reeves, H. 1971, *A&A*, 15, 337
- Meneguzzi, A., & Reeves, H. 1975, *A&A*, 40, 99
- Mercer, D.J., et al. 2001, *Phys. Rev. C*, 63, 065805
- Michaud, G., Fontaine, G., & Beaudet, G. 1984, *ApJ*, 282, 206
- Montmerle, T. 1977, *ApJ*, 216, 177
- Nakamura, K., Inoue, S., Wanaajo, S., & Shigeyama, T. 2006, *ApJ*, submitted [astro-ph/0601415]
- Nakamura, K. & Shigeyama, T. 2004, *ApJ*, 610, 888
- Nissen, P.E., Akerman, C., Asplund, M., Fabbian, D., & Pettini, M. 2005a, in *IAU Symp. 228, From Li to U: Elemental Tracers of Early Cosmic Evolution*, eds. V. Hill, P. Francois, & F. Primas (Cambridge: CUP), in press
- Nissen, P.E., Asplund, M., Hill, V., & D'Odorico, S. 2000, *A&A*, 357, L49
- Nissen, P.E., Asplund, M., Lambert, D., Primas, F., & Smith, V.V. 2005b, in: *Cosmic abundances as records of stellar evolution and nucleosynthesis*, Bash FN, Barnes TG (eds.), ASP Conf. series vol. 336, p. 55
- Nissen, P.E., Chen, Y.Q., Asplund, M., & Pettini, M. 2004, *A&A*, 415, 993
- Nissen P.E., Lambert D.L., Primas F., Smith V.V., 1999, *A&A*, 348, 211
- Nissen, P.E., Primas, F., Asplund, M., & Lambert, D.L. 2002, *A&A* 390, 235
- Nissen, P.E., & Schuster, W.J. 1997, *A&A*, 326, 751
- Nordlund, Å. 1982, *A&A*, 107, 1
- Nordström, B., et al. 2004, *A&A*, 418, 989
- Norris, J.E., Ryan, S.G., & Stringfellow, G.S. 1994, *ApJ*, 423, 386
- O'Brian, T.R., Wickliffe, M.E., Lawler, J.E., Whaling, W., & Brault, J.W. 1991, *J. Opt. Soc. Am.*, B8, 1185
- Parizot, E. 2000, *A&A*, 362, 786
- Parizot, E., & Drury, L. 1999, *A&A* 349, 673
- Piau, L. 2005, submitted to *ApJ* [astro-ph/0511402]
- Pinsonneault, M. H., Deliyannis, C. P., & Demarque, P. 1992, *ApJS*, 78, 179
- Pinsonneault, M. H., Steigman, G., Walker, T. P., & Narayanan, V. K. 2002, *ApJ*, 574, 398
- Pinsonneault, M. H., Walker, T. P., Steigman, G., & Narayanan, V. K. 1999, *ApJ*, 527, 180
- Prantzos, N. 2005, in: *Chemical abundances and mixing in stars in the Milky Way and its Satellites*, Ed. L. Pasquini & S. Randich, (Heidelberg: Springer), in press
- Prantzos, N. 2006, submitted to *A&A* [astro-ph/0510122]
- Proffitt, C.R., & Michaud, G. 1989, *ApJ*, 346, 976
- Proffitt, C.R., & Michaud, G. 1991, *ApJ*, 371, 584
- Przybilla, N., & Butler, K. 2004, *ApJ*, 610, L61
- Ramaty, R., Scully, S. T., Lingenfelter, R. E., & Kozlovsky, B. 2000, *ApJ*, 534, 747
- Ramírez, I., & Melendéz, J. 2005a, *ApJ*, 626, 446
- Ramírez, I., & Melendéz, J. 2005b, *ApJ*, 626, 465
- Reader, J., Corliss, C.H., Wiese W.L., & Martin, G.A. 1980 *Wavelengths and Transition Probabilities for Atoms and Atomic Ions*, NSRDS-NBS, (Washington: National Bureau of Standards)
- Reddy, B.E., Lambert, D.L., Laws, C., Gonzalez, G., & Covey, K. 2002, *MNRAS*, 335, 1005
- Reeves, H., Fowler, W.A., & Hoyle, F. 1970, *Nature*, 226, 727
- Richard, O., Michaud, G., & Richer, J. 2002, *ApJ*, 580, 1100
- Richard, O., Michaud, G., & Richer, J. 2005, *ApJ*, 619, 538
- Rollinde, E., Vangioni, E., & Olive, K. 2005, *ApJ*, 627, 666
- Ryan, S.G., & Elliott, L. 2005, in *ESO Astrophysics Symposia Ser., Chemical Abundances and Mixing in Stars in the Milky Way and its Satellites*, ed. L. Pasquini & S. Randich, (Heidelberg: Springer), in press
- Ryan, S.G., Beers, T.C., Olive, K.A., Fields, B.D., & Norris, J.E. 2000, *ApJ*, 530, L57
- Ryan, S.G., Gregory, S.G., Kolb, U., Beers, T.C., & Kajino, T. 2002, *ApJ*, 571, 501
- Ryan, S.G., Norris, J.E., & Beers, T.C. 1996, *ApJ*, 471, 254
- Ryan, S.G., Norris, J.E., & Beers, T.C. 1999, *ApJ*, 523, 654
- Salaris, M., & Weiss, A. 2001, *A&A*, 376, 955
- Sansonetti, C.J., Richou, B., Engleman, R., & Radziemski, L.J. 1995, *Phys. Rev. A.*, 52, 2682
- Schuster, W.J., & Nissen, P.E. 1988, *A&AS*, 73, 225
- Smith, G., & Raggett, D. St. J. 1981, *J. Phys. B*, 14, 4015
- Smith, V.V., Lambert, D.L., & Nissen, P.E. 1993, *ApJ*, 408, 262
- Smith, V.V., Lambert, D.L., & Nissen, P.E. 1998, *ApJ*, 506, 405
- Smith, V.V., Vargas-Ferro, O., Lambert, D.L., & Olgin, J.G. 2001, *AJ*, 121, 453
- Spergel, D.N., et al. 2003, *ApJS*, 148, 175
- Spite, F., & Spite, M. 1982, *A&A*, 115, 357
- Stehlé, C., & Hutcheon, R. 1999, *A&AS*, 140, 93
- Steigman, G. 2005, *Journal of Modern Physics E*, in press [astro-ph/0511534]
- Stein, R.F., & Nordlund, Å. 1998, *ApJ*, 499, 914
- Suzuki, T.K., & Inoue, S. 2002, *ApJ*, 573, 168
- Suzuki, T.K., & Inoue, S. 2004, *PASA*, 21, 148
- Suzuki, T.K., & Yoshii, Y. 2001, *ApJ*, 549, 303
- Takeda, Y., Zhao, G., Chen, Y.Q., Qui, H., & Takada-Hidai, M. 2002, *PASJ*, 54, 275
- Talon, S., & Charbonnel, C. 2004, *A&A*, 418, 1051
- Thévenin, F., & Idiart, T. 1999, *ApJ*, 521, 753
- Thorburn, J.A. 1994, *ApJ*, 421, 318
- VandenBerg, D.A., Swenson, F.J., Rogers, F.J, Iglesias, C.A., & Alexander, D.R. 2000, *ApJ*, 532, 430
- Vangioni-Flam, E., Cassé, M., & Audouze, J. 2000, *Phys. Rep.*, 333, 365
- Vauclair, S. 1988, *ApJ*, 335, 971
- Vauclair, S., & Charbonnel, C. 1995, *A&A*, 295, 715
- Volz, U., & Schmoranzler, H. 1996, *Phys. Scripta*, T65, 48
- Welty, D.E., & Hobbs, L.M. 2001, *ApJS*, 133, 345
- Wiese, W.L., Fuhr, J.R., & Deters, T.M. 1996, *J. Phys. Chem. Ref. Data*, Monograph No. 7
- Woosley, S.E., Hartmann, D.H., Hoffman, R.D., & Haxton, W.C. 1990, *ApJ*, 356, 272
- Yan, Z.-C., & Drake, G.W.F. 1995, *Phys. Rev. A*, 52, 4316
- Yan, Z.-C., Tambasco, M., & Drake, G.W.F. 1998, *Phys. Rev. A*, 57, 1652
- Yoshii, Y., Kajino, T., & Ryan, S.G. 1997, *ApJ*, 485, 605

TABLE 1. OBSERVATIONAL DETAILS, INCLUDING DATE OF OBSERVATION, UNIVERSAL TIME FOR THE MIDDLE OF THE EXPOSURE, TOTAL EXPOSURE TIME, SIGNAL-TO-NOISE AROUND THE LI I 670.8 nm LINE IN THE REDUCED SPECTRUM, AND THE MEASURED HELIOCENTRIC RADIAL VELOCITY OF THE STAR.

Star	V [mag]	Date	UTC	t_{exp} [min]	S/N	v_{rad} [km s $^{-1}$]
HD 3567	9.26	2000-07-24	08:43	45	560	-47.3
HD 19445	8.05	2000-08-04	10:13	20	790	-139.7
HD 59392	9.73	2002-02-05	02:53	60	710	267.9
HD 102200	8.74	2002-02-05	07:36	40	610	161.1
HD 106038	10.18	2000-07-23	23:57	60	450	99.6
		2000-07-24	23:56	40	350	99.9
HD 140283	7.21	2000-07-24	23:15	13	1020	-170.4
		2002-02-05	08:52	15	770	-170.4
		2004-08-28	00:38	19	820	-170.6
HD 160617	8.73	2000-07-25	01:34	25	650	100.6
HD 213657	9.66	2000-08-04	07:23	45	640	50.8
HD 298986	10.05	2002-02-05	06:24	80	470	198.3
HD 338529	9.37	2000-07-25	04:12	60	680	-128.3
G 013-009	10.00	2000-07-25	00:43	60	530	58.4
G 020-024	11.13	2000-07-24	02:19	90	430	34.2
		2000-07-25	02:47	90	420	34.5
G 075-031	10.52	2000-07-24	09:46	60	500	57.8
		2000-08-04	09:26	60	500	57.8
G 126-062	9.48	2000-08-04	06:30	45	700	-288.6
BD +09°2190	11.15	2002-02-05	04:25	90	400	266.6
		2002-02-06	05:16	90	400	266.0
BD +03°0740	9.80	2002-02-05	01:03	60	740	174.2
BD -13°3442	10.29	2002-02-06	06:27	90	400	116.1
CD -30°18140	9.95	2000-07-24	05:51	60	450	17.9
		2000-07-25	06:03	25	350	17.9
CD -33°1173	10.94	2002-02-06	01:13	90	610	47.6
CD -33°3337	9.08	2002-02-05	01:57	30	740	73.7
CD -35°14849	10.57	2000-07-24	07:27	90	550	108.0
		2000-07-25	06:33	25	350	108.1
CD -48°2445	10.55	2002-02-06	03:01	100	640	319.2
LP 815-43	10.91	2000-07-24	04:12	90	400	-3.8
		2000-07-25	05:35	40	300	-3.5
		2004-08-30	04:52	150	420	-3.6
		2004-08-31	01:35	150	490	-3.9

TABLE 2. DERIVED VALUES OF EFFECTIVE TEMPERATURE, SURFACE GRAVITY, METALLICITY (AS MEASURED BY Fe II LINES), OXYGEN ABUNDANCE (NON-LTE VALUES FROM THE O I TRIPLET), MICROTURBULENCE AND ABSOLUTE MAGNITUDE.

Star	T_{eff} [K]	$\log g$ [cgs]	[Fe/H]	[O/H]	ξ_{turb} [km s $^{-1}$]	M_V
HD 3567	6026	4.08	-1.14	-0.79	1.5	4.01
HD 19445	5980	4.42	-2.02	-1.38	1.3	5.13
HD 59392	5936	3.99	-1.61	-1.04	1.5	3.97
HD 102200	6062	4.15	-1.25	-0.85	1.3	4.27
HD 106038	5905	4.30	-1.35	-0.76	1.2	4.84
HD 140283	5753	3.70	-2.40	-1.74	1.5	3.35
HD 160617	5990	3.79	-1.76	-1.43	1.5	3.35
HD 213657	6180	3.92	-1.90	-1.34	1.5	3.60
HD 298986	6103	4.22	-1.33	-0.98	1.3	4.41
HD 338529	6335	4.04	-2.26	-1.68	1.5	3.73
G 013-009	6298	3.99	-2.30	-1.71	1.5	3.70
G 020-024	6247	3.98	-1.89	-1.35	1.5	3.72
G 075-031	6000	4.08	-1.02	-0.68	1.3	3.96
G 126-062	6183	4.11	-1.51	-1.05	1.5	4.05
G 271-162	6230	3.93	-2.30	-1.79	1.5	3.61
BD +09°2190	6392	4.09	-2.66	-2.22	1.5	3.89
BD +03°0740	6266	4.04	-2.65	-2.06	1.5	3.93
BD -13°3442	6311	3.86	-2.71	-2.09	1.5	3.43
CD -30°18140	6222	4.11	-1.90	-1.28	1.5	4.06
CD -33°1173	6390	4.28	-2.92	-2.33	1.5	4.36
CD -33°3337	5897	4.01	-1.31	-0.76	1.3	3.92
CD -35°14849	6244	4.30	-2.27	-1.70	1.5	4.56
CD -48°2445	6222	4.25	-1.93	-1.40	1.5	4.42
LP 815-43	6400	4.17	-2.74	-2.20	1.5	4.10

TABLE 3. LI ISOTOPIC ABUNDANCES DERIVED FROM THE LII 670.8NM RESONANCE LINE TOGETHER WITH THE LI ABUNDANCES ESTIMATED FROM THE LII 610.4NM SUBORDINATE LINE. BOTH THE 1D LTE AND NON-LTE LI ABUNDANCES ARE LISTED FOR THE TWO LINES. THE QUOTED UNCERTAINTIES IN THE LTE ABUNDANCES ARE THOSE ONLY DUE TO THE FINITE S/N AND DO NOT FOR EXAMPLE TAKE INTO ACCOUNT ERRORS IN THE STELLAR PARAMETERS. THE SECOND AND THIRD COLUMN GIVE THE PROJECTED ROTATIONAL VELOCITY $v_{\text{rot}} \sin i$ (ASSUMED TO BE 0.5 km s^{-1} FOR ALL STARS) AND THE MACROTURBULENCE ζ_{macro} ; NOTE THAT INSTRUMENTAL BROADENING HAS ALSO BEEN APPLIED. THE LISTED EQUIVALENT WIDTHS FOR THE 670.8 AND 610.4 NM LINES ARE THOSE COMING FROM THE BEST-FITTING THEORETICAL LINE PROFILES TO THE OBSERVED PROFILES.

Star	$v_{\text{rot}} \sin i$ [km s^{-1}]	ζ_{macro} [km s^{-1}]	Li I 670.8 nm				Li I 610.4 nm		
			W_{λ} [pm]	$\log \epsilon_{\text{Li}}$ (LTE)	$\log \epsilon_{\text{Li}}$ (non-LTE)	${}^6\text{Li}/{}^7\text{Li}$	W_{λ} [pm]	$\log \epsilon_{\text{Li}}$ (LTE)	$\log \epsilon_{\text{Li}}$ (non-LTE)
HD 3567	0.50	4.71 ± 0.19	3.83	2.32 ± 0.01	2.32	0.017 ± 0.012	0.19	2.30 ± 0.04	2.36
HD 19445	0.50	3.83 ± 0.13	3.51	2.21 ± 0.01	2.20	0.002 ± 0.008	0.16	2.19 ± 0.05	2.24
HD 59392	0.50	4.37 ± 0.35	3.92	2.24 ± 0.01	2.24	0.021 ± 0.016	0.15	2.16 ± 0.03	2.22
HD 102200	0.50	4.44 ± 0.24	3.30	2.25 ± 0.01	2.25	0.047 ± 0.013	0.18	2.30 ± 0.03	2.36
HD 106038	0.50	3.88 ± 0.12	6.31	2.49 ± 0.01	2.48	0.031 ± 0.006	0.30	2.45 ± 0.02	2.52
HD 140283	0.50	4.87 ± 0.07	4.78	2.17 ± 0.01	2.20	0.008 ± 0.006	0.18	2.11 ± 0.03	2.20
HD 160617	0.50	4.54 ± 0.18	4.05	2.28 ± 0.01	2.28	0.036 ± 0.010	0.19	2.28 ± 0.03	2.34
HD 213657	0.50	5.02 ± 0.08	3.00	2.27 ± 0.01	2.25	0.011 ± 0.011	0.15	2.24 ± 0.04	2.29
HD 298986	0.50	4.70 ± 0.20	3.04	2.25 ± 0.01	2.24	0.017 ± 0.015	0.15	2.24 ± 0.04	2.29
HD 338529	0.50	5.65 ± 0.09	2.37	2.25 ± 0.01	2.22	0.010 ± 0.013	0.13	2.24 ± 0.05	2.28
G 013-009	0.50	5.85 ± 0.07	2.39	2.22 ± 0.01	2.19	0.048 ± 0.019	0.11	2.15 ± 0.06	2.20
G 020-024	0.50	5.12 ± 0.22	2.49	2.21 ± 0.01	2.18	0.070 ± 0.017	0.11	2.14 ± 0.07	2.18
G 075-031	0.50	4.95 ± 0.22	3.78	2.30 ± 0.01	2.30	0.015 ± 0.012	0.24	2.40 ± 0.03	2.46
G 126-062	0.50	4.76 ± 0.30	2.76	2.26 ± 0.01	2.24	0.001 ± 0.015	0.14	2.22 ± 0.04	2.27
G 271-162	0.50	5.78 ± 0.13	2.91	2.27 ± 0.01	2.25	0.019 ± 0.012	0.11	2.14 ± 0.05	2.19
BD +09° 2190	0.50	6.27 ± 0.35	1.66	2.13 ± 0.01	2.10	-0.033 ± 0.027	< 0.11	< 2.20	< 2.25
BD +03° 0740	0.50	6.71 ± 0.15	2.08	2.12 ± 0.01	2.11	0.015 ± 0.017	< 0.10	< 2.10	< 2.15
BD -13° 3442	0.50	6.38 ± 0.20	2.04	2.16 ± 0.01	2.14	0.001 ± 0.028	0.11	2.15 ± 0.08	2.19
CD -30° 18140	0.50	5.07 ± 0.11	2.76	2.25 ± 0.01	2.22	0.042 ± 0.013	0.14	2.23 ± 0.03	2.27
CD -33° 1173	0.50	5.82 ± 0.61	1.60	2.08 ± 0.01	2.05	0.013 ± 0.041	0.07	2.01 ± 0.10	2.04
CD -33° 3337	0.50	4.91 ± 0.14	3.90	2.23 ± 0.01	2.24	0.020 ± 0.010	0.20	2.27 ± 0.03	2.34
CD -35° 14849	0.50	4.68 ± 0.12	2.84	2.27 ± 0.01	2.24	0.020 ± 0.012	0.15	2.26 ± 0.05	2.30
CD -48° 2445	0.50	5.18 ± 0.10	2.56	2.22 ± 0.01	2.19	0.032 ± 0.014	0.15	2.27 ± 0.03	2.31
LP 815-43	0.50	6.20 ± 0.19	1.89	2.16 ± 0.01	2.13	0.046 ± 0.022	0.11	2.17 ± 0.06	2.21

TABLE 4. EFFECTS OF THE DERIVED ${}^6\text{Li}/{}^7\text{Li}$ RATIO TO THE STELLAR PARAMETERS AND SUITE OF 1D MODEL ATMOSPHERES

Star	${}^6\text{Li}/{}^7\text{Li}$					
	normal	ΔT_{eff}	$\Delta \log g$	$\Delta[\text{Fe}/\text{H}]$	$\Delta \xi_{\text{turb}}$	Kurucz ^a
HD3567	0.017	0.016	0.015	0.017	0.015	0.018
HD19445	0.002	0.000	0.002	0.002	0.001	0.003
HD59392	0.021	0.020	0.021	0.021	0.020	0.021
HD102200	0.047	0.043	0.045	0.047	0.046	0.044
HD106038	0.031	0.028	0.030	0.032	0.029	0.028
HD140283	0.008	0.008	0.008	0.008	0.007	0.006
HD160617	0.036	0.033	0.034	0.035	0.035	0.035
HD213657	0.011	0.008	0.011	0.011	0.010	0.011
HD298986	0.017	0.014	0.016	0.017	0.017	0.018
HD338529	0.010	0.008	0.011	0.010	0.011	0.011
G013-009	0.048	0.047	0.049	0.048	0.049	0.049
G020-024	0.070	0.070	0.069	0.070	0.069	0.070
G075-031	0.015	0.013	0.014	0.015	0.013	0.016
G126-062	0.001	-0.001	0.000	0.000	-0.001	0.003
G271-162	0.019	0.018	0.019	0.018	0.018	0.019
BD +09°2190	-0.033	-0.035	-0.033	-0.033	-0.032	-0.033
BD +03°0740	0.015	0.013	0.015	0.014	0.013	0.015
BD -13°3442	0.001	-0.001	0.001	0.001	0.001	0.001
CD -30°18140	0.042	0.039	0.043	0.041	0.041	0.044
CD -33°1173	0.013	0.010	0.012	0.013	0.013	0.011
CD -33°3337	0.020	0.019	0.019	0.021	0.017	0.021
CD -35°14849	0.020	0.017	0.020	0.020	0.020	0.020
CD -48°2445	0.032	0.031	0.033	0.032	0.033	0.034
LP815-43	0.046	0.045	0.046	0.048	0.046	0.046

^aDerived ${}^6\text{Li}/{}^7\text{Li}$ when using Kurucz model atmospheres (without convective overshoot as computed by Castelli et al. 1997) instead of the standard MARCS models otherwise used

TABLE 5. ESTIMATED PROJECTED STELLAR ROTATIONAL VELOCITIES AND ${}^6\text{Li}/{}^7\text{Li}$ BASED ON A 3D ANALYSIS

Star	$v_{\text{rot}} \sin i$ [km s^{-1}]	${}^6\text{Li}/{}^7\text{Li}$ (3D)	${}^6\text{Li}/{}^7\text{Li}$ (1D)
HD3567	0.35 ± 0.60	0.000 ± 0.012	0.017 ± 0.012
HD19445	2.55 ± 0.14	0.030 ± 0.008	0.002 ± 0.008
HD140283	2.01 ± 0.14	0.023 ± 0.006	0.008 ± 0.006
HD160617	1.19 ± 0.61	0.052 ± 0.012	0.036 ± 0.010
HD213657	1.93 ± 0.23	0.030 ± 0.012	0.011 ± 0.011
HD338529	2.50 ± 0.18	0.017 ± 0.013	0.010 ± 0.013
G013-009	2.77 ± 0.24	0.056 ± 0.021	0.048 ± 0.019
G020-024	2.30 ± 0.17	0.081 ± 0.016	0.070 ± 0.017
G075-031	0.67 ± 0.82	0.000 ± 0.012	0.015 ± 0.012
G271-162	2.65 ± 0.20	0.026 ± 0.012	0.019 ± 0.012
BD +09°2190	2.84 ± 0.58	0.000 ± 0.027	-0.033 ± 0.027
BD +03°0740	3.80 ± 0.27	0.026 ± 0.019	0.015 ± 0.017
BD -13°3442	3.02 ± 0.39	0.000 ± 0.028	0.001 ± 0.028
CD -30°18140	2.21 ± 0.26	0.058 ± 0.014	0.042 ± 0.013
CD -33°1173	1.81 ± 1.45	0.012 ± 0.027	0.013 ± 0.041
CD -35°14849	0.10 ± 0.19	0.026 ± 0.011	0.020 ± 0.012
CD -48°2445	2.34 ± 0.19	0.046 ± 0.014	0.032 ± 0.014
LP815-43	2.82 ± 0.25	0.036 ± 0.021	0.046 ± 0.022

TABLE 6. PREDICTED ${}^7\text{Li}$ AND ${}^6\text{Li}$ DEPLETION FACTORS (IN DEX) FOR OUR PROGRAM STARS INTERPOLATED FROM PREDICTIONS BY RICHARD ET AL. (2002, 2005; AND 2005, PRIVATE COMMUNICATION). THE SECOND AND THIRD COLUMNS GIVE THE EXPECTED DEPLETION DURING THE PRE-MAIN SEQUENCE (PMS) WHILE THE OTHERS ARE FOR THE EVOLUTION THEREAFTER TO WHICH THE PMS DEPLETION FACTORS SHOULD BE ADDED. DIFFUSION DENOTES THE CASE OF PURE DIFFUSION WHILE T6.09 AND T6.25 ARE FOR TWO DIFFERENT MODELS OF TURBULENT DIFFUSION (SEE TEXT FOR DETAILS).

Star	PMS		Diffusion		T6.09		T6.25	
	${}^7\text{Li}$	${}^6\text{Li}$	${}^7\text{Li}$	${}^6\text{Li}$	${}^7\text{Li}$	${}^6\text{Li}$	${}^7\text{Li}$	${}^6\text{Li}$
HD 3567	0.01	0.8	0.3	0.3	0.2	0.6	0.5	2.1
HD 19445	0.01	0.9	0.2	0.2	0.2	0.6	0.5	2.2
HD 59392	0.02	1.0	0.2	0.2	0.2	0.6	0.5	2.3
HD 102200	0.01	0.8	0.3	0.3	0.2	0.6	0.5	2.0
HD 106038	0.02	1.1	0.2	0.2	0.2	0.7	0.6	2.5
HD 140283	0.01	0.4	0.2	0.3	0.2	0.4	0.5	1.9
HD 160617	0.01	0.6	0.4	0.3	0.2	0.3	0.5	1.8
HD 213657	0.01	0.5	0.4	0.4	0.2	0.4	0.5	1.8
HD 298986	0.01	0.7	0.3	0.3	0.2	0.5	0.5	1.9
HD 338529	0.00	0.3	0.7	0.7	0.2	0.4	0.4	1.7
G 013-009	0.00	0.4	0.6	0.6	0.2	0.4	0.4	1.7
G 020-024	0.00	0.4	0.5	0.5	0.2	0.4	0.4	1.8
G 075-031	0.01	0.9	0.3	0.3	0.2	0.6	0.5	2.1
G 126-062	0.01	0.5	0.4	0.4	0.2	0.4	0.4	1.8
G 271-162	0.00	0.5	0.5	0.5	0.2	0.4	0.4	1.8
BD +09°2190	0.00	0.3	0.9	0.8	0.2	0.3	0.4	1.6
BD +03°0740	0.00	0.4	0.5	0.5	0.2	0.4	0.4	1.7
BD -13°3442	0.00	0.4	0.6	0.6	0.2	0.4	0.4	1.7
CD -30°18140	0.00	0.5	0.5	0.5	0.2	0.4	0.4	1.8
CD -33°1173	0.00	0.3	0.8	0.9	0.2	0.3	0.4	1.6
CD -33°3337	0.02	1.1	0.2	0.2	0.2	0.7	0.6	2.5
CD -35°14849	0.00	0.4	0.5	0.5	0.2	0.4	0.4	1.7
CD -48°2445	0.00	0.5	0.5	0.5	0.2	0.4	0.4	1.8
LP 815-43	0.00	0.3	0.9	0.8	0.2	0.3	0.4	1.6